



THE HONG KONG
POLYTECHNIC UNIVERSITY

香港理工大學

Pao Yue-kong Library

包玉剛圖書館

Copyright Undertaking

This thesis is protected by copyright, with all rights reserved.

By reading and using the thesis, the reader understands and agrees to the following terms:

1. The reader will abide by the rules and legal ordinances governing copyright regarding the use of the thesis.
2. The reader will use the thesis for the purpose of research or private study only and not for distribution or further reproduction or any other purpose.
3. The reader agrees to indemnify and hold the University harmless from and against any loss, damage, cost, liability or expenses arising from copyright infringement or unauthorized usage.

IMPORTANT

If you have reasons to believe that any materials in this thesis are deemed not suitable to be distributed in this form, or a copyright owner having difficulty with the material being included in our database, please contact lbsys@polyu.edu.hk providing details. The Library will look into your claim and consider taking remedial action upon receipt of the written requests.

**DEVELOPING A NOVEL STRATEGY TO
TREAT GLIOBLASTOMA: IMPROVING
BRAIN BIOAVAILABILITY OF
SORAFENIB WITH A SYNTHETIC
FLAVONOID DIMER TO INHIBIT DRUG
EFFLUX IN BLOOD BRAIN BARRIER**

HU XUESEN

Ph.D

The Hong Kong Polytechnic University

2018

The Hong Kong Polytechnic University

**Department of Applied Biology & Chemical
Technology**

**Developing a Novel Strategy to Treat
Glioblastoma: Improving Brain Bioavailability of
Sorafenib with a Synthetic Flavonoid Dimer to
Inhibit Drug Efflux in Blood Brain Barrier**

HU Xuesen

**A thesis submitted in partial fulfilment of the requirements for
the degree of Doctor of Philosophy**

September 2017

CERTIFICATE OF ORIGINALITY

I hereby declare that this thesis is my own work and that, to the best of my knowledge and belief, it reproduces no material previously published or written, nor material that has been accepted for the award of any other degree or diploma, except where due acknowledgement has been made in the text.

_____ (Signed)

HU Xuesen _____ (Name of student)

ACKNOWLEDGEMENT

My deepest gratitude goes first and foremost to Professor Larry Chow, my supervisor, for his constant encouragement, invaluable advice, and unconditional support. I am grateful that Prof. Larry Chow initiated this project with ingenious insights. Prof. Larry Chow is not only an experienced supervisor for my research and study but also a great tutor for my life in many aspects. He is one of the most respectable researchers I have ever met in my life. I have benefited a lot from his attitude to research. I feel lucky I have ever worked with him. And I am sure these five years are an unexceptionable experience of my life.

I would also like to show my gratitude to my dearest teammates Dr. Iris Wong, Mr. George Chong, Dr. Jiahua Cui, Mr. Zhen Liu, Mr. Terry Chan, Dr. Clare Yan, Dr. Jason Kan, Mr. Xuezhen Zhu for their generous assistance in my project, and for the team spirit we all built. Especially, Dr. Iris Wong has provided tremendous support, and encouragement in my project. She has also provided so much advice to my future career. I would like to thank all technical officers in the department of Applied Biology and Chemical Technology for their convenient lab-management and comprehensive technical support. I would like to thank our collaborator Prof. Gilberto Leung of the Department of Surgery at The University of Hong Kong and his postdoc Dr. Grace Zhang for their

generous help in my establishment of the orthotopic tumor model.

I owe my deepest gratitude to the Hong Kong PhD Fellowship Scheme (HKPFS) established by the Research Grants Council (RGC) of Hong Kong. It is an honor for me to be awarded by HKPFS, so that I have the opportunity to study my Ph.D. degree in Hong Kong.

Finally, I must express my very profound gratitude to my family for providing me with unfailing support and continuous encouragement throughout my years of study and through the process of researching and writing this thesis. This accomplishment would not have been possible without them. Thank you.

Abstract

Glioblastoma (GBM) is the most common form of brain cancer with a short median survival time (around 15 months). Chemotherapy is limited to temozolomide (TMZ) and resistance occurs frequently in GBM patients. There is an urgent need to develop new chemotherapeutic agents for GBM. Sorafenib, a potent multi-kinase inhibitor (TKI), being used clinically as an anti-cancer drug for hepatocarcinoma or renal cell carcinoma patients, was more potent than TMZ in killing U87MG (glioblastoma cell line) *in vitro*. Phase I/II clinical trials of sorafenib, however, failed to demonstrate any therapeutic effect on GBM. One possible explanation is that blood brain barrier (BBB) keep sorafenib out of the brain. The two ATP-binding cassette (ABC) transporters expressed at the BBB, P-glycoprotein (P-gp) and Breast Cancer Resistance Protein (ABCG2), might prevent the accumulation of sorafenib in the brain by active efflux. Here, a novel dual inhibitor of P-gp and BCRP (flavonoid dimer Ac12Az9, FD 12-9) shows extraordinary inhibitory effect on both P-gp and BCRP in *in vitro* assay with an EC₅₀ of 285 nM and 0.9 nM, respectively. Using canine MDCKII-P-gp and MDCKII-GFP-BCRP cell lines to mimic the trans-epithelial efflux in the BBB, it was demonstrated that FD 12-9 can inhibit the efflux of sorafenib. Pharmacokinetic studies indicate that FD 12-9 is able to increase the accumulation level of sorafenib in the brain by more than 9-fold. Pharmacokinetic profiles of sorafenib in the brain and plasma with or without

co-administered FD 12-9 were studied. No toxicity response was found in *in vivo* toxicity studies when 10 mg/kg of sorafenib and 10 mg/kg of FD 12-9 were co-administered at the same time. *In vivo* efficacy studies demonstrated that the increased brain concentration of sorafenib, after co-administration with FD 12-9, is high enough to significantly reduce the tumor size of the U87MG-RedFluc orthotopic xenograft glioblastoma model in immunocompromised mice. In addition, a TMZ-relapse model of GBM was developed by a single round of TMZ treatment in Balb/c nu nu mice. TMZ was ineffective in reducing the tumor volume in the relapse stage (34 days after initial treatment), even though the initial treatment stage seems to be completely effective. In contrast, sorafenib in combination with FD 12-9 was highly effective, suggesting that sorafenib, in combination with FD 12-9, can be used in both initial treatment as well as relapse (and TMZ-resistant) case of GBM. In summary, we have discovered a new approach to potentially treat glioblastoma by using a combination of FD 12-9 and sorafenib.

TABLE OF CONTENTS

CERTIFICATE OF ORIGINALITY	i
ACKNOWLEDGEMENT	ii
Abstract	iv
LIST OF TABLES	xii
LIST OF ABBREVIATIONS.....	xiii
CHAPTER 1: INTRODUCTION.....	1
Section 1.1 Glioblastoma multiform	1
1.1.1 Classification of brain tumors	1
1.1.2 Epidemiology of glioblastoma multiform and risk factors.....	3
1.1.3 Prognosis of glioblastoma multiform.....	4
1.1.4 Treatments for glioblastoma patients.....	5
Section 1.2 Sorafenib	10
1.2.1 Chemical and biological properties of sorafenib	10
1.2.2 Clinical application of sorafenib	11
1.2.3 Sorafenib for treating GBM.....	13
Section 1.3 Blood brain barrier (BBB) and multi-drug resistance (MDR)	17
1.3.1 Structure and function of the blood brain barrier (BBB)	17
1.3.2 The structure and evolution of ABC transporters.....	19
1.3.3 ABC transporters in BBB.....	27
1.3.4 Flavonoid dimers can reverse multidrug resistance (MDR)	28
Section 1.4 Objectives and rationales of study.....	30
CHAPTER 2: METHODOLOGY	33
2.1 Chemicals and drugs	33
2.2 <i>In vitro</i> studies.....	34
2.2.1 Cell lines	34
2.2.2 Cell culture	34
2.2.3 Cell proliferation assay	35

2.2.4 Cytotoxicity assay	36
2.2.5 Western blot analysis	36
2.2.6 Immunofluorescence labeling	38
2.2.7 Confocal fluorescence microscopy studies	39
2.2.8 Directional transport assay	39
2.3 <i>In vivo</i> studies.....	43
2.3.1 Animals.....	43
2.3.2 Pharmacokinetic studies of sorafenib in plasma and brain	43
2.3.3 <i>In vivo</i> toxicity studies	47
2.3.4 Orthotopic xenograft model of glioblastoma in mice.....	47
2.3.5 Monitoring of tumor growth by bioluminescent imaging	49
2.3.6 <i>In vivo</i> efficacy studies of sorafenib on U87MG-RedFluc orthotopic ...	49
CHAPTER 3: THE POTENTIAL OF SORAFENIB TO TREAT GBM AND THE POTENTIAL OF FLAVONOID DIMER AC12AZ9 (FD 12-9) TO MODULATE P-GP AND BCRP IN BBB	51
3.1 Introduction	51
3.2 Results.....	53
3.2.1 <i>In vitro</i> cytotoxicity of several TKIs and TMZ towards U87MG-RedFluc cells	53
3.2.2 <i>In vitro</i> effect of FD 12-9 in modulating P-gp- and BCRP- mediated resistance in different cell lines	54
3.2.3 <i>In vivo</i> modulating activity of FD 12-9 on P-gp and BCRP.....	58
3.3 Summary	69
CHAPTER 4: TRANS-EPITHELIAL MOVEMENT OF SORAFENIB IN MIMIC BBB MODEL USING MDCKII CELLS OVEREXPRESSING P-GP OR BCRP	70
4.1 Introduction	70
4.2 Results.....	71
4.2.1 Expression level and localization of P-gp and BCRP in MDCKII-P-gp and MDCKII-GFP-BCRP cells	71
4.2.2 Directional transport assay of sorafenib across MDCKII monolayer	74
4.3 Summary	80

CHAPTER 5: PHARMACOKINETIC STUDIES OF SORAFENIB WITH OR WITHOUT MODULATORS.....	81
5.1 Introduction	81
5.2 Result.....	82
5.2.1 Selection of suitable formulation for FD 12-9 for pharmacokinetic studies.....	82
5.2.2 Pharmacokinetics of sorafenib with or without modulators.....	85
5.3 Summary	92
CHAPTER 6: THE <i>IN VIVO</i> EFFICACY STUDIES OF SORAFENIB ON U87MG-REDFLUC ORTHOTOPIC XENOGRAFT GLIOBLASTOMA IN BALB/C NUDE MICE.....	94
6.1 Introduction	94
6.2 Results.....	95
6.2.1 <i>In vivo</i> toxicity studies in Balb/c mice	95
6.2.2 <i>In vivo</i> efficacy studies of sorafenib on U87MG-RedFluc orthotopic xenograft GBM in Balb/c nude (nu nu) mice with or without modulators....	98
6.2.3 The <i>in vivo</i> efficacy study of sorafenib combined with FD 12-9 in mice with TMZ-resistant recurrent GBM tumor	108
6.3 Discussion and summary	114
CHAPTER 7: CONCLUSIONS AND PERSPECTIVES	118
References	123

LIST OF FIGURES

Figure 1.1.1 Classification of brain tumors.....	2
Figure 1.2.1 Chemical structure and molecular model of sorafenib.....	10
Figure 1.2.3 The summary clinical use of TMZ and different TKIs.....	14
Figure 1.3.1A The structure model of blood brain barrier (BBB).	17
Figure 1.3.1B The model of localization of multidrug resistance transporters on brain capillary endothelial cell.	19
Figure 1.3.2 The structure model of P-glycoprotein (P-gp), multi-drug resistance protein 1 (MRP1) and breast cancer resistance protein (BCRP).	22
Figure 1.3.4 The general structure of flavonoid dimer.	29
Figure 2.2.8 The model of directional transport assay.	40
Figure 3.2.2A Synthesis of flavonoid dimers.	55
Figure 3.2.2B Modulating effect of triazole-containing flavonoid dimers towards P-gp, MRP1 and BCRP.	55
Figure 3.2.2C Chemical structure of flavonoid dimer AC12AZ9 (FD 12-9).	56
Figure 3.2.3.1A The effect of FD 12-9 on the pharmacokinetics studies of PTX.	60
Figure 3.2.3.1B The effect of FD 12-9 on the pharmacokinetics studies of TPT.	61
Figure 3.2.3.2A Chemical structure of erlotinib and the pharmacokinetic study of erlotinib with or without FD 12-9.	63
Figure 3.2.3.2B Chemical structure of axitinib and the pharmacokinetic study of afatinib with or without FD 12-9.....	64
Figure 3.2.3.2C Chemical structure of afatinib and the pharmacokinetic study of lapatinib with or without FD 12-9.	65
Figure 3.2.3.2D Chemical structure of lapatinib and the pharmacokinetic study of gefitinib with or without FD 12-9.....	66
Figure 3.2.3.2E Chemical structure of gefitinib and the pharmacokinetic study of axitinib with or without FD 12-9.	67
Figure 3.2.3.2F Chemical structure of sorafenib and the pharmacokinetic study of	

sorafenib with or without FD 12-9.....	68
Figure 4.2.1A Expression Level P-gp and BCRP in MDCKII Cells.	72
Figure 4.2.1B Expression level and localization of P-gp in MDCKII cells.	73
Figure 4.2.1C Expression level and localization of BCRP in MDCKII cells.....	74
Figure 4.2.2A Directional transport assay of sorafenib across three subtypes of MDCKII.....	76
Figure 4.2.2B Transport of sorafenib across P-gp-transfected MDCKII monolayer in the presence and absence of FD 12-9 or GF120918.	77
Figure 4.2.2C Transport of sorafenib across BCRP-transfected MDCKII monolayer in the presence and absence of FD 12-9 or GF120918.	78
Figure 4.2.2D Apparent permeability of sorafenib across wild-type, P-gp-transfected and BCRP-transfected MDCKII monolayers with or without modulators (FD 12-9 and GF120918).....	79
Figure 5.2.1A Effect of formulations on the accumulation of FD 12-9 in brain.....	83
Figure 5.2.1B Effect of formulations on plasma pharmacokinetics of FD 12-9.....	84
Figure 5.2.2A Pharmacokinetics studies of different dose of sorafenib with FD 12-9 or GF120918 in brain.	86
Figure 5.2.2B Pharmacokinetics studies of different dose of sorafenib with FD 12-9 or GF120918 in plasma.	87
Figure 5.2.2C The Brain-to-Plasma (B-to-P) ratio of sorafenib in seven groups of different dosages.....	88
Figure 5.2.2D Pharmacokinetics studies of FD 12-9 and GF120918 in brain.	91
Figure 5.2.2E Pharmacokinetics studies of FD 12-9 and GF120918 in Plasma.....	92
Figure 6.2.1 In vivo toxicity evaluation studies in BALB/c mice with different treatments.	96
Figure 6.2.2A Implantation of U87MG-RedFluc cells in the brain of nude mice to establish orthotopic model of GBM.....	98
Figure 6.2.2B In vivo efficacy of sorafenib against orthotopic model of GBM with or without FD 12-9.....	100
Figure 6.2.2C In vivo efficacy of sorafenib against orthotopic model of GBM as	

monitored by IVIS technique.....	100
Figure 6.2.2D Survival curve of orthotopic GBM-bearing mice after receiving treatment of sorafenib with or without FD 12-9.....	102
Figure 6.2.2E Body weight changes in U87MG-RedFluc-bearing mice receiving treatment of sorafenib with or without FD 12-9.....	102
Figure 6.2.2F Relative BLI signal changes of U87MG-RedFluc tumors in 6 different groups of mice receiving sorafenib with or without FD 12-9 or GF120918.....	104
Figure 6.2.2G In vivo efficacy of sorafenib with or without different modulators against orthotopic model of GBM as monitored by IVIS technique.....	105
Figure 6.2.2H Survival curve of orthotopic GBM-bearing mice after receiving treatment of sorafenib with or without different modulators.....	106
Figure 6.2.2I Body weight changes of U87MG-RedFluc-bearing mice after receiving sorafenib with or without FD 12-9 or GF120918.....	107
Figure 6.2.3A Establishment of TMZ-resistant relapse model of GBM and its response to combination treatment of TMZ and FD 12-9.....	110
Figure 6.2.3B Establishment of TMZ-resistant relapse model of GBM and its response to combination treatment of TMZ and FD 12-9 (IVIS signals).....	111
Figure 6.2.2C Survival curve of TMZ-resistant GBM animal model in response to TMZ or combination.....	112
Figure 6.2.3D Body weight changes of TMZ-resistant GBM-bearing mice in response to TMZ or combination (FD 12-9 + sorafenib) treatment.....	113

LIST OF TABLES

Table. 1.2.3 Clinical trials of using sorafenib to treat GBM.....	16
Table. 3.2.1 The IC ₅₀ of different TKIs towards U87MG-RedFluc.....	53
Table. 3.2.2 Effects of different compounds in modulating P-gp and BCRP mediated resistance in different cell lines <i>in vitro</i>	57
Table. 3.2.3.1 Effect of FD 12-9 on the pharmacokinetics studies of PTX and TPT by oral administration <i>in vivo</i>	61
Table. 5.2.2 Plasma and brain pharmacokinetic parameters after a single intravenous injection of different doses of sorafenib with or without modulators in BALB/c mice.....	90
Table. 6.2.1 <i>In vivo</i> toxicity evaluation studies in BALB/c mice with different treatments.....	97

LIST OF ABBREVIATIONS

ABC	ATP-binding cassette
ABCA	ATP-binding cassette transporter subfamily A
ABCB	ATP-binding cassette transporter subfamily B
ABCC	ATP-binding cassette transporter subfamily C
ABCD	ATP-binding cassette transporter subfamily D
ABCE	ATP-binding cassette transporter subfamily E
ABCF	ATP-binding cassette transporter subfamily F
ABCG	ATP-binding cassette transporter subfamily G
ABCH	ATP-binding cassette transporter subfamily H
ADESC	Animal Subjects Ethics Sub-committee
ATP	Adenosine-triphosphate
ATP2B1	Plasma membrane calcium-transporting ATPase 1
AUC	Area under curve
BAY 43-9006	Sorafenib
BBB	Blood brain barrier
BCRP	Breast Cancer Resistance Protein
BLI	Bioluminescent imaging
B-RAF	Serine/threonine-protein kinase B-Raf
BSA	Bovine Serum Albumin
CCI-779	mTOR inhibitor temsirolimus
CHO	Chinese hamster ovary
CNS	Central nervous system
C-RAF	RAF proto-oncogene serine/threonine-protein kinase
DMEM	Dulbecco's Modified Eagle Medium
DNA	Deoxyribonucleic acid
DTC	Differentiated thyroid cancer
EC ₅₀	Half maximal effective concentration
EDTA	Ethylenediaminetetraacetic acid
ERK	Extracellular signal–regulated kinases
FBS	Fetal bovine serum
FD 12-9	Flavonoid dimer Ac12Az9

FDA	Food and Drug Administration
GBM	Glioblastoma
GF120918	Elacridar
GFP	Green fluorescent protein
GI	Gastrointestinal
GLUT1	Glucose transporter 1
GSH	Glutathione
GS-X	Glutathione S-conjugate
HCC	Hepatocellular carcinoma
HKPFS	Hong Kong PhD fellowship scheme
HKSAR	Hong Kong Special Administrative Region
HKU	The University of Hong Kong
HPLC	High performance liquid chromatography
HRP	Horse Radish Peroxidase
I.P.	Intraperitoneal
I.V.	Intravenous
IC ₅₀	Half maximal inhibitory concentration
IDH1	Isocitrate dehydrogenase 1
IDH2	Isocitrate dehydrogenase 2
IUPAC	International Union of Pure and Applied Chemistry
IVIS	<i>In vivo</i> imaging system
JAM	Junctional adhesion molecule
LAS X	Leica Application Suite X
LAU	Laboratory of Animal Unit
LC-MS/MS	Liquid chromatography-tandem mass spectrometry
MAP2K	Mitogen-activated protein kinase kinase
MAPK	Extracellular signal-regulated kinases
MAPKK	Mitogen-activated protein kinase kinase
MDCK	Madin-Darby canine kidney
MDR	Multiple drug resistance
MDR1	P-glycoprotein
MEK	Mitogen-activated protein kinase kinase
MGMT	O-6-methylguanine methyltransferase
MRP1	Multidrug resistance-associated protein 1

MTD	Maximum tolerated dose
mTOR	Mammalian target of rapamycin
MXR1	Breast Cancer Resistance Protein
NBD	Nucleotide binding domain
Nexavar	Sorafenib
NMP	N-Methyl-2-pyrrolidone
NOD-SCID	Non-dose diabetic- severe combined immunodeficient
NP-40	Nonyl phenoxyethoxyethanol
NSCLC	Non-small cell lung carcinoma
OAT	Organic anion transporter
OATP1A2	Organic Anion Transporting Polypeptide 1A2
OS	Overall survival
P.O.	Oral
P/S	Penicillin/streptomycin
P _{app}	Apparent permeability
PBS	Phosphate buffered saline
PDGF	Platelet-derived growth factor
PDGFR	Platelet-derived growth factor receptor
PEG	Polyethylene glycol
P-gp	P-glycoprotein
PK	Pharmacokinetics
PMSF	Phenylmethanesulfonyl fluorid
PTX	Paclitaxel
PVC	Polyvinyl chloride
Q.o.D.	Quaque Ommi Die (every other day)
RAF	Rapidly Accelerated Fibrosarcoma
RAF1	RAF proto-oncogene serine/threonine-protein kinase
RCC	Renal cell carcinoma
RGC	Research grants council
RNA	Ribonucleic acid
RPMI	Roswell Park Memorial Institute
SDS	Sodium dodecyl sulfate
SV40	Simian vacuolating virus 40
TBST	tris-buffered saline (TBS) and Polysorbate 20

TEER	transepithelial electrical resistance
TKI	Tyrosine kinase inhibitor
TMD	Transmembrane domain
TMZ	Temozolomide
TPT	Topotecan
TTFields	Tumor treating fields
U.S.A.	United States of America
UCLA	The University of California, Los Angeles
UPLC	Ultra-performance liquid chromatography
VEGF	Vascular endothelial growth factor
VEGFR	Vascular endothelial growth factor receptor
WHO	World Health Organization

CHAPTER 1: INTRODUCTION

Section 1.1 Glioblastoma multiform

1.1.1 Classification of brain tumors

Brain tumors can be classified into primary brain tumors or secondary brain tumors. Secondary brain tumors are metastasized tumors from other organs. Primary brain tumors are tumors that originate in the brain. Unlike metastatic tumors, primary brain tumors rarely spread to other parts of the body. Primary brain tumors are classified according to their cellular origin, such as glioma, meningioma, pituitary adenoma, craniopharyngioma and nerve sheath tumor (Molnár, 2011). Around 80% of tumors that originate in the brain are gliomas, which are the most common type of primary brain tumors. Gliomas originate from glial tissue. According to World Health Organization (WHO), gliomas can be further classified into astrocytomas, oligodendrogliomas, ependymomas or brainstem gliomas based on their origins. Furthermore, gliomas are graded from I to IV according to their malignancy level (Figure 1.1.1) (Dolecek et al., 2012; Ostrom et al., 2013). Glioblastomas, also known as glioblastoma multiforme (GBM), are grade IV astrocytic brain tumors and are considered as the most malignant glioma.

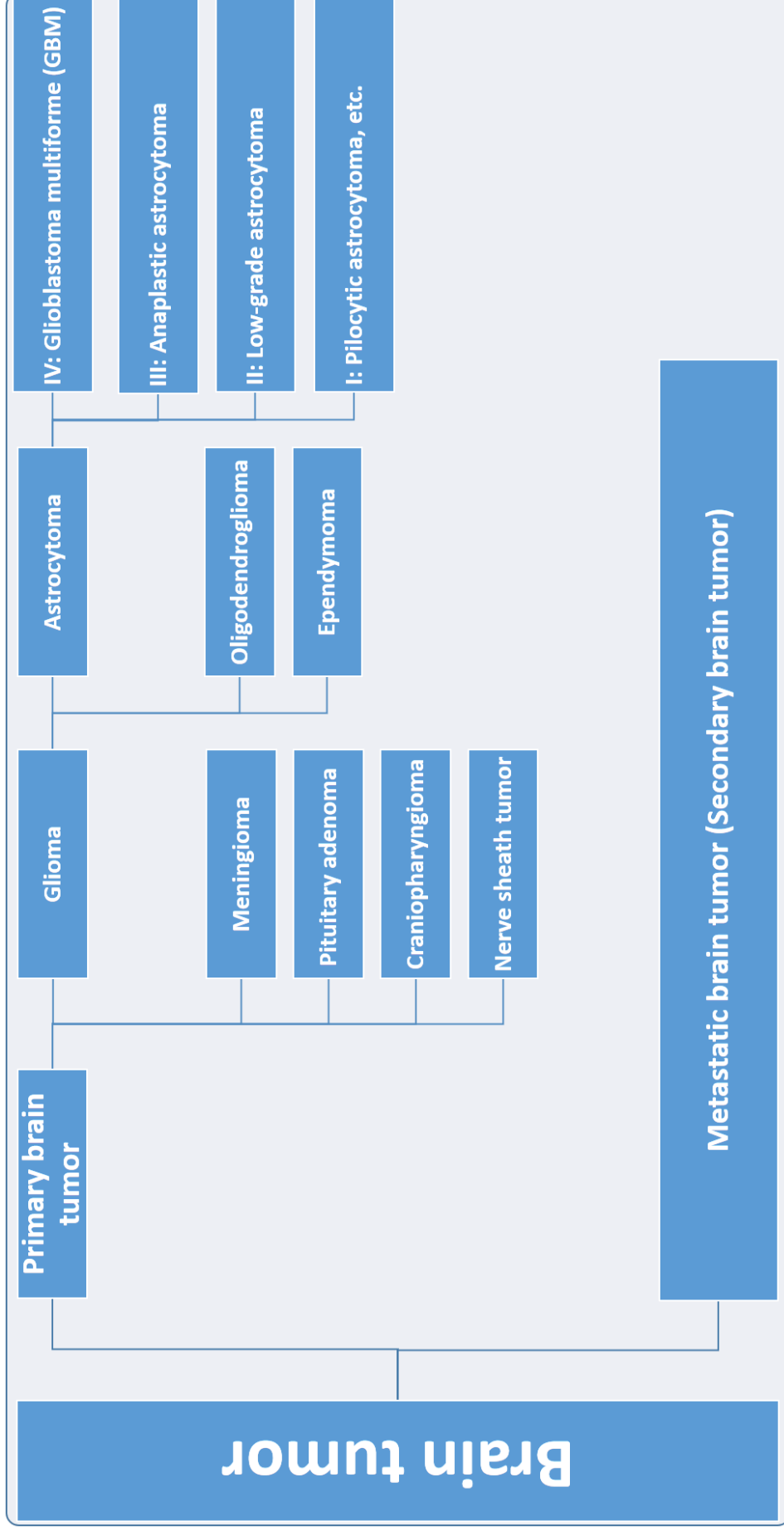


Figure 1.1.1 Classification of brain tumors.

Brain tumors are generally classified into primary brain tumors or secondary brain tumors (also known as metastatic brain tumors).

Common types of primary brain tumors are classified according to the cell types and the location where they originate in brain.

Secondary brain tumors mean tumors that spread from other organs to the central nervous system (CNS).

1.1.2 Epidemiology of glioblastoma multiform and risk factors

GBM is the most common form of brain tumor, representing 15% of all cases. More than 90% of brain tumors are grade IV GBM when first diagnosed, and are classified as primary glioblastomas. Most primary GBMs cases are found in patients above the age of 50. A small number (< 10%) of GBMs are developed from lower-grade glioma, and they are classified as secondary GBMs. Secondary glioblastomas generally occur in younger patients (< 50 years) (Nupponen and Joensuu, 2006; Ohgaki and Kleihues, 2007). Since primary and secondary GBMs respond differently to therapies, with primary GBMs having poorer prognosis (Molenaar et al., 2014b), it is important to distinguish between them. Unfortunately, in many cases, lower-grade gliomas do not show any symptoms until they are found to have progressed to GBMs. More than 80% of secondary GBMs progressing from lower-grade gliomas have a mutation in IDH1 or IDH2 (isocitrate dehydrogenase 1 or 2) whereas primary GBMs only have around 5 - 10% of such mutation (Molenaar et al., 2014a). It has been reported that mutation in IDH1 or IDH2 might be a reliable criterion to define primary and secondary GBMs (Molenaar et al., 2014a; Molenaar et al., 2014b; Ohgaki and Kleihues, 2013).

GBMs account for 15% of all brain tumors and 50% of all gliomas (Young et al., 2015). There are around 32 people in every 1 million diagnosed with either primary GBM or secondary GBM every year, with 12,500 cases diagnosed every year in U.S.A. alone. Most GBM patients are male with median diagnosis

age of 64 (Gallego, 2015).

It is unclear why GBM appears more frequently in elderly males. Younger adults or women have much lower risk of GBM. It has been reported that there is no direct causal relationship between GBM and smoking, cured meat, frequent use of cellphone or exposure to electromagnetic radiation (Huncharek et al., 2003; Inskip et al., 2001; Savitz et al., 1998; Zheng et al., 2001). There might be some relationship between GBM and alcohol consumption or ionizing radiation (Baglietto et al., 2011; Cavenee, 2000). Others have reported that GBMs could be associated with simian vacuolating virus 40 (SV40) (Vilchez et al., 2003). SV40 can be transmitted to humans by *Anopheles* mosquito (COBBS, 2009; Lehrer, 2010). Some occupational risks, including exposure to lead or polyvinyl chloride (PVC), might be associated with GBM (Preston-Martin et al., 1989; Van Wijngaarden and Dosemeci, 2006).

1.1.3 Prognosis of glioblastoma multiform

The median overall survival (OS) for all GBM patients is less than 15 months (Gallego, 2015). Typically, the median OS for GBM patients, without any treatment, is only 3 months (Schapira, 2007). Even with the most comprehensive treatments, the median OS can only be extended to 12 - 24 months. Cerebral edema and intracranial pressure are the major causes of death (Krex et al., 2007). Five-year survival rate for all GBM patients is poor with less than 6% (Gallego, 2015). In addition, relapse rate is high irrespective

of treatments used. Only a very small number of patients show no recurrence for more than 10 years (Gallego, 2015).

An extensive OS study for GBM patients have been performed by UCLA Neuro-Oncology, a brain tumor program launched by UCLA to provide real-time OS data of patients with GBM diagnosed and treated by UCLA Neuro-Oncology from 03-Jun-2010 onwards. Different chemotherapy agents had been applied to different patients in different groups of GBM patients in the following age ranges: 18 - 34; 36 - 50; 50 - 70 and 70 – 93. The estimated mean survival time (Kaplan-Meier plot) for these groups is 36.9 months, 21.1 months, 19.9 months and 16.4 months, respectively. The overall survival of these patients is 20.4 months. There was a clear association between poor prognosis and the age of GBM patients.

1.1.4 Treatments for glioblastoma patients

There has been no significant improvement in OS rates in GBM patients for more than 30 years (1973-2004) since relapse is almost ubiquitous after symptomatic or palliative therapies (Barnholtz-Sloan et al., 2003; Tait et al., 2007).

1.1.4.1 Symptomatic therapy

Symptomatic therapies aim at relieving symptoms of patients. Anticonvulsants

and corticosteroids are two major types of symptomatic agents. Anticonvulsants are widely used in GBM patients even though less than half of them actually need them. Anticonvulsants might not be beneficial to GBM patients. Instead, anticonvulsants should only be taken when spasm occurs (Stevens, 2006). Corticosteroids can effectively lower intracranial pressure to relieve the symptom of headache or drowsiness.

1.1.4.2 Palliative therapy

Unlike symptomatic therapies which only focus on symptoms but not the cause of disease, palliative therapies are treatments that help to prolong the survival time and improve the quality of life for patients. Standard palliative therapies for GBM include surgery and adjuvant radiation therapy followed by chemotherapy. Some new therapies such as alternating electric field therapy have been approved in recent years.

1.1.4.2.1 Surgical resection

Surgical resection is the first-choice of treatment for GBM patients after initial diagnosis because it can reduce up to 99% of tumor bulk. Surgical resection significantly improves prognosis. GBM patients with more than 98% tumor resected live much longer and healthier than those with less than 98% resected (Lacroix et al., 2001). δ -Aminolevulinic acid, a fluorescent dye, has been used as a surgical guide to increase the possibility of total removal of the tumor.

Surgical resection can relieve intracranial pressure and headache and the resected tumor cells can be used for histological diagnosis.

GBM tumors are relatively large and some tumor cells are undetectable at initial diagnosis. Surgical resection, therefore, can only remove most of the GBM cells. Recurrence occurs in most patients. Recurrent GBM could occur either at the original location or nearby. Surgical resection is, therefore, usually followed by radiation therapy and chemotherapy.

1.1.4.2.2 Radiation therapy

For GBM patients, the most common treatment after surgical resection is radiotherapy. An early clinical trial in U.S.A. has reported that the OS of GBM patients improved by more than 2 times with radiotherapy after surgical resection compared that without radiotherapy (Walker et al., 1978). Radiotherapy, therefore, has been widely used in GBM patients after surgery. The average size of a GBM tumor is around 10^{11} cells at diagnosis and 10^9 cells after surgical resection. Three-dimensional conformal radiotherapy is more specific and better to GBM patients in comparison to whole-brain radiotherapy (Showalter et al., 2007). To achieve optimal effect, the dose of the radiotherapy should be controlled between 60 – 65 Gy (Fulton et al., 1992).

The core area of GBM tumor is hypoxic. GBM cells exposed to such hypoxic condition are more resistant to radiotherapy, which significantly impairs the efficiency of radiotherapy. Many radiosensitizers aiming to improve the

radiosensitivity of GBM have been reported (Sheehan et al., 2008; Sheehan et al., 2010).

1.1.4.2.3 Chemotherapy

There are only a few chemotherapy options for GBM. These include bevacizumab, carmustine, lomustine, and temozolomide (TMZ).

Bevacizumab is an anti-angiogenic agent, which can only relieve the symptoms of GBM and shows no effect in prolonging OS and preventing recurrence (Norden et al., 2009).

Carmustine is a DNA alkylating agent which can form inter-strand crosslink in DNA. It is implanted under the skull in a form of biodegradable wafer or disc by surgical operation (Ewend et al., 2007). With this special administration method, carmustine is able to bypass the blood brain barrier (BBB) to enhance the exposure of GBM to carmustine (Gabathuler, 2010).

Lomustine is an oral drug for GBM. Benefiting from its high hydrophobicity (Chen et al., 2016), lomustine can get through the BBB, which makes it ideal for treating GBM. It can alkylate both DNA and RNA (Pizzo and Poplack, 2015).

Temozolomide (TMZ), as the first-line cancer drug for GBM, can methylate guanine to give O-6-methylguanine, causing DNA damage and induce apoptosis (Brandes et al., 2004). TMZ is the most widely-used chemotherapy agent for both newly-diagnosed and recurrent GBM patients. TMZ is the standard treatment following surgical treatment and radiotherapy. TMZ

resistance, however, is almost ubiquitous (Brandes et al., 2006). It has been reported that TMZ treatment can induce O-6-methylguanine methyltransferase (MGMT) in GBM. TMZ resistance is due to elevated MGMT which can repair DNA damage by removing methyl group from the O-6-position of guanine. Elevated level of MGMT significantly desensitizes GBM to TMZ (Jacinto and Esteller, 2007; Pegg, 1990; Pegg et al., 1995).

1.1.4.2.4 Alternating electric field therapy

Alternating electric field therapy, also known as tumor treating fields (TTFields), is a treatment that uses low-frequency electric field at 200 +/- 50 kHz to interfere with mitosis of GBM cells (Swanson et al., 2016). In the anaphase of mitosis, when the plane of mitosis is parallel to TTFields, membrane blebbing occurs in cells and mitosis fails (Kirson et al., 2004). α/β -Tubulin and the septin 2, 6, 7 heterotrimer have been reported to be associated with this antimitosis activity of TTFields. As a novel treatment, TTFields had been approved by the Food and Drug Administration (FDA) of the United States in 2011 for treating recurrent GBM (Fonkem and Wong, 2012) and in 2015 for treating newly diagnosed GBM (Stupp et al.), though its therapeutic effect remains controversial (Wick, 2016). The first TTFields medical device for clinical use, NovoTTF-100A or Optune, has been launched by a company in Israel named Novocure. OS of newly-diagnosed GBM patients can be extended by 3 months (Stupp et al., 2015).

Section 1.2 Sorafenib

1.2.1 Chemical and biological properties of sorafenib

Sorafenib (free base), whose molecular weight is 464.825 g/mol, is a yellowish or brownish powder. The IUPAC name and molecular formula of sorafenib are 4-[4-[[4-chloro-3-(trifluoromethyl)phenyl]carbamoylamino]phenoxy]-*N*-methylpyridine-2-carboxamide and $C_{21}H_{16}ClF_3N_4O_3$ respectively (Figure 1.2.1).

Sorafenib tosylate ($C_{28}H_{24}ClF_3N_4O_6S$, 637.027 g/mol) is the salt form of sorafenib.

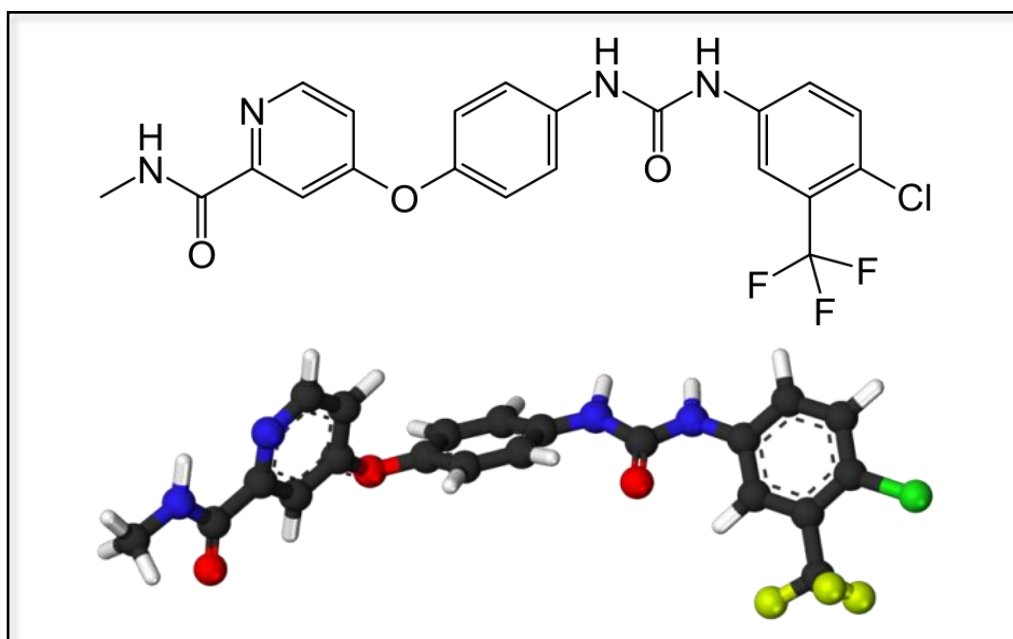


Figure 1.2.1 Chemical structure and molecular model of sorafenib.

The upper panel is the chemical structure of sorafenib. The bottom panel is the molecular model of sorafenib. Atoms are represented as different color of spheres or stick: carbon is tinted with black, hydrogen is tinted with white, nitrogen is tinted with blue, oxygen is tinted with red, fluorine is tinted with yellow and chlorine is tinted with green.

Sorafenib is one of the tyrosine kinase inhibitors (TKIs) which include dasatinib, imatinib, nilotinib, gefitinib, sunitinib, axitinib, erlotinib, afatinib, and lapatinib. Sorafenib acts mainly against RAF proto-oncogene serine/threonine-protein kinase (C-RAF or RAF1) and its V600E mutant form B-RAF (Smalley et al., 2009). Sorafenib can also inhibit the downstream part of the Ras-Raf-MEK-ERK pathway, namely MEK (mitogen-activated protein kinase kinase, also known as MAP2K, MAPKK) and ERK (extracellular signal-regulated kinase, also known as MAPK, mitogen-activated protein kinases) (Wilhelm et al., 2008). Besides the Ras-Raf-MEK-ERK pathway, sorafenib also inhibits vascular endothelial growth factor receptor family (VEGFR) and platelet-derived growth factor receptor (PDGFR) to reduce blood vessels formation (Wilhelm et al., 2008). As a potent inhibitor for both Ras-Raf-MEK-ERK pathway and VEGFR/PDGFR signaling, which are the two important pathways for tumor growth and angiogenesis, sorafenib has been investigated for its potential in treating different tumors (Adnane et al., 2006).

1.2.2 Clinical application of sorafenib

Sorafenib has been approved by the Food and Drug Administration (FDA) of the United States in a formulation of sorafenib tosylate tablet, which is manufactured and launched by Bayer Healthcare Pharmaceuticals in the brand name of Nexavar[®] (BAY 43-9006).

Nexavar has been approved by the FDA for treating kidney cancer (renal cell carcinoma, RCC), liver cancer (hepatocellular carcinoma, HCC) and differentiated thyroid cancer (DTC) in 2005, 2007 and 2013 respectively (Chang et al., 2007; Llovet et al., 2008; Thomas et al., 2014). With the treatment of sorafenib, the median OS of advanced RCC patients is around 167 days, which is significantly longer than those patients without sorafenib therapy (placebo) (84 days). Severe side effect for sorafenib treatment is low, with grade III adverse reactions like hand-foot skin reaction, fatigue and hypertension occurring in less than 6% of all cases, and grade IV adverse reactions are rare (Kane et al., 2006).

Sorafenib is also approved for treating hepatocellular carcinomas (HCC). The median OS of patients with advanced HCC, which is usually untreatable by surgery, can be increased by sorafenib (10.7 months for sorafenib versus 7.9 months for placebo). Advanced HCC means HCC that cannot be cured by surgery, or that HCC cells have spread to other parts of the liver and possibly other parts of the body.

Sorafenib has also been approved by the FDA to be used for treating differentiated thyroid cancer (DTC) in 2013. The standard therapies for thyroid cancer patients are surgery and radioactive iodine treatment. Surgical treatment can remove most of the cancer cells in the thyroid. Radioactive iodine can target thyroid cancer cells in the thyroid. When the thyroid cancer does not respond to radioactive iodine treatment anymore or recurs at the same location

of the thyroid or even metastasizes to other parts of the body, sorafenib can still improve the progression-free survival significantly but not the overall survival. However, side effects like hand-foot skin reaction occur frequently during sorafenib treatment for thyroid cancer patients (Brose et al., 2013; Thomas et al., 2014).

1.2.3 Sorafenib for treating GBM

Other than renal cell carcinoma (RCC), hepatocellular carcinomas (HCC) and differentiated thyroid cancer (DTC), the cytotoxic effect of sorafenib is also investigated in different preclinical cancer models like breast, colon, ovarian and pancreatic carcinoma, melanoma and non-small cell lung carcinoma (NSCLC) or in phase II/III clinical trials for melanoma and NSCLC (Eisen et al., 2006; Monk et al., 2014; Paz-Ares et al., 2015a; Paz-Ares et al., 2015b).

Besides sorafenib, many TKIs have been used to treat different kinds of cancers, such as NSCLC, pancreatic cancer, breast cancer, etc. Among all these clinical uses of TKIs, none of them is related to treating GBM. However, some researchers did try using TKIs to treat GBM in clinical trials.

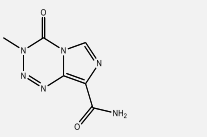
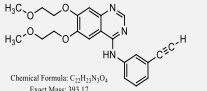
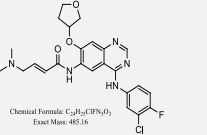
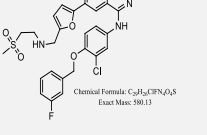
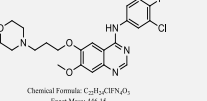
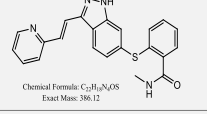
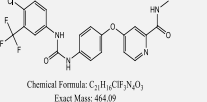
Drugs	Structure	Trade name	Route of administration	Dose	Dosing regimen	Clinical use
Temozolomide	 Chemical Formula: $C_4H_5N_5O_2$ Exact Mass: 194.06	Temodar	PO or Infuse IV over 90 minutes	150 mg/m ² /day	5 consecutive days per 28-day treatment cycle	Newly diagnosed GBM
						Recurrent astrocytoma
Erlotinib	 Chemical Formula: $C_{22}H_{25}N_3O_4$ Exact Mass: 393.17	Tarceva	PO	150 mg/day	Treatment should continue until disease progression or unacceptable toxicity occurs	NSCLC
				100 mg/day with gemcitabine		Pancreatic cancer
Afatinib	 Chemical Formula: $C_{24}H_{24}ClFN_3O_3$ Exact Mass: 485.16	Gilotrif	PO	40 mg/day (Dose escalation to a max of 50 mg/day may be considered if the patient can tolerate a 40 mg/day starting dose)	1. Daily per 21-day treatment cycle for NSCLC 2. Daily per 28-day treatment cycle for squamous NSCLC	NSCLC
Lapatinib	 Chemical Formula: $C_{27}H_{26}ClFN_3O_3S$ Exact Mass: 500.13	Tykerb	PO	1. HER2-overexpressing metastatic breast cancer: 1250 mg/day + capecitabine (2000 mg/m ² /day; PO divided q12hr) 2. Hormone-positive and HER2-positive advanced breast cancer: 1500 mg/day + letrozole (2.5 mg/day; PO)	1. Tykerb on Days 1-21 continuously + capecitabine on Days 1-14 in a 21-day cycle 2. Tykerb + letrozole continuously	Breast cancer
Gefitinib	 Chemical Formula: $C_{22}H_{24}ClFN_3O_3$ Exact Mass: 446.15	Iressa	PO	250 mg/day	Treatment should continue until disease progression or unacceptable toxicity occurs	NSCLC
Axitinib	 Chemical Formula: $C_{17}H_{16}N_4OS$ Exact Mass: 336.12	Inlyta	PO	5 mg/12hr	Treatment should continue as long as clinical benefit is observed until disease progression or unacceptable toxicity occurs	RCC
Sorafenib	 Chemical Formula: $C_{21}H_{19}ClF_3N_2O_2$ Exact Mass: 464.09	Nexavar	PO	400 mg/12hr	Treatment should continue as long as clinical benefit is observed until unacceptable toxicity occurs	Advanced RCC
						Advanced primary HCC

Figure 1.2.3 The summary clinical use of TMZ and different TKIs.

The structures, trade name, therapeutic dose, route of administration, dosing regimen and clinical indication of TMZ and different TKIs.

Attempts have been made to use sorafenib to treat GBM, but the results were unsatisfactory. Sorafenib induces autophagy in GBM cells (T98G) (Jakubowicz-Gil et al., 2014a). Clinical trials results, however, varied. First, it has been hypothesized that vertical blockade of VEGF signaling by combining upstream anti-VEGF antibody bevacizumab (avastin) and downstream Ras-Raf-MEK-ERK pathway inhibitor sorafenib, could have a potential synergistic effect. Such

bevacizumab/sorafenib combination, however, did not improve outcome of patients as compared with conventional bevacizumab treatment alone (Galanis et al., 2013). Second, combining sorafenib with metronomic temozolomide treatment of relapsed glioblastoma was found to be feasible and safe in a phase II study (Zustovich et al., 2013). Third, a phase I study in 2011 found that the maximum tolerated dose (MTD) of sorafenib in recurrent glioma patients was 800 mg, twice a day (Nabors et al., 2011). Fourth, a phase I study in 2014 found that radiation therapy combined with TMZ and sorafenib had significant side effects (Hottinger et al., 2014b). Fifth, combining sorafenib with a mTOR inhibitor temsirolimus (CCI-779) was found to be too toxic in a phase I study for treating recurrent GBM or gliosarcoma (Lee et al., 2012). There was no beneficial effect on recurrent GBM at the MTD of the therapy (800 mg sorafenib daily and 25 mg temsirolimus once weekly). In summary, even though sorafenib is more cytotoxic against GBM cells *in vitro* than TMZ, sorafenib is currently not considered as a viable therapeutic strategy for treating glioblastoma.

Table 1.2.3 Clinical trials of using sorafenib to treat GBM.

Year	2010	2011	2012	2013
Interventions	Radiation Therapy Temozolomide Sorafenib	Sorafenib Temozolomide	Sorafenib Temsirrolimus	Sorafenib Erlotinib
Condition	Glioblastoma Multiforme	Recurrent Glioblastoma Multiforme	Recurrent Malignant Gliomas	Recurrent Glioblastoma Multiforme
Phase	2	2	2	2
Participants	47	32	19	56
OS (Months)	12	9.7	NA	5.7
PFS6 (%)	NA	0.094	0	0.14
Median PFS	6 months	NA	8 weeks	2.5 months
Conclusion	The addition of sorafenib did not appear to improve the efficacy of treatment when compared with the results expected with standard therapy.			The study did not meet its objective of a 30% increase in overall survival.
Reference	https://www.ncbi.nlm.nih.gov/pubmed/20564147?dopt=Abstract	https://www.ncbi.nlm.nih.gov/pubmed/20443129?dopt=Abstract	https://www.ncbi.nlm.nih.gov/pmc/articles/PMC3499017/	https://www.ncbi.nlm.nih.gov/pubmed/23328813?dopt=Abstract

The clinical trials including sorafenib in the past few years. Interventions, conditions, different kinds of survival and conclusions have been listed in the table.

A possible reason for sorafenib's failure in clinical trials even though it is cytotoxic at cellular level is its low penetration in brain, which is limited by the BBB.

Section 1.3 Blood brain barrier (BBB) and multi-drug resistance (MDR)

1.3.1 Structure and function of the blood brain barrier (BBB)

The blood brain barrier (BBB) refers to the membrane barrier between blood and brain tissue, which is mainly composed of endothelial cells with tight junction or occluding junction between them (Ballabh et al., 2004; de Vries et al., 1997; Pardridge, 2005). Such tight junction is composed of transmembrane proteins including occludin, claudins and junctional adhesion molecule (JAM) (Stamatovic et al., 2008). Besides, endothelial cells of the BBB are surrounded by a continuous layer of basement membrane known as basal lamina, and around 85% of the BBB surface is covered by astrocytic feet of astrocyte cells (Figure 1.3.1A) (Pardridge, 2005; Van Dorpe et al., 2012).

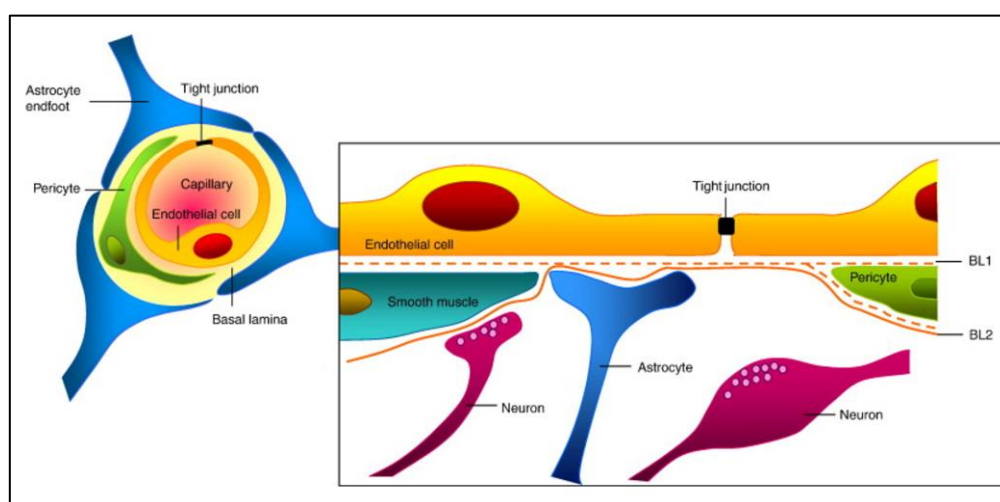


Figure 1.3.1A The model of blood brain barrier (BBB).

The BBB is formed by brain endothelial cells lining brain capillaries. The endothelial cells connect to each other by a special structure named tight junction which seal the lumen of brain capillaries, keeping unwanted

xenobiotics from getting in the CNS. The brain capillaries are also surrounded and stacked by many other kinds of cells like neuron, astrocyte and pericyte etc. This figure is adopted from (Abbott et al., 2010).

The complex composition of the BBB forms a multi-layered structure of brain capillaries and constitutes a protective barrier of brain tissue. The two major functions of the BBB are to protect the central nervous system (CNS) from unwanted xenobiotics and pathogens and to supply necessary nutrients to the brain (Van Tellingen et al., 2015). Water and oxygen can pass through the BBB by passive diffusion while nutrients like glucose and iron can cross the BBB with the help of several carriers such as glucose transporter 1 (GLUT1) and transferrin (Kusuhara and Sugiyama, 2005; Shitara et al., 2013). Interestingly, some carriers such as organic anion transporting polypeptide 1A2 (OATP1A2) and plasma membrane calcium-transporting ATPase 1 (ATP2B1) can mediate the transport of some drugs and compounds in or out the brain through the BBB (Kusuhara and Sugiyama, 2005; Shitara et al., 2013). Unwanted substances, however, are excluded from the brain due to its inherent low penetration and active efflux by membrane transporters present on the endothelial cells. These membrane transporters include three ATP-binding cassette (ABC) transporters, namely P-glycoprotein (P-gp or ABCB1), multi-drug resistance related protein 1 (MRP1 or ABCC1) and breast cancer resistance protein (BCRP or ABCG2) (Figure 1.3.1B) (Cooray et al., 2002; Cordon-Cardo et al., 1989; Löscher and Potschka, 2005).

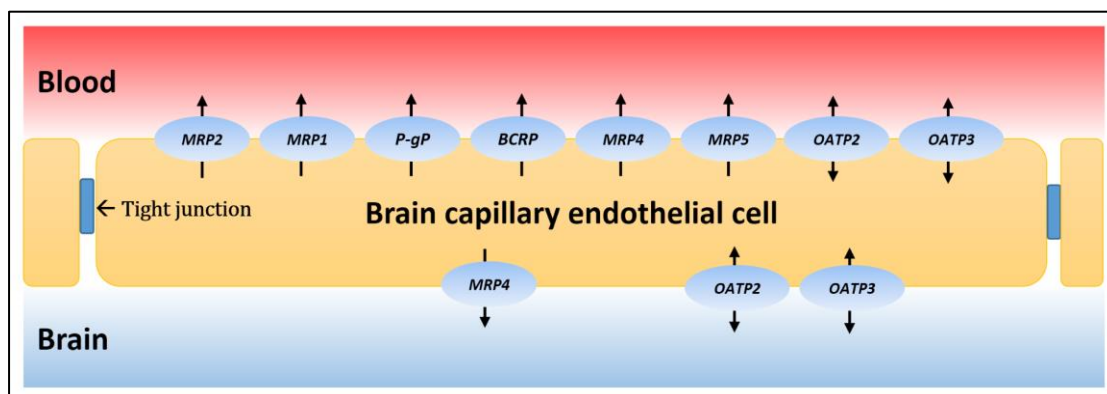


Figure 1.3.1B The model of localization of multidrug resistance transporters on brain capillary endothelial cell.

P-gp, MRPs and BCRP are the major transporters locating unidirectionally on the apical (plasma) side of the brain capillary endothelial cell which are responsible for the active efflux of compounds on BBB. Besides, there are other transporters locating on both sides of the brain capillary like organic anion transporting polypeptides (OATPs).

These membrane transporters on the BBB ensure the health, safety and stability of the environment of the central nervous system (CNS). With the protection by the BBB, brain infection from blood is extremely rare. On the other hand, if brain diseases like infection, GBM or epilepsy occur, the BBB will restrict the penetration of most antibiotics or drugs from entering the brain tissue due to the active efflux by transporters (P-gp, MRPs and BCRP) in BBB, making CNS therapy much more difficult (Raza et al., 2005; Van Dorpe et al., 2012).

1.3.2 The structure and evolution of ABC transporters

Many transporters, including glucose transporters, nucleoside transporters, amino acid transporters, oligopeptide transporters, vitamins transporters,

organic ions transporters and ATP-binding cassette transports (ABC transporters) family have been extensively studied (Dean et al., 2001). Among these transporters, P-gp and BCRP are closely associated with the active efflux process found in the BBB (Goldstein et al., 1992; Krishna and Mayer, 2000; Raza et al., 2005).

P-gp, MRP1 and BCRP belong to the same superfamily of ABC transporters. They have similar functional domains but contribute to different distinct physiological functions. P-gp, MRPs and BCRP are responsible for multi-drug resistance (MDR) in many types of cancer cells through their ATP-dependent drug efflux activity (Figure 1.3.2).

One of the major function of ABC transporters is ABC-dependent efflux of substances out of the cell. Besides active efflux, ABC-transporters are also involved in the absorption and accumulation of many compounds, and play an important role in body defense by actively removing xenobiotics in liver, small intestine and placenta (Childs and Ling, 1994; Higgins, 1992).

ABC transporters can be found in both animals and plants. Out of the 56 ABC transporters identified, 48 are present in human. They are divided into seven subtypes (ABCA~ABCG). ABCB1, ABCC1 and ABCG2 proteins are involved in the MDR of cancer cells (Dean et al., 2001).

There are 12 ABCA subfamily members in human; 7 in zebrafish. The ABCB subfamily was found only in vertebrates; 11 ABCB genes have been found in human; 12 in rats and mice and 9 in zebrafish. P-glycoprotein (P-gp, ABCB1)

is the first ABC transporter found in human. ABCC subfamily contains 12 complete transporters with the function of an ion transporter, cell surface receptor and has toxin secreting activity. Some ABCC family members are organic anion transporter (OAT). ABCD, ABCE and ABCF genes are so conserved in mammals and zebrafish that the number of gene is constant: 4 for ABCD, 1 for ABCE and 3 for ABCF (except for mouse, which is 4). ABCG subfamily has 5 members, wherein ABCG2 (BCRP) gene is important in multi-drug resistant (Lander et al., 2001; Venter et al., 2001). ABCH is the least understood subfamily. Only one gene, Abch1, was found in zebrafish and blowfish but not in mice or human.

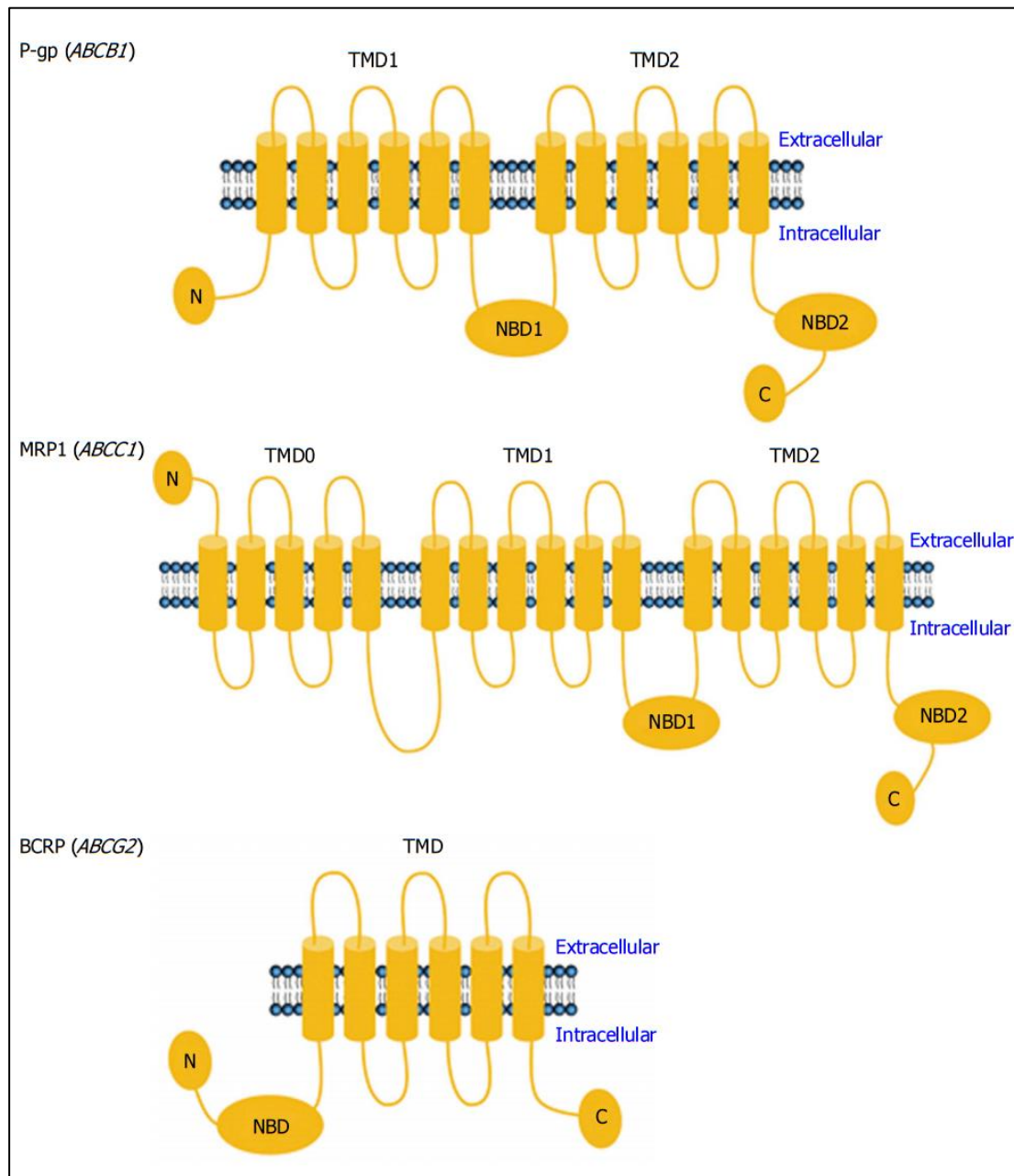


Figure 1.3.2 The model of P-glycoprotein (P-gp), multi-drug resistance related protein 1 (MRP1) and breast cancer resistance protein (BCRP).

P-gp, MRP1 and BCRP are typical ABC transporters responsible for multi-drug resistance (MDR) in cancer cells. Generally, ABC transporters are composed of transmembrane domains (TMDs) and nucleotide binding domains (NBDs). The figure is adopted from (Hu, Li et al. 2016).

1.3.2.1 The general structure of ABC transporters

The general structure of ABC transporters is similar. They are composed of dimer or monomer. Each monomer contains transmembrane domain (TMD) and nucleotide binding domain (NBD). P-gp is pseudo-dimeric in structure, i.e. it has two TMDs and two NBDs. It remains controversial whether BCRP works as a dimer or monomer, or both (Hyde et al., 1990; Ogura et al., 2015). The TMD is formed by six transmembrane alpha helices. It makes a transmembrane channel to transport the substrates, and also participates in the recognition of substrates. The NBD is made up of highly conserved Walker A, Walker B and Walker C, an ABC transporter specific binding site. Walker C is a specific structure of ABC transporters. The NBD is involved in nucleotide binding and hydrolysis, which provides energy to ABC transporters (Figure 1.3.2).

1.3.2.2 The structure of P-glycoprotein (P-gp, ABCB1)

P-glycoprotein (P-gp), encoded by ABCB1 (also known as MDR1) gene, is a functional transmembrane transporter using the energy from ATP hydrolysis to pump drugs outside the cell. Substrates include hydrophobic drugs such as vinblastine, anthracycline, etoposide and paclitaxel (Ferreira et al., 2012). Interestingly, purified P-gp proteins are not able to bind vinblastine while P-gp on membrane is able to, indicating P-gp function is associated with the structure of membrane. Expression level of P-gp is different from tissue to tissue. For example, P-gp is highly expressed in the brain, liver, adrenal, and testis tissue,

while it is expressed moderately in the lungs, stomach, pancreas and kidney. For ovaries, thymus and marrow, expression level of P-gp is very low or even absent (Ferreira et al., 2012; Thiebaut et al., 1987).

Overexpression of P-gp transporter is a classic mechanism of MDR of cancer cells. It is also the most widely-studied mechanism of drug resistance (Nielsen and Skovsgaard, 1992). In 1976, Juliano RL and Ling V found that P-gp was amplified in colchicine-resistant Chinese hamster ovary (CHO) cell line (Reeve et al., 1987). P-gp is composed of 1280 amino acid residues, and its molecular weight is 170 kD.

N-terminal and C-terminal halves of P-gp are similar to each other in structure. Both halves have a TMD and a highly conserved NBD. The TMD of N-terminal is located between residues 50 to 350, while the NBD of N-terminal is located at residues 426 - 433 / 541 - 551. The TMD of C-terminal is located between residues 700 to 1000, while the NBD of C-terminal is located at residues 1068 – 1075 / 1184 - 1196. P-gp has eight N-terminal glycosylation sites located at residues 14, 73, 91, 96, 103, 702, 887 and 998, respectively (Figure 1.3.2) (Aller et al., 2009; Dean et al., 2001; Ueda et al., 1987).

1.3.2.3 The structure of multidrug resistance related proteins (MRPs, ABCCs)

The ABCC subfamily has 13 proteins and 9 of them have been found to be related to multidrug resistance (Chen and Tiwari, 2011). For example, MRP1 is

one of the major MRP proteins whose molecular weight is 190kD. MRP1 contains three transmembrane domains (TMD).

Two TMDs (TMD1 & TMD2) from C-terminal and two NBDs (NBD1 & NBD2) form the core structure of MRP1. Another TMD from N-terminal (TMD0) is linked to the TMD1 through the L0 Linker (Figure 1.3.2). It is believed that TMD0 (amino acid residue 1 to 203) has nothing to do with MRP1 function because MRP1 without TMD0 still presents the same activity as the wild type MRP1. The L0 linker (amino acid residue 204 to 281) may be an important structure which is necessary for MRP1 to transport substrates (Cole et al., 1992).

MRP1-mediated drug efflux is associated with the presence of glutathione (GSH). GSH regulates MRP1 mediated drug transport. The mechanism of MDR induced by MRP1 is probably due to MRP1's efflux of the drugs-GSH complex (Cole et al., 1992; Cole and Deeley, 1993).

So far, the cancers reported to be related to MRP1 include leukemia, multifocal myeloma, stomach cancer, esophageal cancer, breast cancer, lung cancer, fibrosarcoma, neuroblastoma and cervical cancer. Besides pumping out drugs, MRP1 can also induce MDR by changing the intracellular drug distribution. It has been reported that in cells with high expression of MRP1, anthracycline is concentrated in regions out of the nucleus and cytoplasm but not in the nucleus. MRP1 exists widely in normal human body as GS-X pump. It is mainly distributed in the cytoplasm and is slightly expressed on the plasma membrane. A normal expression level of MRP1 helps to maintain the function of body while

an abnormal expression may lead to MDR (Basselin et al., 1996).

MRP2 is responsible for platinum resistance and is mainly expressed in liver cells and renal epithelial cells. MRP2 can mediate the secretion of a variety of organic anions. MRP2 may play a role different from that of MRP1 because most substrates of MRP2 are inhibitors of MRP1.

MRP3 is mainly expressed in the liver, intestine and adrenal gland and is slightly expressed in other tissues. In the liver, MRP3 is concentrated in epithelial cells, and moderately expressed in liver cells. Substrates of MRP3 are different from those of MRP1 and MRP2. MRP3 is not able to transport GSH, but is specific to cholate in liver (Basselin et al., 1996; Begley, 2004; Cole et al., 1992; Cole and Deeley, 1993).

1.3.2.4 The structure of breast cancer resistance protein (BCRP, ABCG2)

Breast cancer resistance protein (BCRP), also known as MXR-1, is encoded by ABCG2 gene which belongs to the ABCG subfamily. BCRP monomer is 70 kD in size and contains one TMD and one NBD. It is widely reported that BCRP works as a homodimer (Allikmets et al., 1996; Doyle et al., 1998). For example, BCRP migrates at 70 kDa in reducing condition, but at 140 kDa in non-reducing condition, suggesting that BCRP dimerize via a cysteine linkage. Moreover, mutated BCRP-15 with defective disulfide linkage does not confer drug resistance, suggesting that BCRP works as a dimer through disulfide bond to

mediate drug resistance [98]. However, it has also been reported that formation of homodimer, which is linked by covalent bridge between BCRP monomers, may not be necessary for BCRP function (Shigeta et al., 2010).

BCRP exists in normal human organs such as the placenta, bile duct, colon, intestine, and brain capillaries. Placental BCRP may protect the fetus. It also protects against poisonous compounds (Vlaming et al., 2009). BCRP is capable of transporting and conferring resistance to mitoxantrone, topotecan, doxorubicin, daunorubicin but not to vincristine, paclitaxel or cisplatin. Both acute granulocytic leukemia and acute lymphocytic leukemia show high levels of BCRP expression (Doyle et al., 1998; Vlaming et al., 2009).

1.3.3 ABC transporters in BBB

While cancer cells overexpress ABC transporters to pump out the anti-cancer drugs for self-protection, endothelial cells of the BBB overexpress ABC transporters on the capillaries lumen to prevent compounds from crossing the BBB. Modulators originally designed to inhibit P-gp and BCRP, for reversing MDR in cancers, may also can be used to facilitate drug penetration through BBB.

This concept stems from the observation that both Bcrp and P-gp knockout mice accumulated more sorafenib, with Bcrp being more important. Surprisingly, P-gp and BCRP double knockout mice accumulated disproportionately higher amounts of sorafenib than either P-gp- or BCRP-single knockout mice (Lagas

et al., 2010a; Lagas et al., 2010b). This result suggested that sorafenib is a stronger substrate of BCRP than P-gp (Agarwal et al., 2011). Coincidentally, trans-epithelial study using MDCKII cells transfected with human P-gp and BCRP as a model of BBB demonstrated that both P-gp and BCRP can transport sorafenib, topotecan and sunitinib, although mouse Bcrp is the major transporter responsible for restricting sorafenib penetration. The highest level of sorafenib accumulation in brain was obtained only when both mouse p-gp and bcrp were inhibited by a dual inhibitor elacridar (GF120918) (Lagas et al., 2010a; Poller et al., 2011b).

Neither monospecific BCRP inhibitor nor monospecific P-gp inhibitor can increase the brain concentration of sorafenib to a level found in P-gp and BCRP double knockout mice. On the other hand, GF120918 (a dual inhibitor of P-gp and BCRP) can increase the brain level of several TKIs, which is better than PSC833 (a well-known P-gp specific inhibitor) or Ko143 (a well-known BCRP specific inhibitor). GF120918, however, is too toxic to use. More potent and non-toxic dual selective inhibitors of P-gp and BCRP are needed (Agarwal et al., 2011; Lagas et al., 2010b; Poller et al., 2011a; Polli et al., 2009).

1.3.4 Flavonoid dimers can reverse multidrug resistance (MDR)

It has been reported by our research group that flavonoid dimers have potent, safe and specific modulating activity for P-gp, MRP1 and BCRP (Chan et al., 2012; Chan et al., 2006; Chan et al., 2009; Yan et al., 2015). Flavonoid dimers

were synthesized by joining two flavonoid moieties together using a biocompatible polyethylene glycol (PEG) linker (Figure 1.3.4). Safety is one advantage of flavonoid dimers as they are composed of two naturally-occurring flavonoid moieties. Another advantage of flavonoid dimer is their high hydrophobicity, which can promote the binding affinity between flavonoid dimers and ABC-transporters in the BBB.

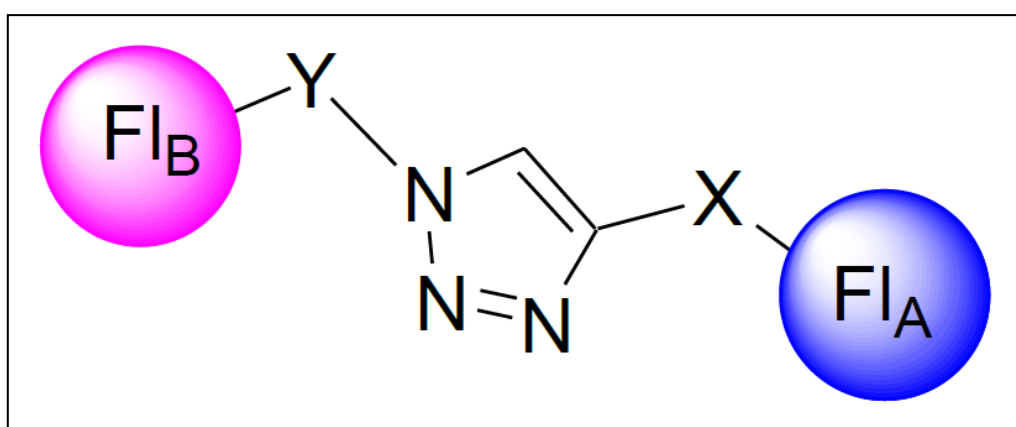


Figure 1.3.4 The general structure of flavonoid dimer.

Two flavonoids are linked together by an azide linker. Sub linker X and Y could be same or different. If the two flavonoids are same, then the dimer is called homo dimer. If the two flavonoids are different, then the dimer is called hetero dimer.

Different flavonoid dimers have different specificities to particular transporters. Some are specific to P-gp, some to MRPs, and some to BCRP. Moreover, some flavonoid dimers have been found to be specific to more than one transporters. The dual or triple selectivity of some flavonoid dimers make them ideal for facilitating drugs across the BBB since many anti-cancer drugs can be transported by more than one transporters.

Section 1.4 Objectives and rationales of study

The major objective of this project is to discover a TKI that can be used to treat GBM. The choices and effect of chemotherapy treatment to GBM are limited. As a standard treatment for GBM patients, TMZ is normally used along with radiotherapy after surgical resection. Although TMZ exhibits a powerful inhibitory effect to newly-diagnosed GBM patients, GBM relapse and TMZ resistance occurs quite often in GBM patients (Lee, 2016; Nagasawa et al., 2012). Recurrent GBM patients cannot benefit any more from TMZ. A novel chemotherapy treatment for GBM is urgently needed. TKIs are an important kind of anti-cancer drugs which are used to treat many different cancers. None of TKIs is used for GBM so far, though TKIs has the potential to be used in treating many other cancers because of its multi-kinase inhibitory activities, which is different from that of TMZ. For example, sorafenib has been tried in treating GBM and exhibit extraordinary potency in killing GBM cells in vitro (Jakubowicz-Gil et al., 2014b), but has failed in clinical trials. It has been demonstrated that sorafenib is a substrate of P-gp and BCRP in pharmacokinetic studies in Balb/c mice and in knocked out mice (Lagas et al., 2010a; Lagas et al., 2010b).

Second objective of this project is to identify a flavonoid dimer with both P-gp and BCRP modulating activity from a newly synthesized triazole-linked flavonoid dimers library. As mentioned before, sorafenib is a substrate of P-gp and BCRP, therefore, inhibiting P-gp or BCRP alone is not enough to increase

the accumulation of sorafenib in brain. A dual modulator for both P-gp and BCRP is needed. It is suggested that P-gp and BCRP work together in a synergistic manner to limit the penetration of TKIs. An inhibitor which can inhibit both P-gp and BCRP will be ideal for improving the penetration of TKIs passing through BBB.

This project also aims to establish an orthotopic GBM model in nude mice. Compared to subcutaneous xenograft model, orthotopic xenograft model can provide a similar kind of tissue microenvironment similar to that of patient. Since GBM is protected by the BBB, an orthotopic model is needed to mimic the limited distribution of cancer drugs by BBB.

This study also tries to understand the *in vivo* efficacy of the combination of candidate TKI and flavonoid dimer using the orthotopic GBM model. For proof of concept, the efficacy study of candidate TKI in treating orthotopic GBM will be carried out in the presence or absence of selected flavonoid dimer.

To further expand the impact of this project, this thesis will also develop a recurrent and TMZ-resistant orthotopic GBM model in nude mice, and treat it with a combination of TKI and flavonoid dimer. Since relapse and TMZ-resistance are two major problem for GBM patients clinically, it is important to develop effective treatment for recurrent and TMZ-resistant GBM.

The long-term aim of this study is to develop novel chemotherapy treatment for GBM. Few drugs are used to treated GBM clinically due to the limitation of BBB which imposes restrictions on most of anti-cancer drugs passing through

capillaries in the brain. It is suggested that BBB restricts compounds out of brain by active efflux, and BCRP and P-gp overexpressed on BBB are responsible for such efflux. This study hypothesizes that a dual selective flavonoid dimer for both P-gp and BCRP can increase the brain penetration of sorafenib and thereby improving the effectiveness of sorafenib in treating GBM. To establish a treatment strategy by inhibiting the efflux of P-gp and BCRP to overcome the BBB may make it possible to treat GBM by using other anti-cancer drugs which are approved for other cancers in clinical use.

CHAPTER 2: METHODOLOGY

2.1 Chemicals and drugs

All TKIs, TMZ, topotecan, GF120918 and paclitaxel used in this study were pure compound in powder form, and were purchased from commercial company. PSC833 (powder) was kindly provided by Novartis. Afatinib (powder, purity > 99%), axitinib (powder, purity > 99%), gefitinib (powder, purity > 99%), lapatinib (powder, purity > 99%), erlotinib (powder, purity > 99%), temozolomide (powder, purity > 99%) and GF120918 (Elacridar; powder, purity > 99%) were purchased from MedChem Express (China), Shanghai, China. Sorafenib (powder, purity >98%), topotecan (powder, purity >98%) and paclitaxel (powder, purity > 98%) were purchased from Wuhan Hezhong Biochemical Manufacture Co, Ltd, Wuhan, China. Dulbecco's Modified Eagle Medium (DMEM), Roswell Park Memorial Institute (RPMI) 1640 medium, trypsin/EDTA acid and penicillin/streptomycin (P/S) were obtained from Gibco. Fetal bovine serum (FBS) was obtained from HyClone. All other drugs and common reagents were of high performance liquid chromatography (HPLC) grade or reagent grade and were purchased from Sigma-Aldrich.

2.2 *In vitro* studies

2.2.1 Cell lines

The passages of all cell lines used in this study were within 5 to 15 from thawing them on. L929, LCC6, LCC6MDR, HEK293, HEK293-R2, MCF7, MCF7-MX100, MDCKII-WT, MDCKII-P-gp, MDCKII-GFP-BCRP, U87MG and U87MG-RedFluc cell lines were used in these experiments. The human breast cancer cell lines LCC6 and LCC6MDR were kindly provided by Dr. Robert Clarke from Georgetown University (U.S.A.). The MDCKII-WT, MDCKII-P-gp cells were generously provided by Prof. Piet Borst (the Netherlands Cancer Institute, Amsterdam, Netherlands). MDCKII-GFP-BCRP was kindly provided by Dr. Laszlo Homolya from Semmelweis University (Budapest, Hungary). U87MG-RedFluc is a human glioblastoma cell line purchased from PerkinElmer.

2.2.2 Cell culture

L929, LCC6, LCC6MDR, 2008MRP1, MDCKII and MDCK subtypes were cultured in supplemented DMEM media with 10% heat inactivated FBS, penicillin (100 U/mL) and streptomycin (100 µg/mL). HEK293, HEK293-R2, MCF7 and MCF7-MX100 cell lines were cultured in supplemented RPMI media with 10% heat inactivated FBS, penicillin (100 U/mL) and streptomycin (100 µg/mL). U87MG-RedFluc cells were cultured in supplemented MEM- α media

with 10% heat inactivated FBS, penicillin (100 U/mL) and streptomycin (100 µg/mL). All cells were maintained at 37°C with 5% CO₂ in a humidified incubator (Chan et al., 2009).

2.2.3 Cell proliferation assay

LCC6MDR, HEK293-R2 or MCF7-MX100 cells were seeded in each well of a 96-well plate at a density of 4500 cells/well. A series of concentrations (a serial dilution from 1000µM to 1 µM) of anticancer drugs, including paclitaxel and topotecan, were added into wells previously seeded with cells, with different concentrations (a serial dilution from 100 µM to 0.01 nM) of modulators (verapamil, PSC833, GF120918, Ko143 or flavonoid dimer 12-9 (FD 12-9)). After 5 days of incubation at 37°C with 5% CO₂ in a humidified incubator, MTS assay was carried out to determine the percentage of survival (Chan et al., 2012). And the MTS assays were carried out as the following protocol:

1. MTS ((3-(4,5-dimethylthiazol-2-yl)-5-(3-carboxymethoxyphenyl)-2-(4-sulfophenyl)-2H-tetrazolium)) and PMS (phenazine methosulfate) solution were prepared in PBS separately prior to the experiment to a concentration of 4 mg/ml (MTS) and 0.92 mg/ml (PMS), respectively.
2. Medium in 96-well plate was discarded and another 50 µL of warm medium was added in to each well with cells and blank control wells for background subtraction.

3. 10 μL of MTS/PMS mixture (V/V=100:5) was added into each well to a final volume of 60 μL .
4. 96-well plate was placed in a 37°C chamber for incubation for 1-2 hours.
5. Absorbance was recorded at 490 nm.

2.2.4 Cytotoxicity assay

About 4,500 cells were seeded in each well of a 96-well plate with a series of concentrations (a serial dilution from 1000 μM to 1 μM) of anticancer drugs or modulators including verapamil, PSC833, GF120918, Ko143, FD 12-9 at 37°C with 5% CO₂ in a humidified incubator for 3 days. Percentage of survival was determined by MTS assay as mentioned in **2.2.3**.

2.2.5 Western blot analysis

LCC6, LCC6MDR, MCF7, MCF7-MX100, MDCKII-WT, MDCKII-P-gp, MDCKII-GFP-BCRP and U87MG-RedFluc cells were washed with PBS (phosphate buffered saline, pH 7.2-7.4) and harvested with trypsin/EDTA solution (0.15% trypsin, 0.06% EDTA), followed by centrifugation at 1,500 rpm for 5 minutes. Cell pellets were washed by PBS, and lysed with 100 μL lysis buffer (50 mM Tris-HCl pH 8.0, 150 mM NaCl, 1.0% NP-40, 0.5% sodium deoxycholate, 0.1% SDS, and 0.2 mM PMSF) for 30 minutes at 4°C. Cells were centrifuged at 14000

rpm for 10 minutes at 4°C. Supernatant was collected to measure the protein concentration by using Bio-Rad Bradford reagent.

Ten microgram cell lysate of each cell line was mixed with Laemmli's sample buffer for 10 minutes at room temperature. Samples were analyzed by SDS-PAGE followed by electroblotting. The transferred membranes were cut into two parts at the size of 55 kDa. Both parts of the membrane were incubated with 5% non-fat powdered milk (dissolved in TBST buffer: 0.05% Tween-20, 10 mM Tris, and 150 mM NaCl, pH 7.5) at room temperature for 60 minutes. The part of the membrane with a lower molecular weight was incubated with β -actin antibody (C4, mouse monoclonal, 1:3000, Santa Cruz Biotechnology) at room temperature for 60 minutes. The other part of the membrane with a higher molecular weight was incubated with P-gp antibody (D-11, mouse monoclonal, 1:1000, Santa Cruz Biotechnology) or BCRP antibody (BXP-21, mouse monoclonal, 1:3000, Santa Cruz Biotechnology) at room temperature for 60 minutes. After the incubation with primary antibodies, all membranes were washed with TBST buffer three times, followed by incubation with a secondary antibody (Goat anti-mouse, 1:3000, IgG HRP conjugated, Santa Cruz Biotechnology) for one hour at room temperature. After three washes with TTBS for 5 to 15 minutes, signal was generated using chemiluminescent HRP substrate (Immobilon Western) and detected by Azure C600 (Azure Biosystems, Inc.) (Yan et al., 2015).

2.2.6 Immunofluorescence labeling

Sterilized circular glass coverslips (diameter = 12 mm, thickness = 0.27 mm) were placed in 24-well plates. 100,000 cells were seeded to each well with coverslip. After 24 hours of incubation (37°C with 5% CO₂ in a humidified incubator), cells were rinsed with PBS. Cells on the coverslips were fixed with 4% paraformaldehyde in PBS for 15 minutes at room temperature, followed by washes with PBS for three times (5 minutes for each time). Non-specific binding was blocked by incubation with 3% bovine serum albumin (BSA) and 0.1% Triton X-100 in PBS (W/V) for 30 minutes at room temperature. After aspirating the blocking solution (Bovine Serum Albumin (BSA) and 0.1% Triton X-100 in PBS (W/V)), cells were incubated with primary antibodies (D-11 or BXP-21, 1:500 in blocking solution) at 4°C overnight, and washed with PBS three times (5 minutes for each time). Cells on the coverslips were then incubated with secondary antibodies (Alexa Flour[®] 594, 1:500 in blocking solution) for one hour at room temperature. After three washes (5 minutes for each time), cells were incubated with Hoechst dye (10 mg/ml) by dilution of 1/1500 for 10 minutes at room temperature. After washes by PBS and distilled water respectively, all coverslips were placed on kimwipes for more than 30 minutes to dry. One drop of FluorSave Reagent (CALBIOCHEM) was placed on the coverslip, and put up-side down the coverslip on a slide to seal the edges. All these slides were stored at 4°C until use (Litman et al., 2002).

2.2.7 Confocal fluorescence microscopy studies

A Leica TCS SPE inverted microscope (lasers: 405nm, 488nm, 561nm and 635nm) was used to study the expression and localization of P-gp or BCRP in MDCKII cells. Laser of 405 nm was used to excite Hoechst dye, 488 nm for GFP and 561 nm for Alexa Fluor® 594 (secondary antibody of D-11 and BXP-21). Image processing was done on the Leica Application Suite X (LAS X) control software.

2.2.8 Directional transport assay

About 200,000 MDCKII cells were seeded on the membrane of each well of a six-well trans-well plate (24mm diameter, 0.4µm polyester membrane, tissue culture treated; Costar, Corning, NY). The six-well plate was incubated at 37°C with 5% CO₂ in a humidified incubator for 4-5 days until a confluent tight monolayer was formed with transepithelial electrical resistance (TEER) > 200 ohm.cm² (Ω.cm²). Two different directional transport experiments may be performed: apical side-to-basal side (A-to-B) and basal side-to-apical side (B-to-A) (Figure 2.2.8).

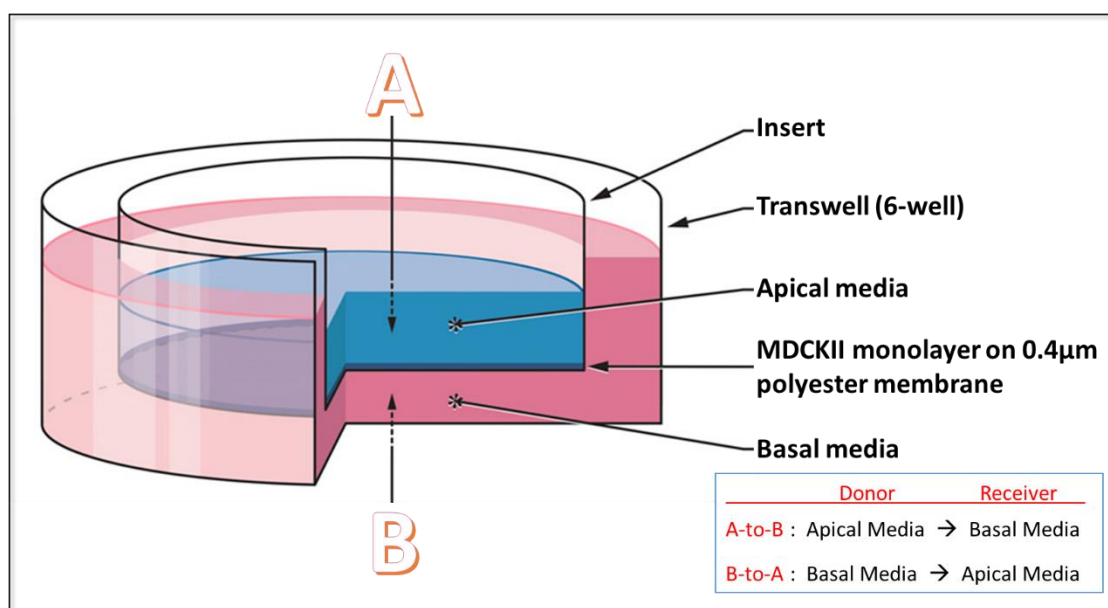


Figure 2.2.8 The trans-well model of directional transport assay.

Drugs or substrates were added in the donor side, and samples were collected in the receiver side at different time points. The concentration of drugs and substrates in the samples were measured by LC-MS/MS.

Prior to the transport assay, the monolayers were washed with warm medium. Ten µg/mL of sorafenib in the medium (total volume = 2 mL) was added to the donor side, and control medium without sorafenib was added to the receiver side. Trans-well plates were kept in incubator at 37°C with 5% CO₂. Twenty microliter of sample from the receiver compartment was collected at various time points (15, 30, 45, 60, 90, 120, 150, 180 min). For assays using inhibitors (FD 12-9 or GF120918), 1 µM of inhibitor was simultaneously added to both donor and receiver side when sorafenib was added. Samples were stored at -20°C before they were quantified (Agarwal et al., 2011).

The concentration of sorafenib was determined by liquid chromatography tandem mass spectrometry (LC-MS/MS). Samples collected were thawed first

and 20 μL of internal standard (carbanilide, 10 $\mu\text{g}/\text{mL}$) was added to each sample. One hundred and sixty microliter of methanol was added, followed by vigorous vortex for 30 seconds. After samples were left to stand for 1 minute, they were centrifuged at 7500 rpm for 10 minutes at 4°C. Supernatant was collected and filtered with a 0.22 μm pore size nylon filter. Samples were transferred into glass vials with micro-volume inserts (Agarwal et al., 2011; Chan et al., 2012; Chan et al., 2006; Chan et al., 2009).

Ten microliter of each sample was injected into a liquid chromatography system (AcQuity, Waters) by auto-sampler (4°C), separated by a BEH C18 column (2.1 X 50 mm, 1.7 μm ; AcQuity UPLC, Waters) fitted with a BEH C18 guard column (2.1 X 5 mm, 1.7 μm ; VanGuard, AcQuity UPLC, Waters). The mobile phase was composed of MilliQ water (containing 0.1% formic acid) (A) and methanol (containing 0.1% formic acid) (B). The flow rate of mobile phase was 0.3 ml/min. The gradient elution program was: 90% A / 10% B at 0 min, 90% A / 10% B at 1 min, 15% A / 85% B at 6 min, 15% A / 85% B at 7 min, 90% A / 10% B at 8 min and 90% A / 10% B at 9 min. Effluent was detected by a triple-quadrupole mass spectrometer (Waters Quattro Ultima). For data acquisition, the capillary voltage was set at 3.0 kV and the cone voltage was set at 30 V. The precursor ions of sorafenib (m/z 465) and carbanilide (m/z 213) were allowed to pass from first quadrupole (Q1) to the collision cell (Q2). Precursor ions were fragmented under a collision energy of 30 eV. Only desired product ion (daughter ion) of sorafenib (m/z 252) and carbanilide (m/z 94) were detected and recorded

through the third quadrupole (Q3). Analysis and quantification was performed using MassLynx Mass Spectrometry Software (Waters) (Agarwal et al., 2011; Yan et al., 2015).

Based on the concentration of sorafenib in the samples, the apparent permeability (P_{app}) was calculated as follows:

$$P_{app} = \frac{\left(\frac{dQ}{dt} \right)}{A \times C_0}$$

Where dQ/dt is mass transport rate of sorafenib, A is the surface area of cell monolayer which is equal to the insert membrane area (4.67 cm²), and C_0 is the initial concentration of sorafenib at the donor side (10 µg/ml) (Agarwal et al., 2011).

2.3 *In vivo* studies

2.3.1 Animals

Female Balb/c mice between 6 to 8 weeks old were used in pharmacokinetics and *in vivo* toxicity evaluation studies. Balb/c nu nu athymic mice, aged from 6 to 8 weeks weighing from 18 to 25 grams, were used in *in vivo* efficacy studies. These studies were approved by the Animal Subjects Ethics Sub-committee (ASESC) of The Hong Kong Polytechnic University. Ethics approvals by ASESC have been obtained with the following reference number: 14-15/02-ABCT-R-GRF and 15-16/82-ABCT-R-HMRF.

2.3.2 Pharmacokinetic studies of sorafenib in plasma and brain

For the pharmacokinetic studies of TKIs:

Each TKI (1.5 mg/ml) was freshly prepared using N-Methyl-2-pyrrolidone (NMP), Cremophor EL, and 5%-Tween 80 (5: 5: 90). For those treatment groups with inhibitors (FD 12-9 or GF120918), the inhibitors were prepared together with TKI in the same solution and same concentration to be co-injected to mice.

Mice were fasted for 15 hours prior to receiving different doses of TKI (10, 20 or 30 mg/kg) by tail vein intravenous (I.V.) injection with or without different inhibitors. Blood and whole brain samples were collected by cardiac puncture

and craniotomy respectively at various time points (15, 30, 60, 120, 240 and 360 min). Blood samples were centrifuged at 3000rpm for 10 minutes at 4°C to obtain plasma. Whole brains were frozen in liquid nitrogen immediately after washing in cold PBS buffer. Plasma and brain tissue samples were stored at -80°C before they were used for quantification.

On the day of analysis, plasma and brain samples collected were thawed first in room temperature. For plasma samples, 90 µL of plasma of each sample was added with 10 µL of internal standard (carbanilide, 10 µg/ml). Three hundred microliter of methanol was added, followed by vigorous vortex for 30 seconds. For brain samples, each weighed brain was added with three-fold (V/W) of ice-cold 5%-FBS-contained PBS, and homogenized by using a homogenizer. Ninety microliter of homogenized mixture was added with 10 µL of internal standard (carbanilide, 10 µg/ml). Three hundred microliter of methanol was added, followed by vigorous vortex for 30 seconds. After all samples were left to stand for 1 minute, they were centrifuged at 7500 rpm for 10 minutes at 4°C. Supernatant was collected and filtered with a 0.22 µm pore size nylon filter. Samples were transferred into glass vials with micro-volume inserts.

The concentration of sorafenib in plasma and brain was determined by liquid chromatography tandem mass spectrometry (LC-MS/MS) as described in **Section 2.2.8** (Agarwal et al., 2011; Chan et al., 2012; Chan et al., 2006; Chan et al., 2009; Yan et al., 2015).

For the pharmacokinetic studies of paclitaxel and topotecan:

Paclitaxel (1.5 mg/ml) and topotecan (1.5 mg/ml) was freshly prepared using N-Methyl-2-pyrrolidone (NMP), Cremophor EL, and 5%-Tween 80 (5: 5: 90). For those treatment groups with FD 12-9, FD 12-9 were prepared together with sorafenib in the same solution to be co-administered to mice. Mice were fasted for 15 hours prior to pharmacokinetic studies. Mice were administered with a dose of paclitaxel (80 mg/kg) or topotecan (30 mg/kg) by tail vein intravenous (I.V.) injection with or without FD 12-9 (30 mg/kg) orally (P.O.) Blood samples were collected by cardiac puncture at various time points (15, 30, 60, 120, 240 and 360 min). Blood samples were centrifuged at 3000rpm for 10 minutes at 4°C to obtain plasma. Plasma samples were stored at -80°C before they were used for quantification.

On the day of analysis, plasma samples collected were thawed first in room temperature. Ninety microliter of plasma of each sample was added with 10 µL of internal standard ([¹³C₆] paclitaxel for PTX, 10 µg/ml; tetracycline for TPT, 10 µg/ml). Three hundred microliter of methanol was added, followed by vigorous vortex for 30 seconds. After all samples were left to stand for 1 minute, they were centrifuged at 7500 rpm for 10 minutes at 4°C. Supernatant was collected and filtered with a 0.22 µm pore size nylon filter. Samples were transferred into glass vials with micro-volume inserts.

The concentration of PTX and TPT in plasma were determined by liquid chromatography tandem mass spectrometry (LC-MS/MS). Ten microliter of

each sample was injected into a liquid chromatography system (AcQuity, Waters) by auto-sampler (4°C), separated by a BEH C18 column (2.1 X 50 mm, 1.7µm; AcQuity UPLC, Waters) fitted with a BEH C18 guard column (2.1 X 5 mm, 1.7µm; VanGuard, AcQuity UPLC, Waters). The mobile phase was composed of MilliQ water (containing 0.1% formic acid) (A) and methanol (containing 0.1% formic acid) (B). The flow rate of mobile phase was 0.3 ml/min. The gradient elution program was: 90% A / 10% B at 0 min, 90% A / 10% B at 1 min, 15% A / 85% B at 6 min, 15% A / 85% B at 7 min, 90% A / 10% B at 8 min and 90% A / 10% B at 9 min. Effluent was detected by a triple-quadrupole mass spectrometer (Waters Quattro Ultima). For data acquisition, the capillary voltage was set at 3.0 kV and the cone voltage was set at 30 V. The precursor ions of paclitaxel (m/z 876), topotecan (m/z 422), [¹³C₆] paclitaxel (m/z 882) and tetracycline (m/z 445) were allowed to pass from first quadrupole (Q1) to the collision cell (Q2). Precursor ions were fragmented under a collision energy of 40, 20, 40 and 20 eV respectively. Only desired product ion (daughter ion) of paclitaxel (m/z 308), topotecan (m/z 377), [¹³C₆] paclitaxel (m/z 314) and tetracycline (m/z 410) were detected and recorded through the third quadrupole (Q3). Analysis and quantification was performed using MassLynx Mass Spectrometry Software (Waters).

2.3.3 *In vivo* toxicity studies

Twenty-four 6-8-week-old Balb/c mice were divided into six groups (n = 4 per group). Groups 1 to 6 were treated with (1) solvent control (NMP: Cremophor EL: 5% Tween-80 = 5: 5: 90), (2) sorafenib (10 mg/kg), (3) FD 12-9 (10 mg/kg), (4) sorafenib (10 mg/kg) + FD 12-9 (10 mg/kg), (5) GF120918 (10 mg/kg), and (6) sorafenib (10 mg/kg) + GF120918 (10 mg/kg) respectively. All treatments were carried out through tail vein intravenous injection (I.V.). Each group received ten injections every other day from day 0 to day 18 (QoD X 10). From day 0 onwards, all mice were monitored for toxicity symptoms like loss of weight, loss of appetite, slowness in activity, and treatment-related mortality. A weight loss of more than 15% would be considered a result of treatment-related toxicity, and such mice would be euthanized. After the last treatment, animals were monitored for ten more days to observe any toxicity response. Remaining mice were euthanized (Yan et al., 2015).

2.3.4 Orthotopic xenograft model of glioblastoma in mice

Balb/c nu nu athymic mice aged from 6 to 8 weeks old and weighing from 18 to 25 grams were purchased from Laboratory of Animal Unit (LAU) of The University of Hong Kong. Ethics approval has been obtained from the Committee on the Use of Live Animals in Teaching and Research (CULATR) of The University of Hong Kong with the reference number of CULATR 4378-17

and CULATR 4018-16. All mice were maintained in a germ-free environment with unlimited supply of sterilized food and water and a 12-hour light/dark cycle. All studies were performed in accordance with the Cap 340 Animal License of Department of Health in Hong Kong. All experiments were approved by Animal Subjects Ethics Sub-committee (ASESC) of The Hong Kong Polytechnic University. Ethics approvals by ASESC have been obtained with the following reference number: 14-15/02-ABCT-R-GRF and 15-16/82-ABCT-R-HMRF.

One hundred thousand of U87MG-RedFluc cells with luciferase marker were implanted intracranially in the striatum of each Balb/c nu nu mouse. Pre-operative skin disinfection was performed by applying iodophor (Betadine® scrub) alternating with 70% alcohol for 3 times, followed by a final soaking with a disinfectant solution (Betadine® solution) at the incision area. Under general anesthesia of ketamine (100mg/kg) and xylazine (10mg/kg), the mice were placed in a stereotactic apparatus (RWD Life Science Co., Ltd) and a burr hole was made 3mm lateral and 1mm anterior to the bregma using an electric drill (1mm diameter). Tumor cell implantation was performed using a 10- μ L Hamilton syringe with a 26-gauge needle to a depth of 3.5mm from dura. The needle was left in place for one more minute after inoculation to minimize reflux. After intracranial implantation, the burr hole was closed with bone wax, and the scalp was sutured with a size 5-0 polypropylene non-absorbable suture. Tumor-bearing mice were returned to their home cage (Baumann et al., 2012; Ozawa and James, 2010).

2.3.5 Monitoring of tumor growth by bioluminescent imaging

The size of the intracranial tumors was monitored by IVIS[®] *in vivo* imaging system (IVIS Lumina III, PerkinElmer). Four to seven days after the implantation of U87MG-RedFluc cells, the mice were anaesthetized with ketamine (100 mg/kg; i.p.) and xylazine (10 mg/kg; i.p.). When the mice were completely under anesthesia (usually 5-10 minutes after anesthesia was applied), they were placed in the imaging station of the IVIS[®] system on a heat pad (37°C). Before image acquisition, black dividers were positioned between each mouse to prevent signal interference from adjacent mice. Thirty sequential images were taken in 30 minutes after injection of D-luciferin (150 mg/kg; i.p.). The highest signal among the 30 images was taken as the BLI signal (Baumann et al., 2012; Clark et al., 2016; Ozawa and James, 2010).

2.3.6 *In vivo* efficacy studies of sorafenib on U87MG-RedFluc orthotopic xenograft glioblastoma in Balb/c nu nu mice with or without modulators

Balb/c nu nu mice with previously-implanted tumor were randomly assigned into different groups (n = 4 - 9 mice per group) to receive different treatments (1) untreated control, (2) solvent control (NMP: Cremophor EL: 5% Tween-80 = 5: 5: 90), (3) sorafenib (10 mg/kg), (4) FD 12-9 (10 mg/kg), (5) sorafenib (10 mg/kg) + FD 12-9 (10 mg/kg), (6) GF120918 (10 mg/kg), and (7) sorafenib (10

mg/kg) + GF120918 (10 mg/kg). From day 0 onwards, the tumor growth of all mice was monitored every few days by a bioluminescent *in vivo* imaging system (PerkinElmer). Bioluminescent imaging (BLI) signal of each mouse at each time point was normalized to the initial BLI signal of this mouse on day 0. At the same time, toxicity symptoms were also monitored during and after the treatments. Mice with more than 15% weight loss in three consecutive days would be euthanized. The rest of mice were euthanized when all experiments were completed.

CHAPTER 3: THE POTENTIAL OF SORAFENIB TO TREAT GBM AND THE POTENTIAL OF FLAVONOID DIMER AC12AZ9 (FD 12-9) TO MODULATE P-GP AND BCRP IN BBB

3.1 Introduction

Glioblastoma multiforme (GBM) is the most common form of brain tumor. Overall survival rate of GBM patients has not been improved for more than 30 years (1973-2004) (Barnholtz-Sloan et al., 2003; Tait et al., 2007). A few brain cancer drugs have been developed in the past four decades. The only widely-used first line drug for GBM is temozolomide (TMZ). It was approved for treating GBM together with radiotherapy in 2005 (Cohen et al., 2005). Resistance to TMZ, however, is frequently found in GBM patients. TMZ is an DNA alkylating agent which methylates DNA and triggers apoptosis of GBM cells. It is believed that TMZ resistance is mainly due to the elevated expression of O-6-methylguanine-DNA methyltransferase (MGMT), which demethylates and repairs the TMZ-induced DNA damage.

To re-sensitize GBM to TMZ, many clinical trials have been carried out but few has succeeded (Kyte et al., 2011; Narayana et al., 2012; Prados et al., 2008). There is an urgent need to develop new chemotherapeutic agents for GBM. Tyrosine kinase inhibitors (TKIs) have caught the attention of many researchers

in recent years. Different TKIs can inhibit different tyrosine kinases to suppress protein phosphorylation in different signaling pathways. In fact, many TKIs have been approved by the U.S. FDA for treating different cancers, for examples, erlotinib and afatinib for non-small cell lung carcinoma (NSCLC) (Miller et al., 2012; Zhou et al., 2011), lapatinib for breast cancer (Blackwell et al., 2010), gefitinib for breast cancer and lung cancer (Gettinger et al., 2014; Tryfonidis et al., 2016), axitinib for renal cell carcinoma (RCC) (Rini et al., 2007), and sorafenib for advanced RCC and unresectable hepatocellular carcinoma (HCC) (Kane et al., 2009; Llovet et al., 2008). Most clinical trials of using a combination of TKIs and TMZ to treat GBM did not show significant improvement (Amaravadi et al., 2007; Karavasilis et al., 2013; Prados et al., 2008; Zustovich et al., 2013). Most clinical trials used TKIs together with TMZ. In fact, some TKIs can kill GBM cells by themselves. It is possible that TKI alone can be used to treat GBM.

Although some TKIs can kill GBM cells *in vitro*, they cannot reach brain tumor *in vivo* due to BBB. It has been reported that the distribution of sorafenib in the brain is mainly limited by the P-gp and BCRP expressed on the endothelial cells present in BBB. Knockout studies in mice showed that absence of both mouse P-gp and BCRP can induce a dramatic increase of the brain-to-plasma ratio of sorafenib (Agarwal et al., 2011; de Vries et al., 2007).

Here we will investigate if flavonoid dimers can block P-gp and BCRP in the BBB to restore the accumulation of TKIs in the brain. Our research group has previously synthesized a series of flavonoid dimers that specifically modulate

P-gp or BCRP. Here, these flavonoid dimers will be tested for their effect in the pharmacokinetics of TKIs in both mice plasma and brain.

3.2 Results

3.2.1 *In vitro* cytotoxicity of several TKIs and TMZ towards U87MG-RedFluc cells

To explore the possibility of using TKIs to treat GBM, the cytotoxicity of various TKIs towards a GBM cell line U87MG-RedFluc cells was determined. Compared to TMZ, TKIs like erlotinib, afatinib, lapatinib, gefitinib, axitinib and sorafenib were more cytotoxic to U87MG-RedFluc cells (IC_{50} = 9, 6, 6, 12, 12 and 8 μ M, respectively) than TMZ (564 μ M) (Table 3.2.1). This result suggested that TKIs might be good alternatives to treat GBM.

Table. 3.2.1 The IC_{50} of different TKIs towards U87MG-RedFluc.

Cytotoxicity of TKIs against U87MG-RedFluc			
TKIs / TMZ	Clinical use (By FDA)	Molecular Weight (g/mol)	IC_{50} (μ M)
Erlotinib	Pancreatic cancer, NSCLC	393.436	9.2±0.4
Afatinib	NSCLC	485.937	5.8±2.5
Lapatinib	Breast cancer	581.058	5.9±1.8
Gefitinib	Breast cancer, Lung cancer	446.902	12.3±5.2
Axitinib	RCC	386.469	12.1±3.1
Sorafenib	Advanced RCC, Advanced primary HCC	464.825	8.0±5.7
Temozolomide	Newly diagnosed GBM, Recurrent astrocytoma	194.151	563.9±60

IC_{50} of TKIs and TMZ towards U87MG-RedFluc cells were measured by using MTS assay. TKIs listed in this table are used clinically for different kinds of cancers including breast, lung, pancreatic, kidney, liver and brain cancers as indicator. Mean±S.D. (n=3-6).

3.2.2 *In vitro* effect of FD 12-9 in modulating P-gp- and BCRP-mediated resistance in different cell lines

Flavonoid dimers were synthesized by joining two flavonoid moieties together using a biocompatible polyethylene glycol (PEG) linker (Chan et al., 2012; Chan et al., 2006; Chan et al., 2009; Yan et al., 2015). They have been demonstrated to have potent P-gp and MRP1 modulating activities. Recently, 'click chemistry' has been utilized to generate a structurally-diversified triazole-containing flavonoid dimer library. The new flavonoid monomers containing alkyne (A) and the other containing azide (B) are joined together by copper-(I)-catalysed 1,2,3-triazole formation to become a triazole-containing flavonoid dimer (C) (Figure 3.2.2A). By using different flavonoids and varying the linkers X and Y, different flavonoid dimers were obtained. These flavonoid dimers were investigated for their modulating effect on three ABC-transporters (P-gp, MRP1 and BCRP) (Figure 3.2.2B). Two flavonoid dimers were found to be specific towards BCRP only (FD 15-8 and FD 15-9) whereas four of them are dual selective towards both BCRP and P-gp (FD 5-5, FD 5-9, FD 12-5, and FD 12-9).

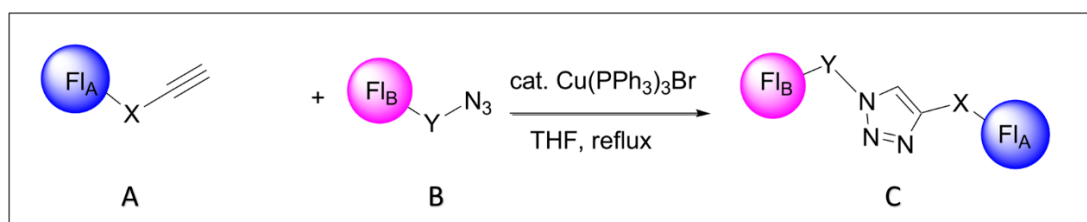


Figure 3.2.2A Synthesis of flavonoid dimers.

One flavonoid moiety contains alkyne (A) and the other containing azide (B) were joined together by copper(I)-catalysed 1,2,3-triazole formation ('click chemistry' reaction) to become triazole-linked flavonoid dimer (C). Fl_A / Fl_B = flavonoid moiety; X / Y = linker. Both Fl_A, Fl_B linker X and Y could be different, resulting in a library of triazole-linked flavonoid dimers (C).

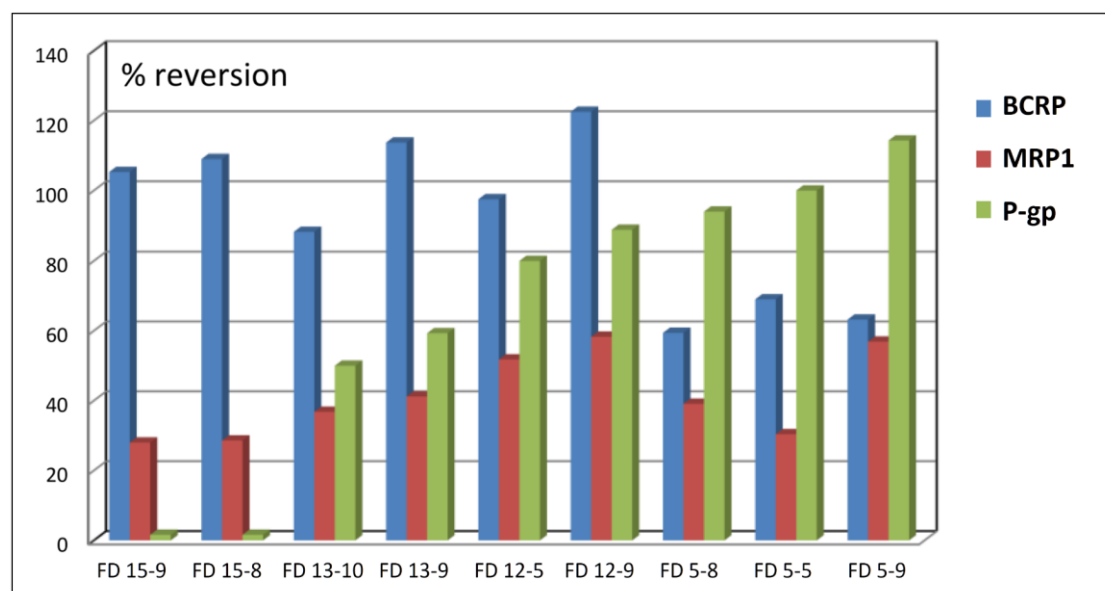


Figure 3.2.2B Modulating effect of triazole-containing flavonoid dimers towards P-gp, MRP1 and BCRP.

Cytotoxicity of 3 cell lines, namely LCCMDR (overexpressing P-gp), 2008MRP1(overexpressing MRP1) and HEK293-R2 (overexpressing BCRP) towards paclitaxel, doxorubicin and topotecan were measured with or without modulators (1 μ M). The percentage of reversion (% reversion) is defined as the ability of a modulator (1 μ M) to lower the IC₅₀ of an anti-cancer drug. All IC₅₀ were measured by MTS assay. Higher % reversion represents a more potent modulating activity.

% reversion is defined as:

$$\% \text{ reversion} = \frac{\text{IC}_{50} \text{ (without } 1\mu\text{M modulator)} - \text{IC}_{50} \text{ (with } 1\mu\text{M modulator)}}{\text{IC}_{50} \text{ (without } 1\mu\text{M modulator)}}$$

This project aims to identify a dual selective modulator towards P-gp and BCRP. FD 12-9 (Flavonoid dimer AC12AZ9, Figure 3.2.2C) exhibited extremely potent BCRP and P-gp modulating effect in a concentration of 1 μM . FD 12-9 was therefore selected as a dual selective inhibitor to determine its EC_{50} in modulating P-gp and BCRP in different cell lines (Table 3.2.2).

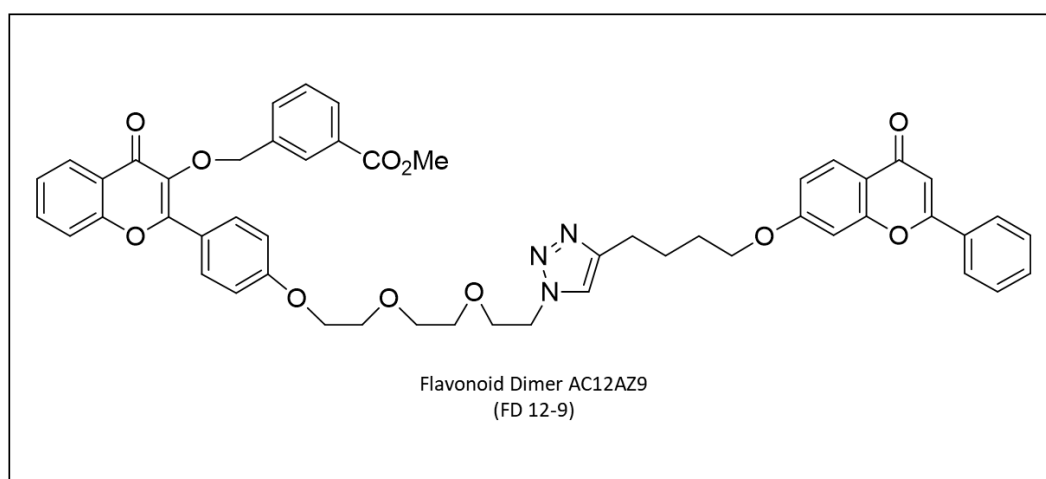


Figure 3.2.2C Chemical structure of flavonoid dimer AC12AZ9 (FD 12-9).

FD 12-9 is a hetero dimer from the flavonoid dimer library synthesized in our group. 'Click chemistry' was applied to link an alkyne-containing flavonoid moiety and a azide-containing flavonoid moiety to generate FD 12-9.

Table. 3.2.2 Effects of different compounds in modulating P-gp and BCRP mediated resistance in different cell lines *in vitro*.

Compounds	Cytotoxicity	Paclitaxel resistance	Topotecan resistance	Topotecan resistance
	of L929	of LCC6MDR	of HEK293/R2	of MCF7-MX100
	IC ₅₀ (μM)	EC ₅₀ (nM)	EC ₅₀ (nM)	EC ₅₀ (nM)
FD 12-9	>100	285.0±25.1	0.9±0.1	1.4±0.6
Verapamil	89.2±8.2	445.7±40.7	>5000	ND
PSC833	>100	2.3±0.5	2800.0±458.8	ND
GF120918	>100	1.1±0.1	20.0±7.1	47.0
Ko143	29.2±1.6	1060.0±120.1	11.4±2.4	9.0±1.5

Flavonoid dimer FD 12-9 was characterized for its P-gp modulating activity in LCC6MDR (a breast cancer cell line with overexpressing P-gp) and BCRP modulating activity in HEK293/R2 (a human embryonic kidney cell line with transfected BCRP) and MCF7-MX100 (a breast cancer cell line selected by a BCRP-specific substrate called mitoxantrone). The IC₅₀ of LCC6MDR cells towards paclitaxel (PTX), HEK293/R2 cells towards topotecan (TPT) and MCF7-MX100 cells towards TPT were measured in the presence of serial dilutions of FD 12-9 or other modulators including P-gp modulators (verapamil and PSC833), P-gp and BCRP modulator (GF120918) and BCRP modulator (Ko143). EC₅₀ is defined as the concentration of FD 12-9 or modulators needed to reduce the IC₅₀ by 50%. Toxicity of FD 12-9 towards normal mouse fibroblasts L929 was also measured. ND means the EC₅₀ is too high to determine. Mean ± S.D. (*n* = 3-6).

FD 12-9 can modulate P-gp-mediated paclitaxel resistance in P-gp-overexpressing human breast cancer LCC6MDR cells with an EC₅₀ at 285 nM. It can also reverse BCRP-mediated topotecan resistance in HEK293/R2 and MCF7-MX100 cells with EC₅₀ at 0.9 nM and 1.4 nM, respectively. HEK293/R2

cells were BCRP-transfected human embryonic kidney cells 293. MCF7-MX100 was obtained by selecting human breast cancer cell line MCF7 with 100 μM mitoxantrone, a BCRP substrate. Unlike verapamil and PSC833 which are P-gp selective or Ko143 which is BCRP-specific, FD 12-9 is dual selective towards P-gp and BCRP. FD 12-9 is about 2-fold more potent than verapamil. FD 12-9 is 12-fold more potent than Ko143. In addition, FD 12-9 was less toxic towards normal L929 fibroblasts ($\text{IC}_{50} > 100 \mu\text{M}$) than Ko143 ($\text{IC}_{50} = 29 \mu\text{M}$) or verapamil ($\text{IC}_{50} = 89 \mu\text{M}$). Even when compared with the gold standard of dual selective inhibitor of both P-gp and BCRP, elacridar (GF120918), FD 12-9 has lower EC_{50} in reversing BCRP-mediated topotecan resistance in HEK239/R2 ($\text{EC}_{50} = 0.9 \text{ nM}$ vs 20 nM) and MCF7-MX100 ($\text{EC}_{50} = 1.4 \text{ nM}$ vs 47 nM) (Table 3.2.2). All these showed that FD 12-9 is a promising dual selective inhibitor of P-gp and BCRP.

3.2.3 In vivo modulating activity of FD 12-9 on P-gp and BCRP

3.2.3.1 Effect of FD 12-9 on the oral bioavailability of paclitaxel (PTX) and topotecan (TPT) in GI tract

Although FD 12-9 can modulate P-gp- and BCRP-mediated drug resistance *in vitro*, its effect of FD 12-9 on *in vivo* drug delivery remains to be confirmed.

Here, a model that is considered to be similar to BBB was used, namely gastrointestinal tract (GI tract). In the process of oral absorption, many drugs

are kept out of the blood circulation by P-gp and BCRP located on the luminal side of intestinal epithelial cells (Estudante et al., 2013). An effective dual modulator of P-gp and BCRP is expected to increase the oral bioavailability of PTX and TPT, which are typical substrate of P-gp and BCRP, respectively.

To determine the effect of FD 12-9 in inhibiting P-gp and BCRP in GI tract, mice were orally fed with PTX, a P-gp substrate, (80 mg/kg) and TPT, a BCRP substrate, (80 mg/kg) with or without FD 12-9 (30 mg/kg). In parallel, PTX and TPT were injected intravenously to another group of mice to calculate oral bioavailability. Blood samples were collected at different time points and plasma concentrations of PTX and TPT were quantified by LC-MSMS. It was found that C_{max} of PTX was increased by 2.5-fold when PTX was co-fed with FD 12-9. T_{max} was postponed from 30 to 60 minutes. Area under curve ($AUC_{0-360min}$) and oral bioavailability of combination group (40.0%) was increased by more than 4-fold compared to PTX alone (9.1%) (Figure 3.2.3.1A, Table 3.2.3.1). Similarly, C_{max} of TPT was increased by two folds when TPT was co-fed with FD 12-9 with T_{max} remaining the same. $AUC_{0-360min}$ and oral bioavailability of TPT with FD 12-9 (14.2%) was increased by 3-fold compared to TPT alone (4.9%) (Figure 3.2.3.1B, Table 3.2.3.1). These results suggest that FD 12-9 can modulating P-gp and BCRP in the GI tract.

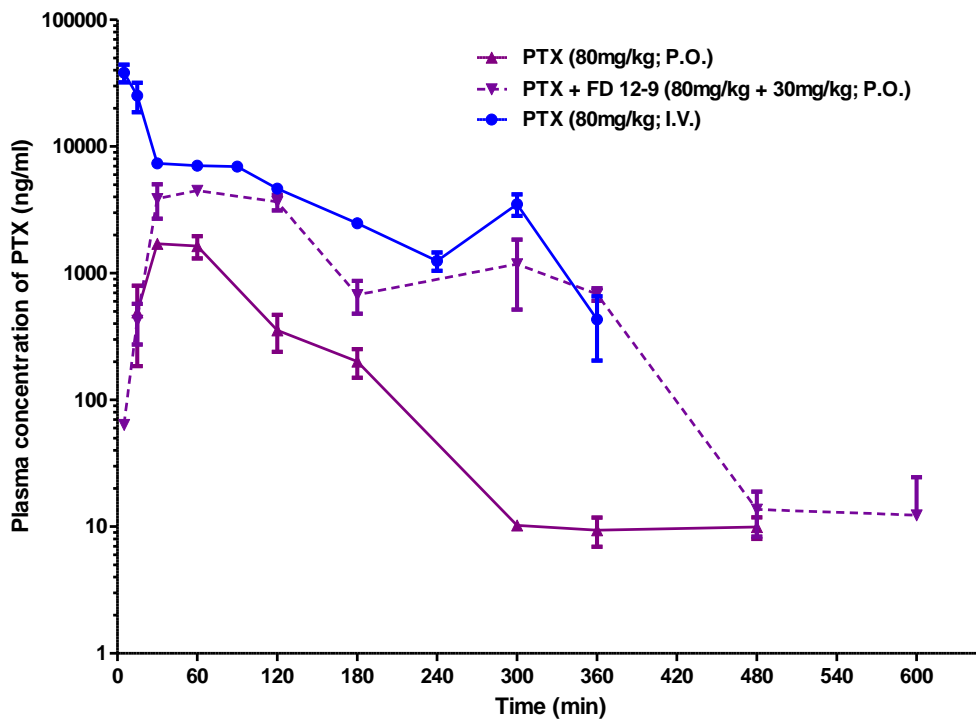


Figure 3.2.3.1A The effect of FD 12-9 on oral bioavailability of PTX.

Balb/c mice were divided into three groups and received one of following 3 treatments: oral PTX (80 mg/kg) with or without oral FD 12-9 (30 mg/kg) and intravenous PTX (80 mg/kg). Plasma PTX was measured by LC-MS/MS at different time points up to 600 minutes. Each time point had 3 Balb/c mice (n = 3).

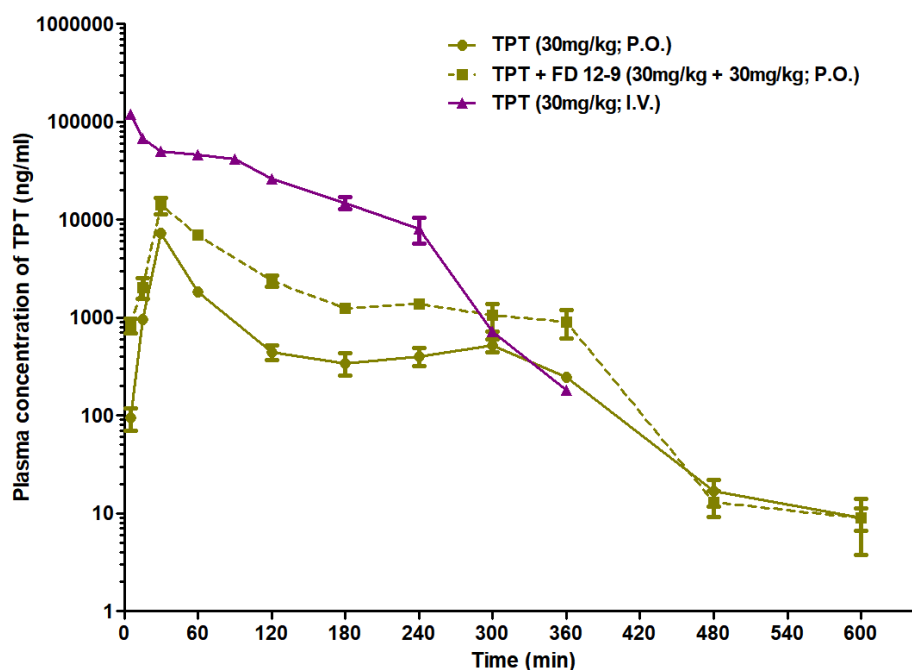


Figure 3.2.3.1B Effect of FD 12-9 on the pharmacokinetics studies of TPT. Balb/c mice were divided into three groups and received one of following 3 treatments: oral TPT (30 mg/kg) with or without oral FD 12-9 (30 mg/kg) and intravenous TPT (30 mg/kg). Plasma TPT was measured by LC-MS/MS at different time points up to 600 mins. Each time point had 3 Balb/c mice (n = 3).

Table. 3.2.3.1 Effect of FD 12-9 on the pharmacokinetics studies of PTX and TPT by oral administration *in vivo*.

Dose of PTX / TPT	mg/kg	Paclitaxel (PTX)			Topotecan (TPT)		
		80	80	80	30	30	30
Dose of FD 12-9	mg/kg	--	--	30	--	--	30
	Administration	I.V.	P.O.	P.O.	I.V.	P.O.	P.O.
AUC_{0-360min}	ng·min/ml	1,749,000	158,776	700,588	7,778,000	383,911	1,105,000
C_{max}	ng/ml	--	1,726	4,483	--	7,194	14,087
T_{max}	Min	--	30	60	--	30	30
Half-life	Min	15	80	140	20	45	60
Half-life (D/A)	Min	90	50	80	90	15	30
AUC_{0-360min}/dose	ng·min·ml ⁻¹ /(mg·kg ⁻¹)	21,863	1,985	8,757	25,927	12,797	36,833
Bioavailability	%	--	9.1	40.0	--	4.9	14.2

Plasma level of PTX and TPT from pharmacokinetic experiments shown in Figure 3.2.3.1A&B were analyzed by GraphPad Prism® 5. Bioavailability (F) was calculated by normalizing the dose-normalized AUC_{0-360min} to that oral ones.

3.2.3.2 Effect of FD 12-9 in improving the brain penetration of various TKIs

Here pharmacokinetic experiments were used to investigate whether FD 12-9 can enhance TKIs to cross BBB. Brain accumulation of 6 TKIs (erlotinib, afatinib, lapatinib, gefitinib, axitinib and sorafenib) were studied with or without co-administration of FD 12-9. The dosage of all six TKIs and FD 12-9 used in these experiments were 10 mg/kg (I.V.).

It was found that the effect of FD 12-9 was TKI-dependent. FD 12-9 has insignificant impact on modulating erlotinib and axitinib to cross the BBB (Figure 3.2.3.2A, B). On the contrary, FD 12-9 can elevate the brain concentration of afatinib, lapatinib, gefitinib and sorafenib, with the effect on sorafenib most significant (Figure 3.2.3.2C - F).

Brain levels of afatinib, lapatinib and gefitinib were still lower than their individual IC_{50} against U87MG-RedFluc cells after the enhancement effect by co-administration of FD 12-9 (Figure 3.2.3.2C - E), suggesting that the potentiation effect of FD 12-9 is not strong enough. In contrast, the increased brain concentration of sorafenib was above its *in vitro* IC_{50} against U87MG-RedFluc cells and could last for 60 minutes (Figure 3.2.3.2F) suggesting that FD 12-9 can increase the concentration of sorafenib in brain to treat GMB.

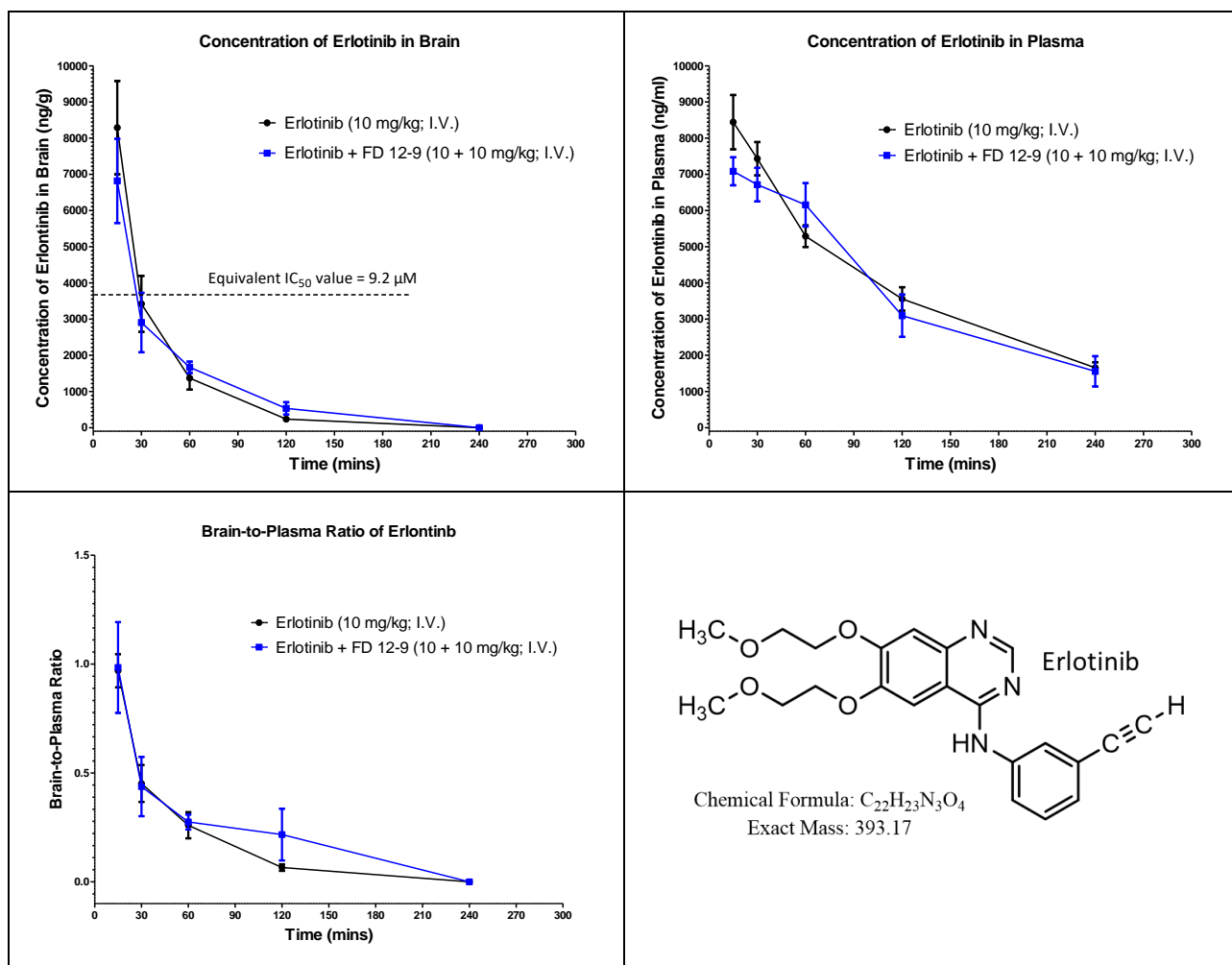


Figure 3.2.3.2A Chemical structure of erlotinib and the pharmacokinetic study of erlotinib with or without FD 12-9.

Balb/c mice were administered with 10 mg/kg of erlotinib with or without co-administration of 10 mg/kg FD 12-9. Plasma and brain concentration of erlotinib was measured by LC-MS/MS at different time points up to 240 minutes post administration. The brain-to-plasma ratio was calculated by dividing brain concentration by plasma concentration (n = 3).

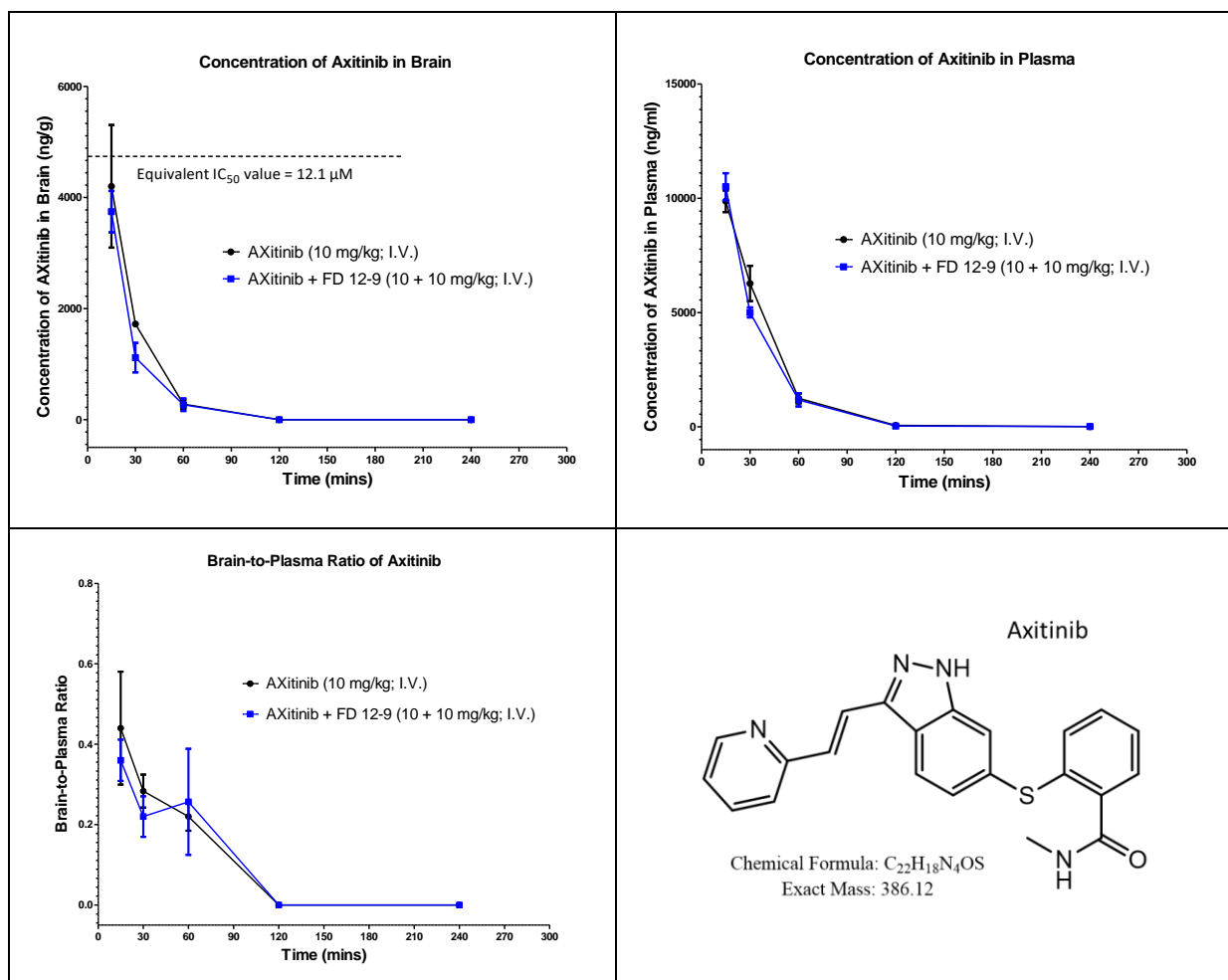


Figure 3.2.3.2B Chemical structure of axitinib and the pharmacokinetic study of axitinib with or without FD 12-9.

Balb/c mice were administered with 10 mg/kg of axitinib with or without co-administration of 10 mg/kg FD 12-9. Plasma and brain concentration of axitinib was measured by LC-MS/MS at different time points up to 240 minutes post administration. The brain-to-plasma ratio was calculated by dividing brain concentration by plasma concentration (n = 3).

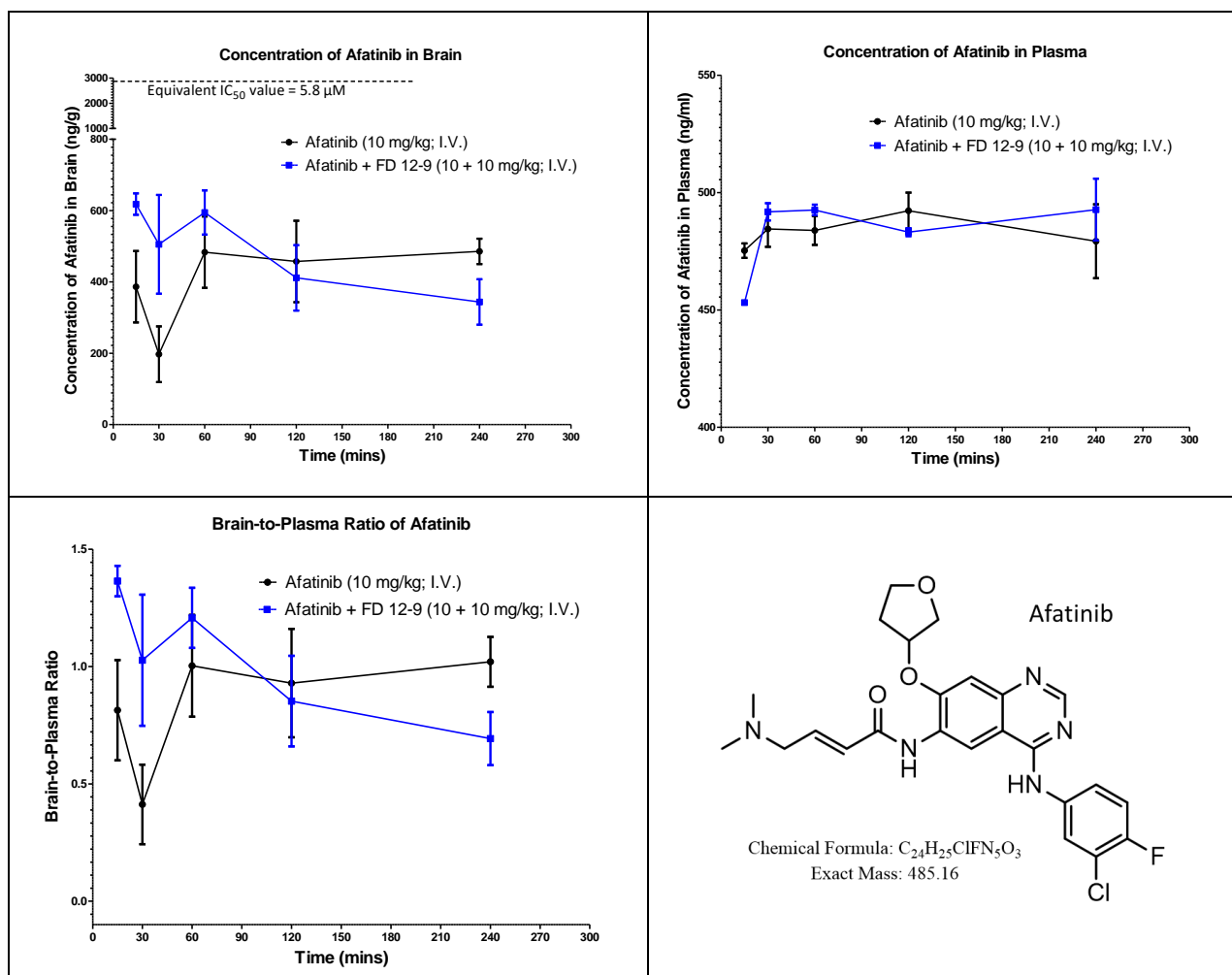


Figure 3.2.3.2C Chemical structure of afatinib and the pharmacokinetic study of afatinib with or without FD 12-9.

Balb/c mice were administered with 10 mg/kg of afatinib with or without co-administration of 10 mg/kg FD 12-9. Plasma and brain concentration of afatinib was measured by LC-MS/MS at different time points up to 240 minutes post administration. The brain-to-plasma ratio was calculated by dividing brain concentration by plasma concentration (n = 3).

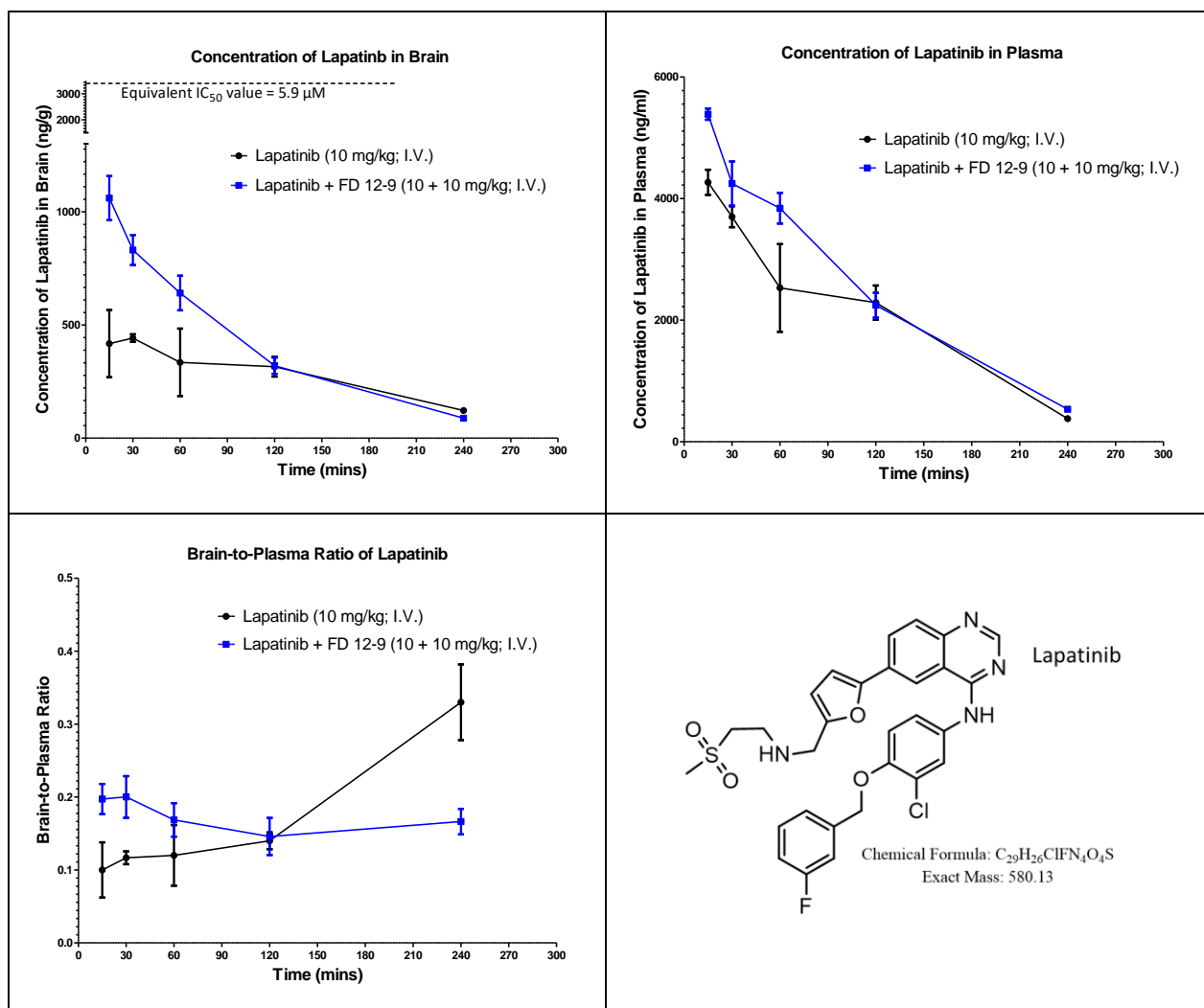


Figure 3.2.3.2D Chemical structure of lapatinib and the pharmacokinetic study of lapatinib with or without FD 12-9.

Balb/c mice were administered with 10 mg/kg of lapatinib with or without co-administration of 10 mg/kg FD 12-9. Plasma and brain concentration of lapatinib was measured by LC-MS/MS at different time points up to 240 minutes post administration. The brain-to-plasma ratio was calculated by dividing brain concentration by plasma concentration (n = 3).

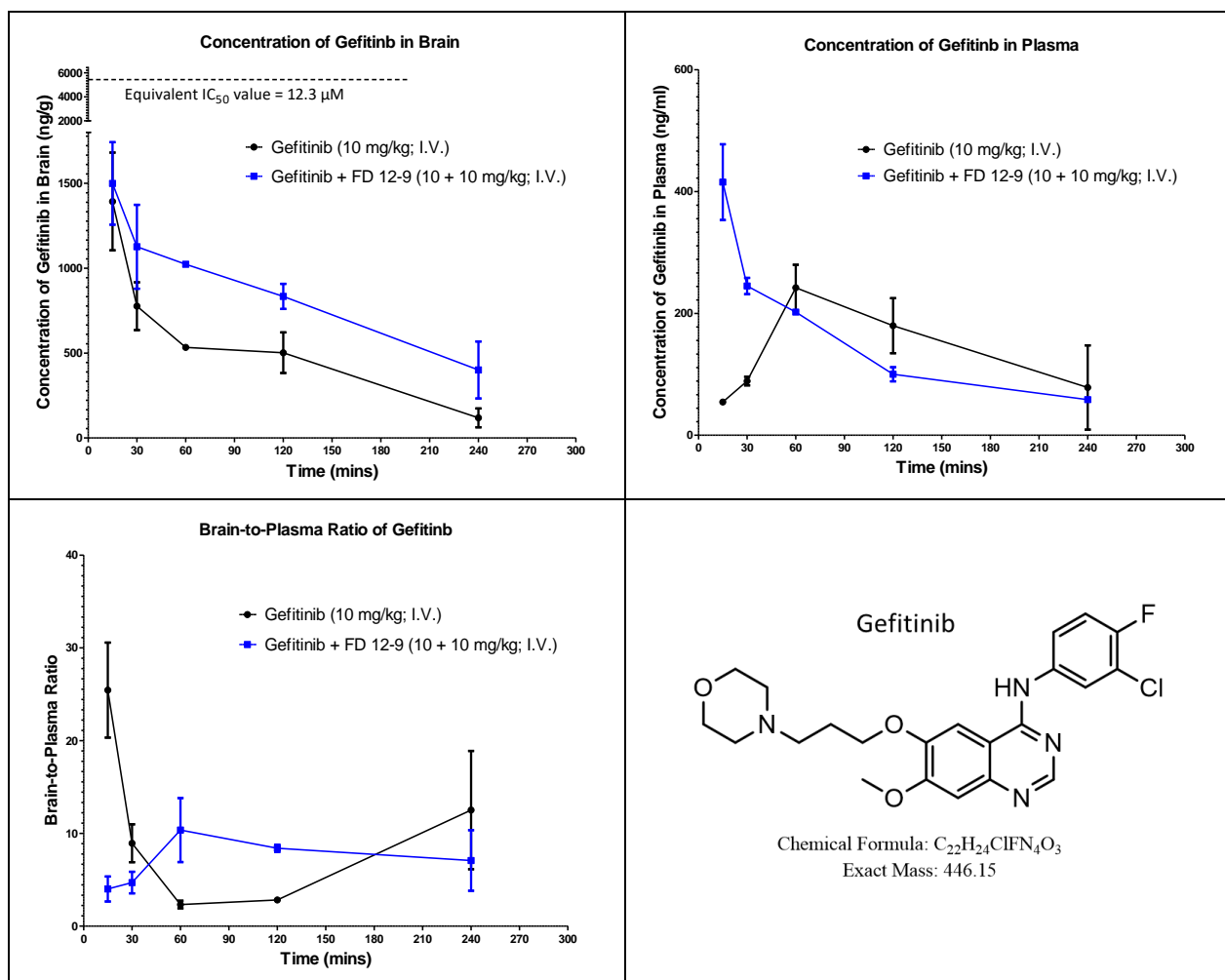


Figure 3.2.3.2E Chemical structure of gefitinib and the pharmacokinetic study of gefitinib with or without FD 12-9.

Balb/c mice were administered with 10 mg/kg of gefitinib with or without co-administration of 10 mg/kg FD 12-9. Plasma and brain concentration of gefitinib was measured by LC-MS/MS at different time points up to 240 minutes post administration. The brain-to-plasma ratio was calculated by dividing brain concentration by plasma concentration (n = 3).

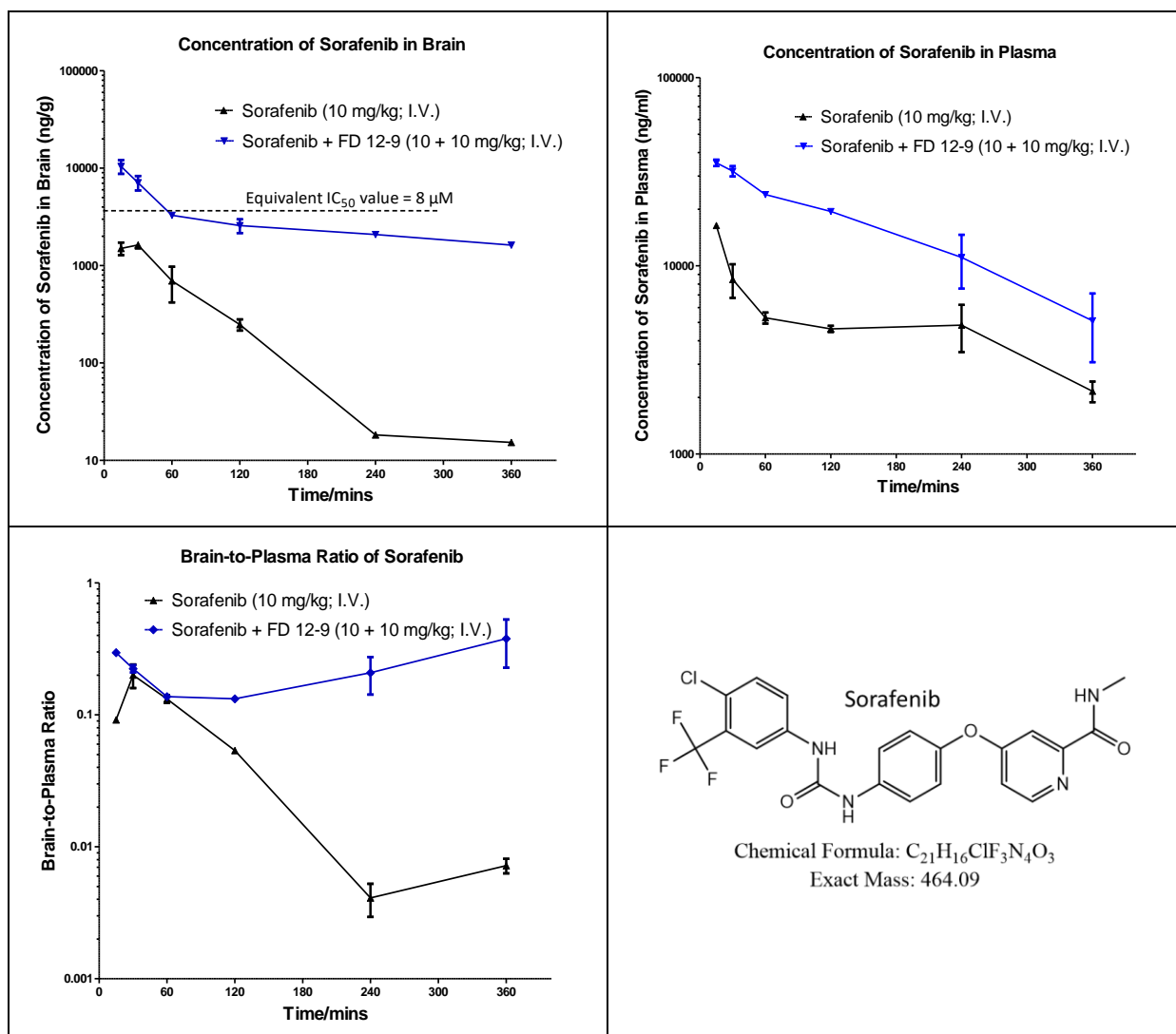


Figure 3.2.3.2F Chemical structure of sorafenib and the pharmacokinetic study of sorafenib with or without FD 12-9.

Balb/c mice were administered with 10 mg/kg of sorafenib with or without co-administration of 10 mg/kg FD 12-9. Plasma and brain concentration of sorafenib was measured by LC-MS/MS at different time points up to 240 minutes post administration. The brain-to-plasma ratio was calculated by dividing brain concentration by plasma concentration (n = 6).

3.3 Summary

The above results suggested that the *in vitro* cytotoxicity activity of TKIs against GBM cell line U87MG-RedFluc cell was better than TMZ, suggesting that TKIs might be used to treat GBM.

FD 12-9 can modulate P-gp and BCRP-mediated drug resistance in three cell lines including LCC6MDR, HEK293/R2 and MCF7/MX100. FD 12-9 is highly potent against BCRP with EC_{50} of 0.9 to 1.4 nM and moderately potent against P-gp with EC_{50} of 285 nM. It is also non-toxic to L929 fibroblasts with $IC_{50} > 100$ μ M. These properties compare favorably against the gold standard dual inhibitor of P-gp and BCRP, elacridar (GF120918).

Among six TKIs tested, sorafenib was most sensitive to the modulating effect of FD 12-9 in pharmacokinetic experiments. FD 12-9 can increase the brain concentration of sorafenib significantly and such increased brain level of sorafenib can be maintained above its *in vitro* IC_{50} (8.0 μ M) by 60 minutes. This encouraging data suggesting that sorafenib in combination with FD 12-9 might be effective in treating GBM model *in vivo*. Further pharmacokinetic studies on different doses of sorafenib with or without different modulators would be discussed in another chapter.

CHAPTER 4: TRANS-EPITHELIAL MOVEMENT OF SORAFENIB IN MIMIC BBB MODEL USING MDCKII CELLS OVEREXPRESSING P-GP OR BCRP

4.1 Introduction

To mimic the BBB for *in vitro* studies, different models have been tried including bovine, porcine or rat brain micro vessel from brain tissue (Culot et al., 2008; Nakagawa et al., 2009; Zhang et al., 2006), Madin-Darby canine kidney (MDCK) cells transfected with human P-gp (Agarwal et al., 2007; Wang et al., 2013) and Caco-2 cells model (Lundquist et al., 2002). Among these models, brain capillary models are too costly to maintain. Whereas, MDCK cells and Caco-2 cells are readily available and easy to maintain.

MDCK is a dog renal epithelial cell line. MDCK cells have been used to mimic different trans-epithelial models (Agarwal et al., 2007; Hansson et al., 1986; Pan et al., 2010; Wang et al., 2013). They can form a confluent and tight monolayer with electrical resistance of 100 ohm/cm² in 3 - 4 days, which is much shorter than another intestinal mucosa model, Caco-2 cells (around 21 days) (Sambuy et al., 2005).

Here, we have employed 3 MDCKII models, namely MDCKII-GFP-BCRP, MDCKII-P-gp and MDCKII-WT cells, to mimic directional transport of sorafenib

in the BBB. The effect of FD 12-9 on such transport was also studied.

4.2 Results

4.2.1 Expression level and localization of P-gp and BCRP in MDCKII-P-gp and MDCKII-GFP-BCRP cells

Among the three MDCKII cell lines used, P-gp and BCRP are overexpressed in MDCKII-P-gp and MDCKII-GFP-BCRP, respectively. MDCKII-WT is untransfected control. To confirm the expression level and the localization of P-gp and BCRP in these three cell lines, both western blot and confocal microscopy were used.

Western blot results indicated that the MDCKII-P-gp cells overexpressed P-gp at a level similar to that of LCC6-MDR cells, a human breast cancer cell line transfected with P-gp (Figure 4.2.1A, top panel). MDCKII-WT, MDCKII-GFP-BCRP and U87MG-RedFluc, as well as LCC6, showed very low expression of P-gp (Figure 4.2.1A, top panel). MDCKII-GFP-BCRP cells are MDCKII cell line transfected with GFP-BCRP fusion. Expression of GFP-BCRP fusion or BCRP was confirmed by western-blot (Figure 4.2.1 bottom panel). Expression level of BCRP in MDCKII-GFP-BCRP was even higher than that of a mitoxantrone-selected MCF7-MX100 cell line which is known to be expressing BCRP (Figure 4.2.1A, bottom panel).

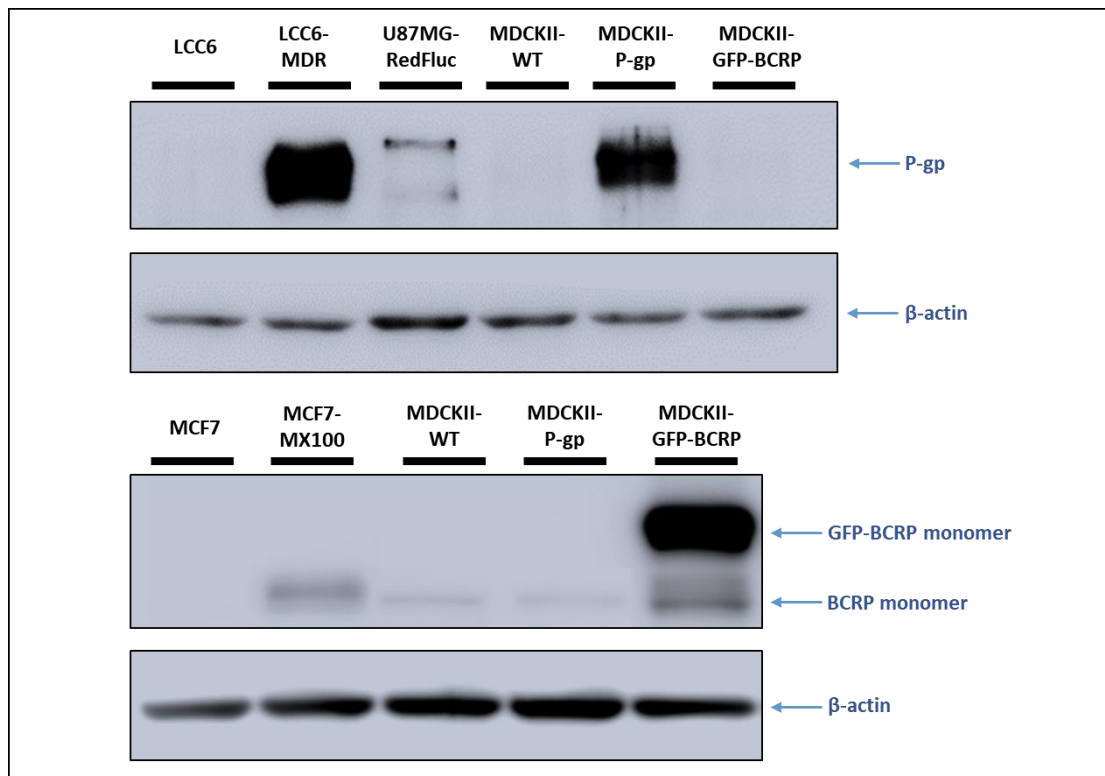


Figure 4.2.1A Expression level of P-gp and BCRP in MDCKII-WT, MDCKII-P-gp and MDCKII-GFP-BCRP cells.

The expression level of P-gp and BCRP in MDCKII-WT, MDCKII-P-gp and MDCKII-GFP-BCRP cells were characterized by western-blot. LCC6 is a human breast cancer cell line, and LCC6-MDR is a P-gp-transfected LCC6 cell line. U87MG-RedFluc is a human glioblastoma cell line. MCF7 is a human breast cancer cell line and MCF7-MX100 is a mitoxantrone selected MCF7 cell line known to overexpress BCRP.

Confocal microscopy results showed that P-gp and BCRP are mainly overexpressed on the surface of MDCKII-P-gp and MDCKII-GFP-BCRP cells, respectively. GFP signal was colocalized with BCRP (Figure 4.2.1B & C).

The above result confirmed that P-gp and BCRP are expressed in MDCKII-P-gp and MDCKII-GFP-BCRP cells and they are localized in the expected cell surface location: plasma membrane.

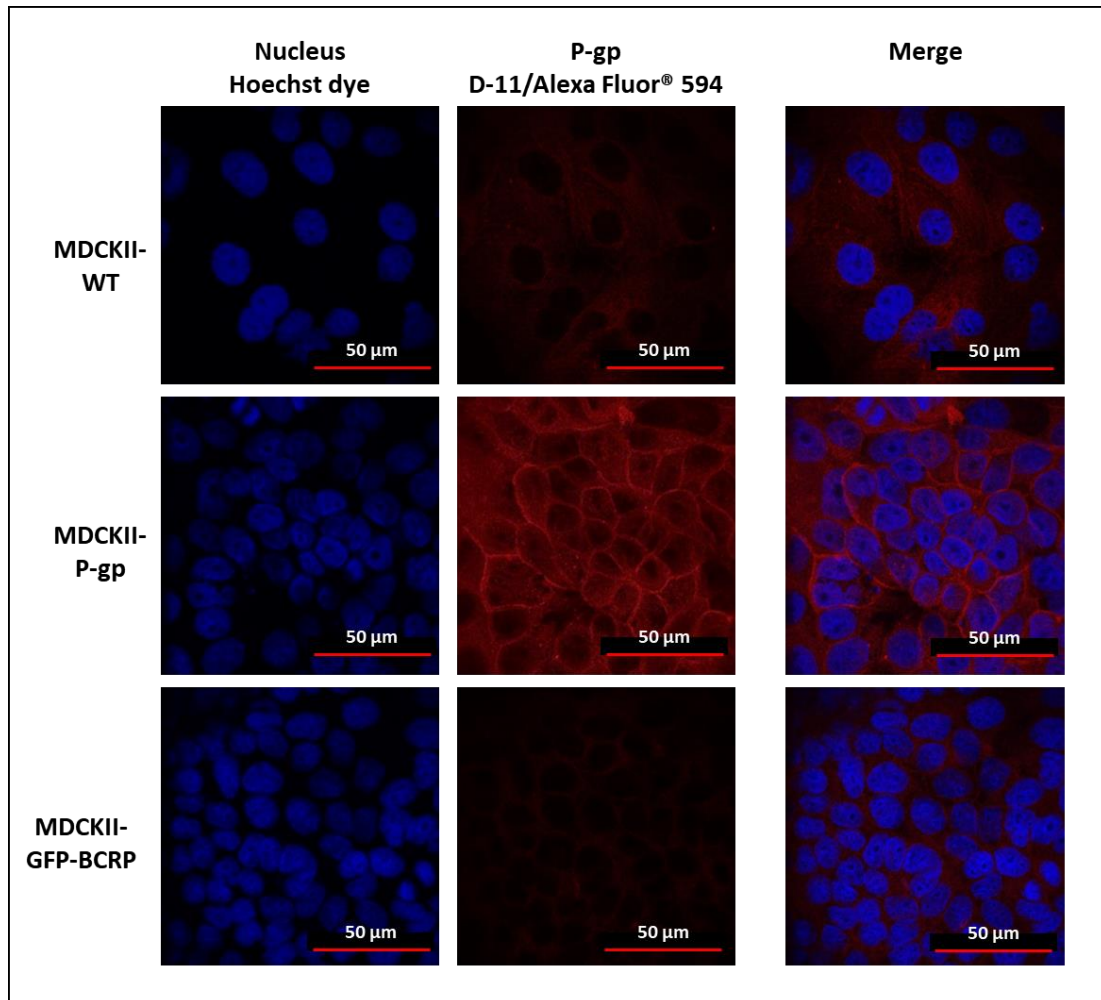


Figure 4.2.1B Expression level and localization of P-gp in different MDCKII cells.

Expression and localization of P-gp in MDCKII cells was detected by confocal microscopy. Nucleus was stained with Hoechst dye (Blue); P-gp was detected by monoclonal anti-mdr-1 (D-11), followed by an Alexa Fluor® 594 donkey anti-mouse IgG secondary antibody (Red).

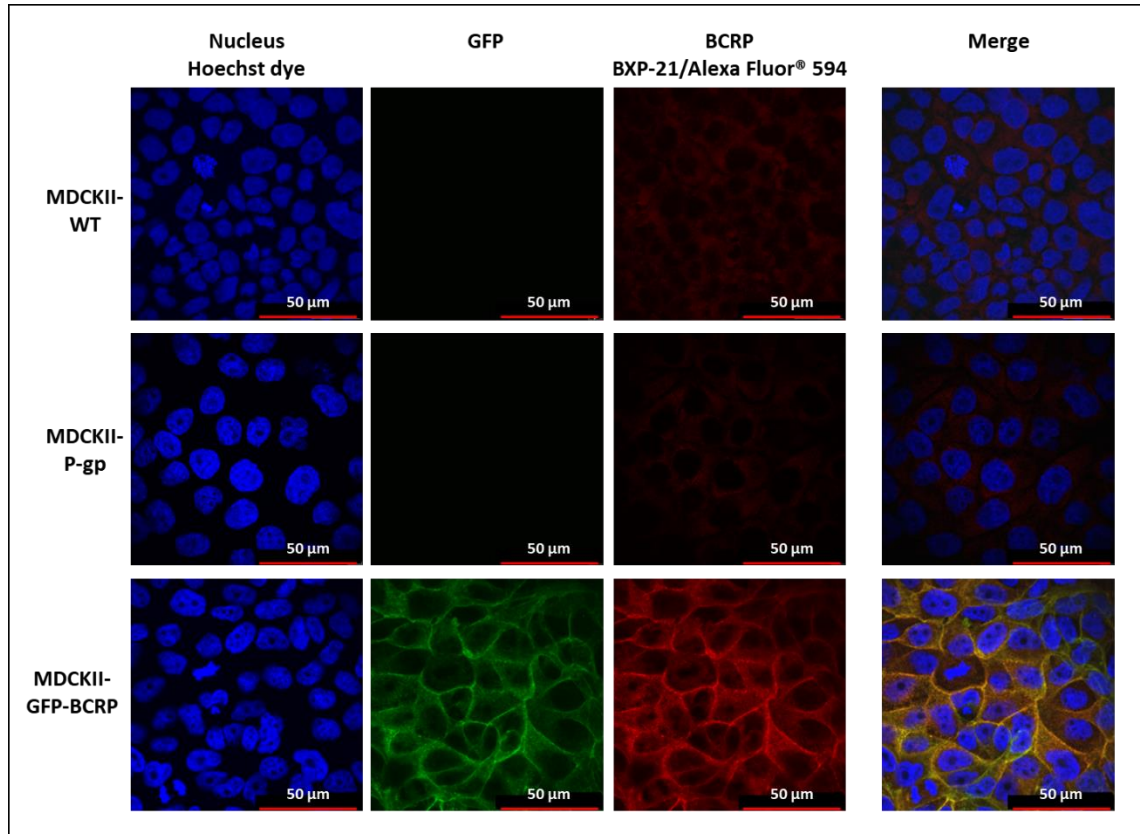


Figure 4.2.1C Expression level and localization of BCRP in different MDCKII cells.

Expression and localization of BCRP in MDCKII cells was detected by confocal microscopy. Nucleus was stained with Hoechst dye (Blue); BCRP was detected by monoclonal anti-BCRP (BXP-21), followed by an Alexa Fluor® 594 donkey anti-mouse IgG secondary antibody (Red). GFP was detected in the green channel.

4.2.2 Directional transport assay of sorafenib across MDCKII monolayer

To measure the directional transport across MDCKII monolayers, sorafenib was added on one side (donor side) and concentration of sorafenib in receiver side was measured at different time points. Two different directional experiments

were conducted: apical-to-basal side (A-to-B) and basal-to-apical side (B-to-A).

Three subtypes of MDCKII cell lines were employed for the sorafenib transport assays with or without modulators of FD 12-9 or GF120918.

As expected, all 3 MDCKII cell lines showed very low transport rate of sorafenib in A-to-B direction because P-gp and BCRP are localized on the apical side of MDCK monolayer (dotted lines in Figure 4.2.2A). There was a low level of B-to-A transport of sorafenib in MDCKII-WT cells and such rate was slightly increased in MDCKII-P-gp cells suggesting sorafenib is not a good P-gp substrate (Figure 4.2.2A). In contrast, B-to-A transport of sorafenib in MDCKII-GFP-BCRP monolayer was significantly higher, suggesting that sorafenib is a good BCRP substrate (Figure 4.2.2A).

Neither FD 12-9 nor GF120918 has significant inhibitory effect on the B-to-A transport of MDCKII-P-gp monolayer (Figure 4.2.2B). In contrast, FD 12-9 (and less so for GF12-0918) can significantly inhibit B-to-A transport of sorafenib in MDCKII-GFP-BCRP monolayer, suggesting that FD 12-9 is a stronger modulator of BCRP in sorafenib transport than GF120198 (Figure 4.2.2C).

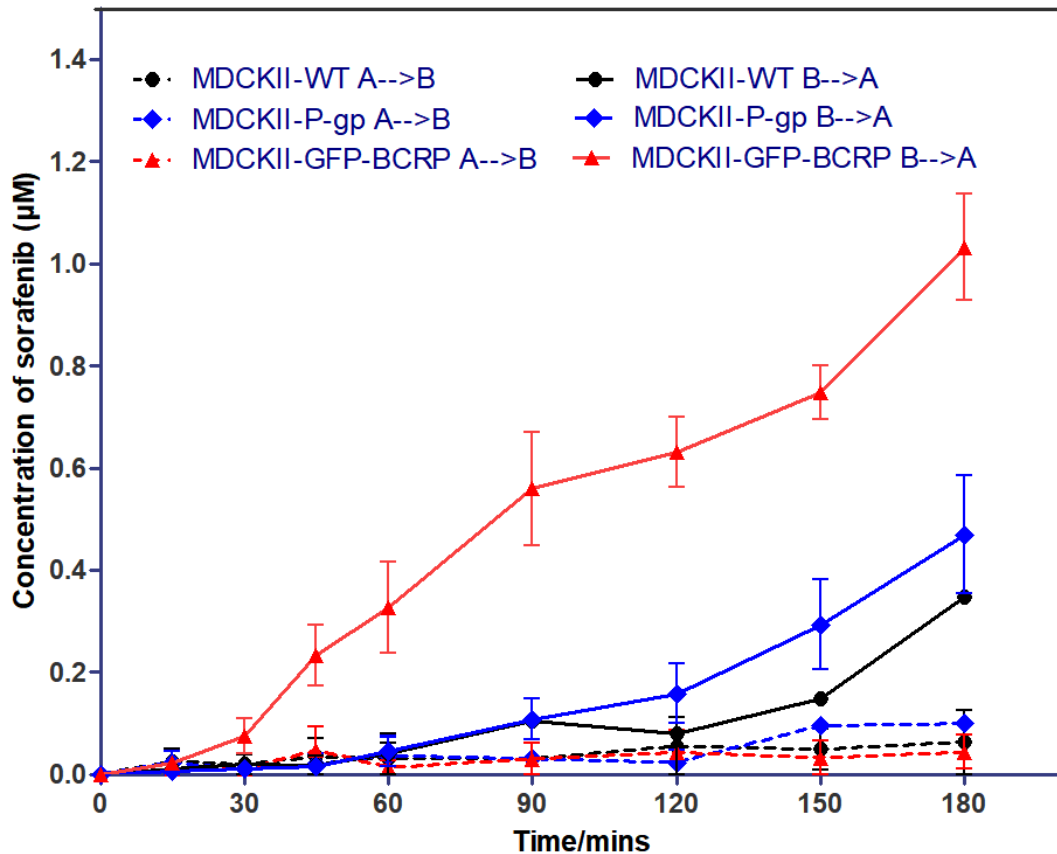


Figure 4.2.2A Directional transport assay of sorafenib across MDCKII-WT, MDCKII-P-gp and MDCKII-GFP-BCRP monolayers.

MDCKII monolayers were grown to form tight junction with TEER > 200 ohm.cm² (Ω .cm²). Sorafenib (10 µg/ml) was added to the donor side of MDCKII monolayers and the concentration of sorafenib at the recipient side was measured at the indicated time points (n = 3 - 4) using LC-MS/MS. Donor side can be either apical (A-to-B) or basal (B-to-A).

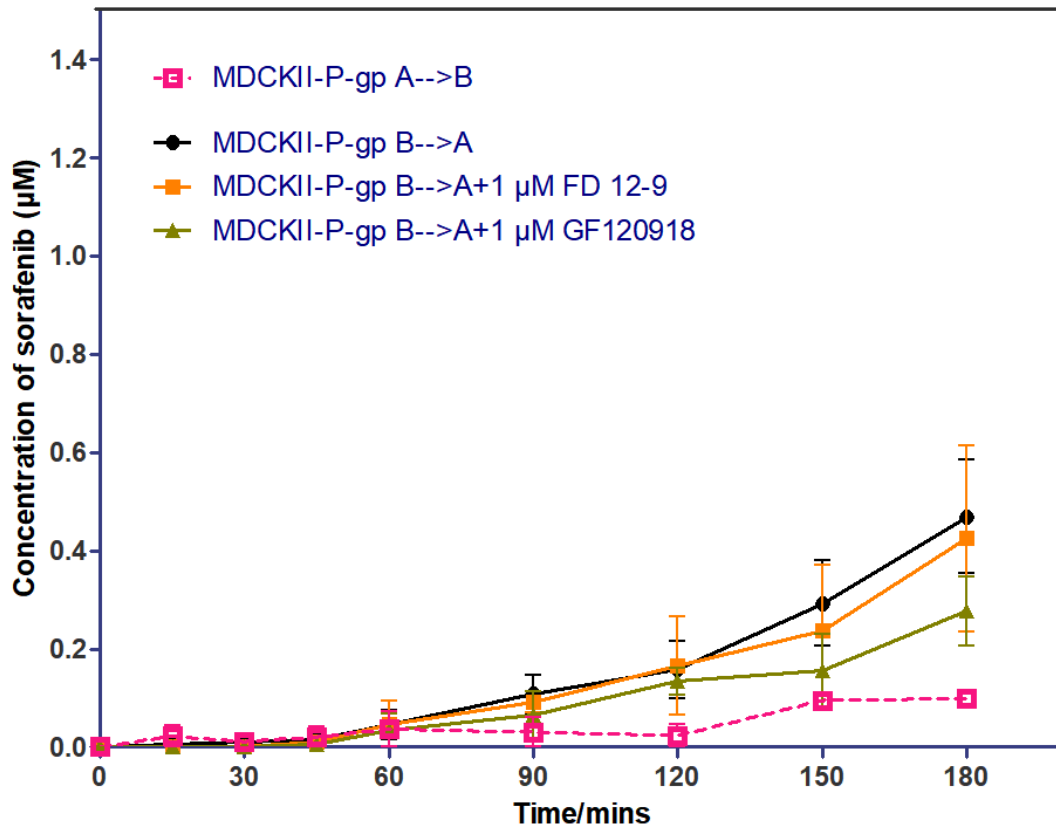


Figure 4.2.2B Transport of sorafenib across MDCKII-P-gp monolayer with or without FD 12-9 or GF120918.

Directional transport assay was performed as in Figure 4.2.2A, except that FD 12-9 or GF120918 (1 µM) was added to donor side and recipient side of MDCKII-P-gp monolayer (n = 4 - 6).

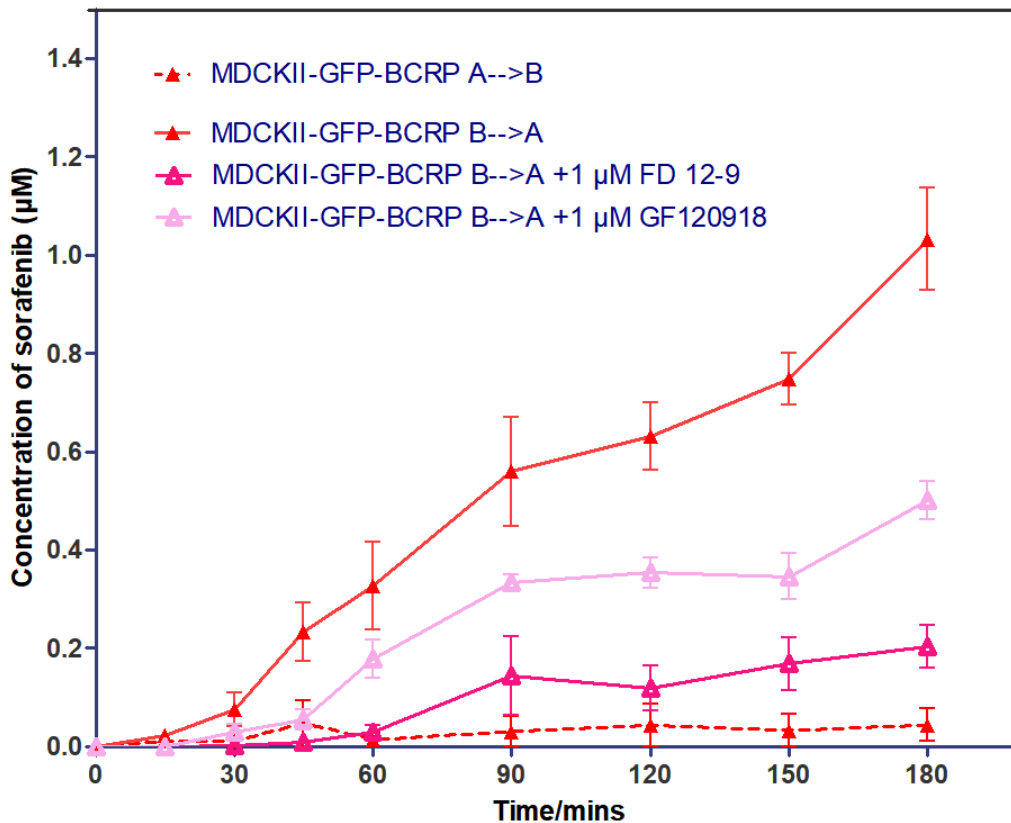


Figure 4.2.2C Transport of sorafenib across MDCKII-GFP-BCRP monolayer with or without FD 12-9 or GF120918.

Directional transport assay was performed as in Figure 4.2.2A, except that FD 12-9 or GF120918 (1 µM) was added to donor side and recipient side of MDCKII-GFP-BCRP monolayer (n = 4 - 6).

Transport rates of sorafenib were quantified in terms of apparent permeability (P_{app} , $\text{cm} \cdot \text{sec}^{-1} \times 10^6$). $P_{app A-to-B}$ was low in all three MDCKII cells (white bars in Figure 4.2.2D). $P_{app B-to-A}$ in MDCKII-WT, MDCKII-P-gp and MDCKII-GFP-BCRP (grey bars in Figure 4.2.2D) were 2.7-, 4.8- and 18.4-fold higher than the corresponding $P_{app A-to-B}$. This suggests that sorafenib is a weak substrate of P-gp but a strong substrate for BCRP. FD 12-9 reduced $P_{app B-to-A}$ in MDCKII-P-gp by only 8% whereas GF120918 reduced it by 45%, suggesting that GF120918 is a better modulator of P-gp in transporting sorafenib. FD 12-9 reduced $P_{app B-$

to-A in MDCKII-GFP-BCRP by 81% ($P < 0.01$) whereas GF120918 reduced it by 52% ($P < 0.01$), suggesting that FD 12-9 is a better modulator of BCRP in transporting sorafenib. Both FD 12-9 and GF120918 are dual selective inhibitor for P-gp and BCRP to transport sorafenib. Since sorafenib is a better substrate of BCRP than P-gp, a good modulator like FD12-9 is expected to have a larger impact on the overall sorafenib transport in BBB where both P-gp and BCRP are expressed.

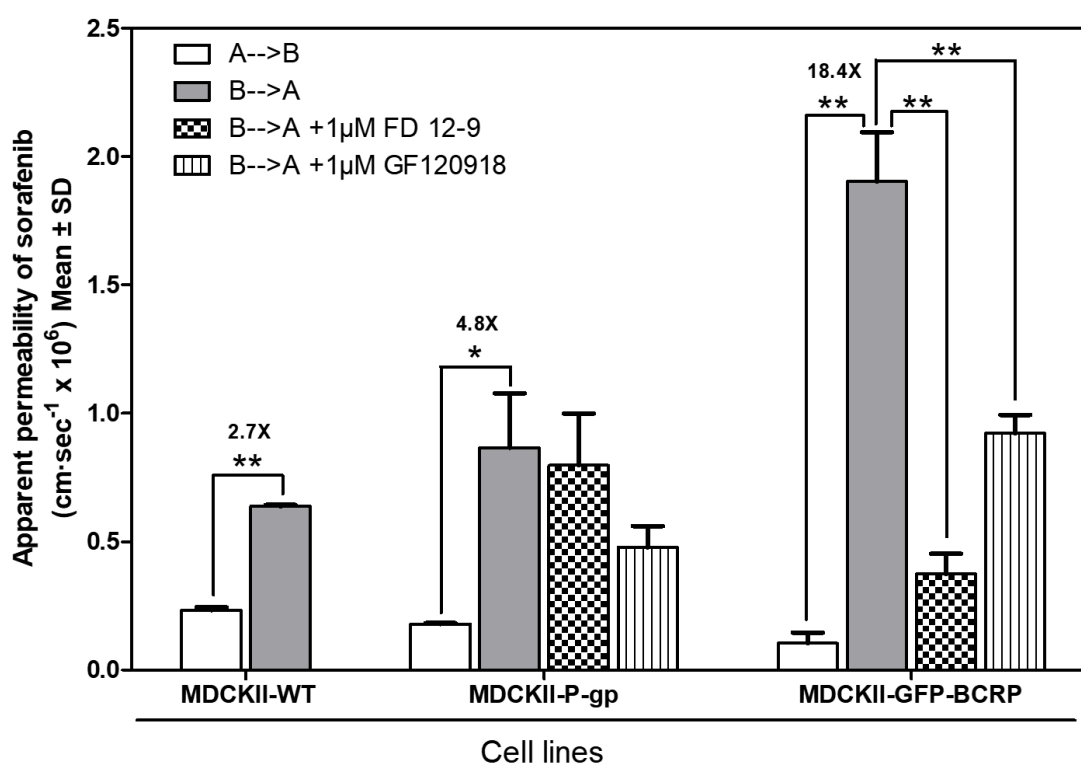


Figure 4.2.2D Apparent permeability (P_{app}) of sorafenib across MDCKII-WT, MDCKII-P-gp and MDCKII-GFP-BCRP monolayers with or without modulators (FD 12-9 and GF120918).

P_{app} was calculated according to $P_{app} = (dQ/dt)/A \cdot C_0$, where dQ/dt is mass transport rate of sorafenib, A is the surface area of cell monolayer which is equal to the insert membrane area (4.67 cm^2), and C_0 is the initial concentration of sorafenib at the donor side (10 µg/ml). Mean \pm S.D. ($n = 3-6$). *, $p < 0.05$; **, $p < 0.01$.

4.3 Summary

MDCKII cells transfected with P-gp or BCRP have been demonstrated to overexpress P-gp and BCRP respectively. Surface localization of both P-gp and BCRP are confirmed to be present on the expected location on the plasma membrane. Directional transport of sorafenib in MDCKII monolayers have been established with a low P_{app} A-to-B transport of sorafenib whereas P_{app} B-to-A of MDCKII-WT, MDCKII-P-gp and MDCKII-GFP-BCRP monolayers were 2.7-, 4.8- and 19- fold higher than the corresponding P_{app} A-to-B suggesting that both P-gp and BCRP can mediate a directional (B-to-A) transport of sorafenib with BCRP a significantly better transporter than P-gp. Both FD 12-9 and GF120918 are dual selective inhibitor of P-gp and BCRP with FD 12-9 being a better BCRP modulator whereas GF120918 is a better P-gp modulator. As both P-gp and BCRP are expressed on the capillary side of endothelial cells in BBB, it is expected that either FD 12-9 or GF120918 can inhibit both P-gp and BCRP to increase the brain accumulation of sorafenib in brain. For further study, co-transfection with more than one transporter into MDCKII cells may mimic the real BBB better. Such efforts have been tried in this project but failed to yield double P-gp and BCRP transfectants of MDCKII cells with unknown reasons.

CHAPTER 5: PHARMACOKINETIC STUDIES OF SORAFENIB WITH OR WITHOUT MODULATORS

5.1 Introduction

Previous chapters demonstrated that sorafenib is active against GBM cell line U87MG-RedFluc with an IC_{50} of 8 μ M which is much more potent than the current GBM drug, temozolomide ($IC_{50} = 564 \mu$ M). In addition, sorafenib is a substrate of BCRP and P-gp as demonstrated in the trans-epithelial transport experiments using MDCKII-P-gp and MCDKII-GFP-BCRP monolayer to mimic BBB. FD 12-9 can inhibit both P-gp and BCRP to transport sorafenib. Putting together, it was hypothesized that co-treatment of FD 12-9 with sorafenib may overcome the BBB by inhibiting P-gp and BCRP there and increasing the brain accumulation of sorafenib to treat GBM.

In this chapter, a series of pharmacokinetic experiments were used to study whether FD 12-9 can increase the brain level of sorafenib in rodents *in vivo*.

5.2 Result

5.2.1 Selection of suitable formulation for FD 12-9 for pharmacokinetic studies

Since formulation could have a significant impact on the solubility, stability and metabolism *in vivo*, a suitable formulation is needed. Here, six formulations were tested to determine which one could yield the best pharmacokinetics profile (Figure 5.2.1A, B). Six formulations were studied, including Formulation A (Ethanol : Cremophor : 5%-Tween80 = 5 : 5 : 90), Formulation B (NMP : Cremophor : 5%-Tween80 = 5 : 5 : 90), Formulation C (NMP : 20%-Tween80 = 5 : 5 : 90), Formulation D (NMP : Solutol : 5%-Tween80 = 5 : 10 : 85), Formulation E (NMP : Solutol : Saline = 5 : 10 : 85) and Formulation F (DMSO : Cremophor : 5%-Tween80 = 5 : 5 : 90).

It was found that formulation B and C can maintain the highest brain level of FD 12-9. Formulation C, however, was too toxic in mice since mice died in 180 mins after injection of formulation C, which suggested that 20% Tween-80 in such formulation is intolerable to mice. As brain accumulation of FD 12-9 in formulation D (with 5% Tween-80) was higher than that in formulation E (with saline), suggesting that 5% Tween-80 was suitable and non-toxic). In addition, brain accumulation of FD 12-9 in formulation B (with Cremophor) was higher than that in formulation D (with Solutol), suggesting that Cremophor is more suitable than Solutol (Figure 5.2.1A). Plasma profile of FD 12-9 dissolved in

different formulations followed similar pattern as in brain profile, except for formulation C, which exhibited a relative high concentration of FD 12-9 in plasma (Figure 5.2.1B). Taken together, formulation B (NMP: Cremophor: 5% Tween-80 = 5: 5: 90) was selected for subsequent pharmacokinetics studies.

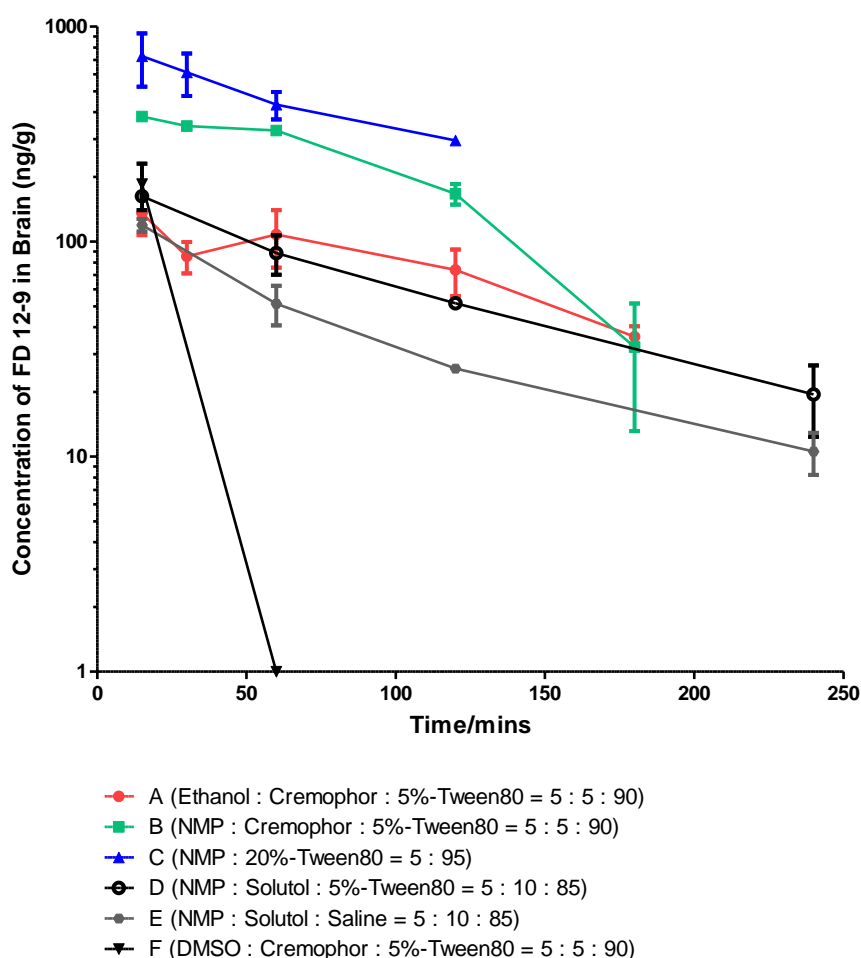


Figure 5.2.1A Effect of formulations on the accumulation of FD 12-9 in brain.

FD 12-9 was prepared in six different formulations with the same concentration (1.5 mg/ml). FD 12-9 (10 mg/kg) from these six formulations was administered intravenously to mice (groups A-F) via tail vein. Brain concentration of FD 12-9 at different time points was measured by LC-MSMS and the pharmacokinetic profiles were plotted. Each time point has 3 animals (n = 3).

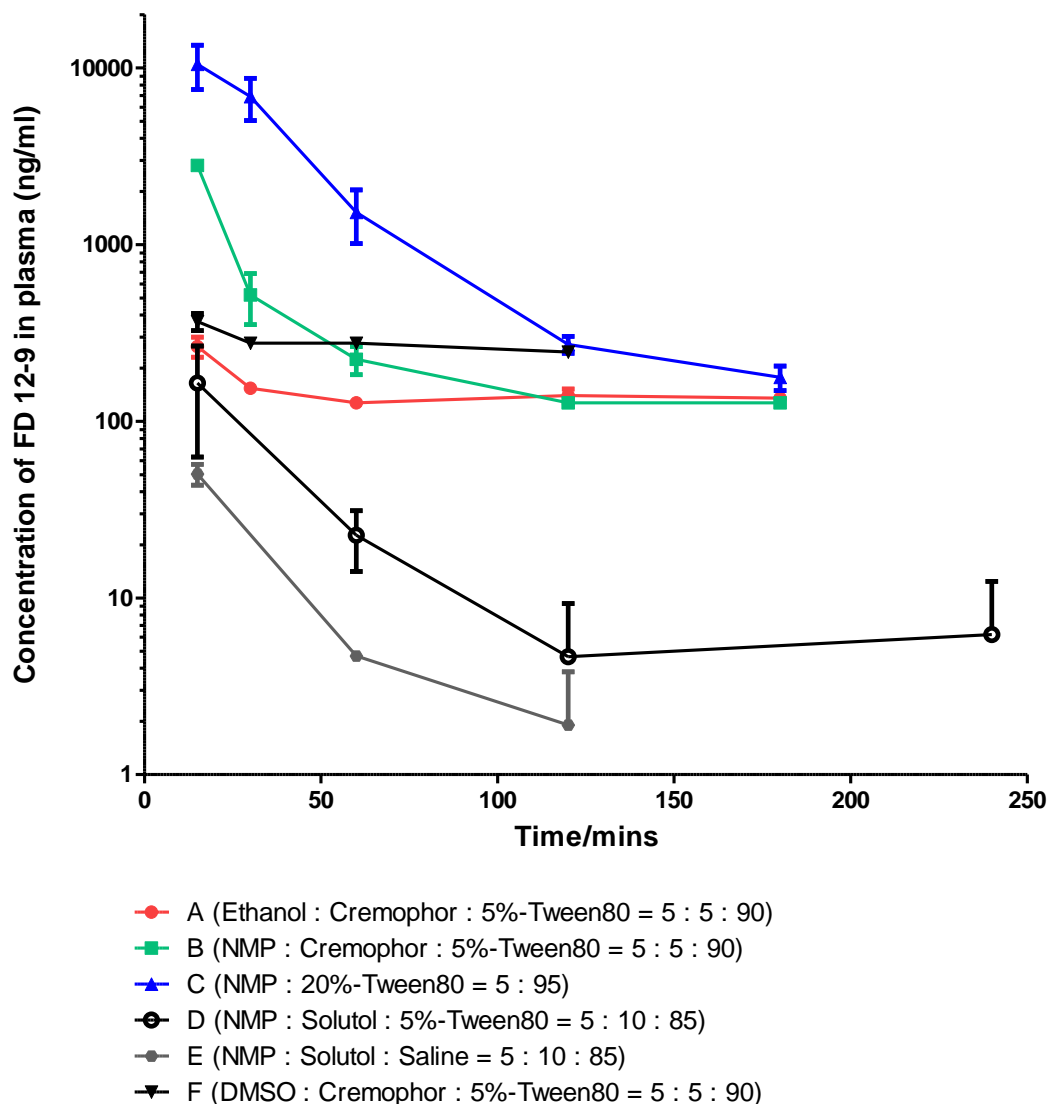


Figure 5.2.1B Effect of formulations on the plasma pharmacokinetics of FD 12-9.

FD 12-9 was prepared in six different formulations with the same concentrations (1.5 mg/kg). FD 12-9 (10 mg/kg) from these six formulations was administered intravenously to mice (groups A-F) via tail vein. Plasma concentration of FD 12-9 at different time points was measured by LC-MSMS and the pharmacokinetic profiles were plotted. Each time point has 3 animals (n = 3).

5.2.2 Pharmacokinetics of sorafenib with or without modulators

Before *in vivo* efficacy experiments were carried out, pharmacokinetic studies were conducted to determine the effect of FD 12-9 on the distribution of sorafenib in mice brain and plasma. Sorafenib (10, 20 or 30 mg/kg) was administered with or without FD 12-9 (10 mg/kg) or GF120918 (10 mg/kg). Brain and plasma level of sorafenib was determined up to 360 minutes post administration (Figure 5.2.2A and B) as well as the brain-to-plasma ratio (B-to-P ratio) (Figure 5.2.2C). It was found that brain concentration of sorafenib (10mg/kg) was significantly increased by co-administration of either FD 12-9 or GF120918. Such level was even higher than sorafenib (20 mg/kg) or sorafenib (30 mg/kg) (Figure 5.2.2A). In addition, it was found that when sorafenib (10 mg/kg) was co-injected with FD 12-9 (10 mg/kg) or GF120918 (10 mg/kg), plasma concentration of sorafenib (10mg/kg) is higher than that without modulators (Figure 5.2.2B). Pharmacokinetic parameters were summarized in Table 5.2.2. Area under curve (AUC) from 15 to 360 minutes (AUC_{15-360}) in brain (AUC_{brain}) and plasma (AUC_{plasma}) were measured to calculate the ratio (AUC_{brain}/AUC_{plasma}) as a measure of the movement from the plasma to the brain.

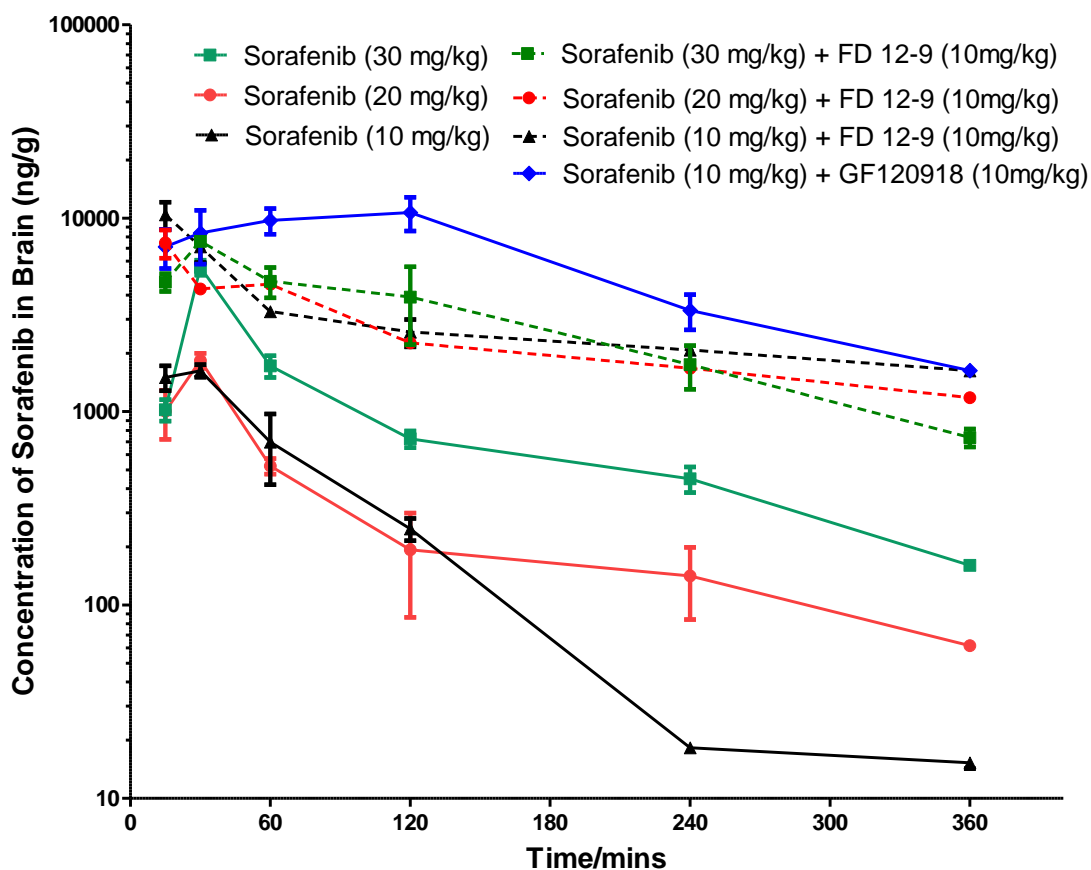


Figure 5.2.2A Pharmacokinetic studies of brain level of sorafenib with or without FD 12-9 or GF120918.

Brain concentration of sorafenib after a single intravenous injection of sorafenib (10, 20 or 30 mg/kg) in the presence or absence of FD 12-9 (10 mg/kg) or GF120918 (10 mg/kg) was measured up to 360 minutes post administration (n = 3 – 6).

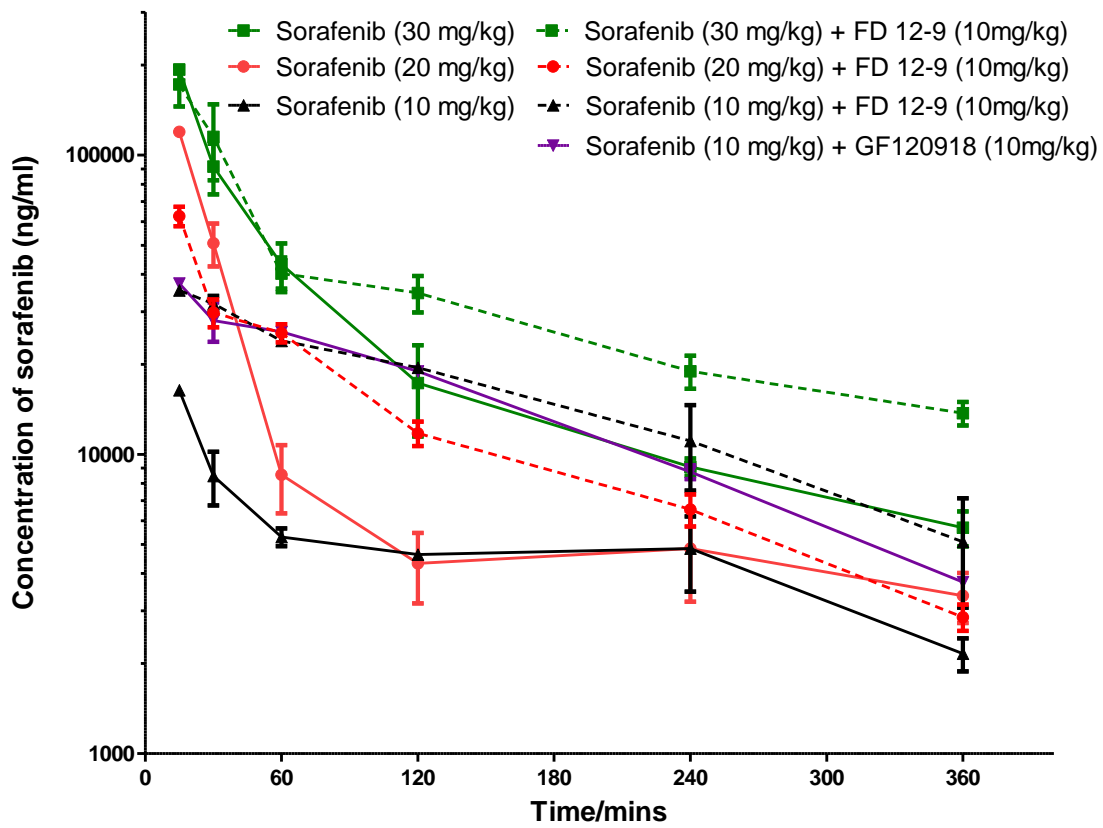


Figure 5.2.2B Pharmacokinetic studies of plasma level of sorafenib with or without FD 12-9 or GF120918.

Plasma concentration of sorafenib after a single intravenous injection of sorafenib (10, 20 or 30 mg/kg) in the presence or absence of FD 12-9 (10 mg/kg) or GF120918 (10 mg/kg) was measured up to 360 minutes post administration (n = 3 – 6).

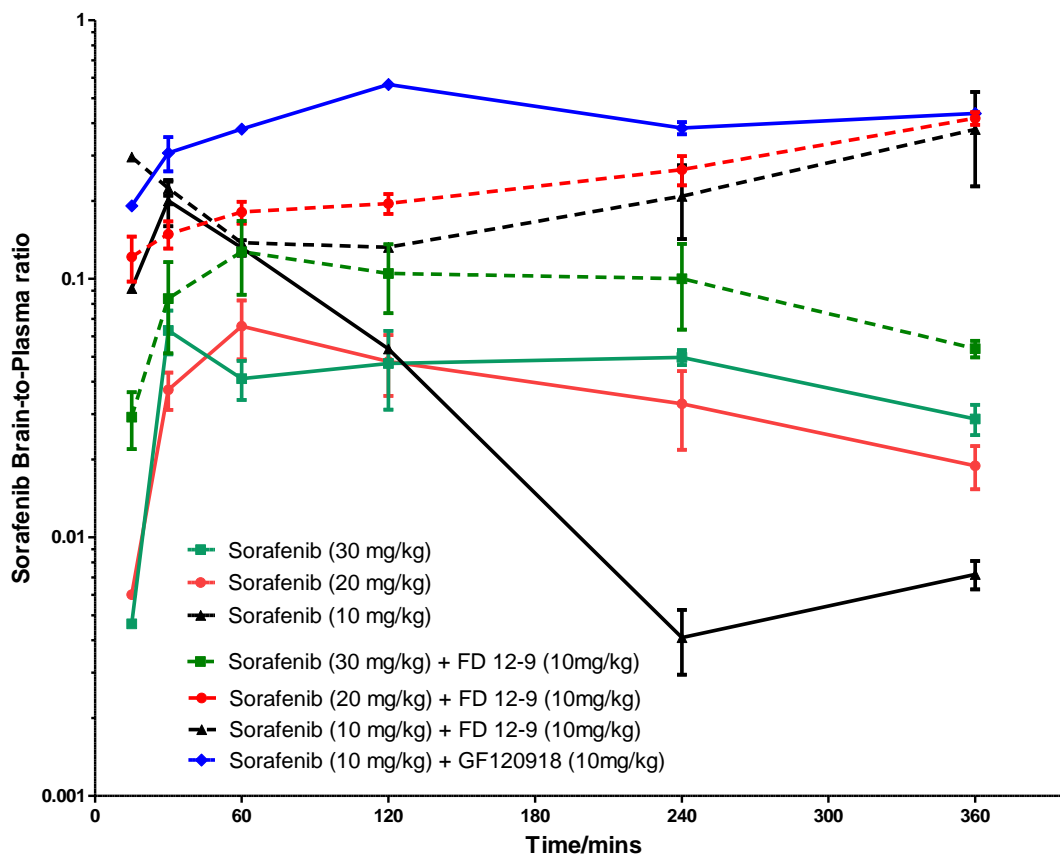


Figure 5.2.2C Effect of FD 12-9 and GF120918 on the Brain-to-Plasma (B-to-P) ratio of sorafenib.

Brain level of sorafenib (from Figure 5.2.2A) was normalized to that of plasma level (from Figure 5.2.2B) to yield the brain-to-plasma (B-to-P) ratio and plotted here (n = 3 – 6).

Dose-normalized AUC of sorafenib in the brain ($AUC_{brain}/dose$) of 10, 20 and 30 mg/kg sorafenib are 10458, 5417 and 11270 $ng \cdot min \cdot g^{-1}/mg \cdot kg^{-1}$ respectively, suggesting that $AUC_{brain}/dose$ cannot be increased by simple increase in the sorafenib used (Table 5.2.2). Dose-normalized AUC of sorafenib in plasma ($AUC_{plasma}/dose$) was 167800, 179700 and 281267 $ng \cdot min \cdot ml^{-1}/mg \cdot kg^{-1}$,

respectively. These results indicated that increasing the dosage of sorafenib can only improve the $AUC_{plasma}/dose$ but not the $AUC_{brain}/dose$.

When FD 12-9 (10 mg/kg) was co-administered with sorafenib (10, 20 or 30 mg/kg), $AUC_{brain}/dose$ can be increased to 96515 $ng \cdot min \cdot g^{-1}/mg \cdot kg^{-1}$ (9.2-fold over sorafenib alone), 41,655 (7.7-fold) and 34,133 (3.0-fold) respectively. These results demonstrated that 10 mg/kg of sorafenib benefited most from the FD 12-9.

Taken together, co-administration with FD 12-9 (10 mg/kg) with sorafenib resulted in an increase in brain-to-plasma ratio (AUC_{brain}/AUC_{plasma}) when sorafenib was used at 10 mg/kg (3.0-fold increase from 0.06 to 0.18), 20 mg/kg (6.3-fold increase from 0.03 to 0.19) and 30 mg/kg (2.3-fold increase from 0.04 to 0.09) (Figure 5.2.2C and Table 5.2.2). Co-treatment with positive control GF120918 (10 mg/kg) can increase AUC_{brain}/AUC_{plasma} by 7.0-fold when sorafenib was used at 10 mg/kg (Figure 5.2.2C and Table 5.2.2).

Table. 5.2.2 Plasma and brain pharmacokinetic parameters after a single intravenous injection of different doses of sorafenib with or without modulators in Balb/c mice.

	Sorafenib (mg/kg; I.V.)	10	20	30	10	20	30	10
	FD 12-9 (mg/kg; I.V.)	-	-	-	10	10	10	-
	GF120918 (mg/kg; I.V.)	-	-	-	-	-	-	10
AUC ₁₅₋₃₆₀	ng·min/g	104,577	108,333	338,094	965,148	833,107	1,024,000	2,142,000
C _{max}	ng/g	1,627	1,839	5,572	10,428	7455	7599	10,706
T _{max}	min	30	30	30	15	15	30	120
Brain Half-life	min	55	45	50	42	85	140	190
Brain Half-life (D/A)	min	25	15	20	27	70	110	70
AUC _{15-360min/dose}	ng·min·g ⁻¹ /(mg·kg ⁻¹)	10,458	5,417	11,270	96,515	41,655	34,133	214,200
Plasma AUC _{15-360min}	ng·min/ml	1,678,000	3,594,000	8,438,000	5,447,000	4,298,000	11,900,000	5,041,000
Plasma Half-life	min	120	25	28	120	30	40	120
Plasma AUC _{15-360min/dose}	ng·min·ml ⁻¹ /(mg·kg ⁻¹)	167,800	179,700	281,267	544,700	214,900	396,666	504,100
	AUC _{Brain} /AUC _{plasma}	0.06	0.03	0.04	0.18	0.19	0.09	0.42

Non-compartmental analysis of brain or plasma level of sorafenib (10, 20 or 30 mg/kg) with or without FD 12-9 (10 mg/kg) of GF120918 (10mg/kg) was performed using GraphPad Prism® 5. $AUC_{Brain} / AUC_{plasma}$ was calculated to reflect the relative accumulation of sorafenib in brain over plasma. $AUC_{15-360min}/dose$ means the normalized AUC value divided by the dose used in the experiment, so that $AUC_{15-360min}/dose$ of different doses could be compared with each other.

Distribution of FD 12-9 and GF120918 in brain and plasma was also determined after they were co-administered with 10 mg/kg of sorafenib (Figure 5.2.2D, E). Brain $AUC_{15-360 \text{ min}}$ of GF120918 ($454984 \text{ ng}\cdot\text{min}\cdot\text{g}^{-1}$) was 6-fold higher than that of FD 12-9 ($74355 \text{ ng}\cdot\text{min}\cdot\text{g}^{-1}$). Plasma $AUC_{15-360 \text{ min}}$ of GF120918 ($939617 \text{ ng}\cdot\text{min}\cdot\text{ml}^{-1}$) was 13-fold higher than that of FD 12-9 ($72824 \text{ ng}\cdot\text{min}\cdot\text{ml}^{-1}$). GF120918, therefore, exhibited a much higher concentration in both brain and plasma, suggesting that GF120918 might penetrate BBB faster than FD 12-9. This may account for the 7-fold increase of $AUC_{\text{brain}}/AUC_{\text{plasma}}$ of sorafenib versus 3-fold increase caused by FD 12-9 co-treatment.

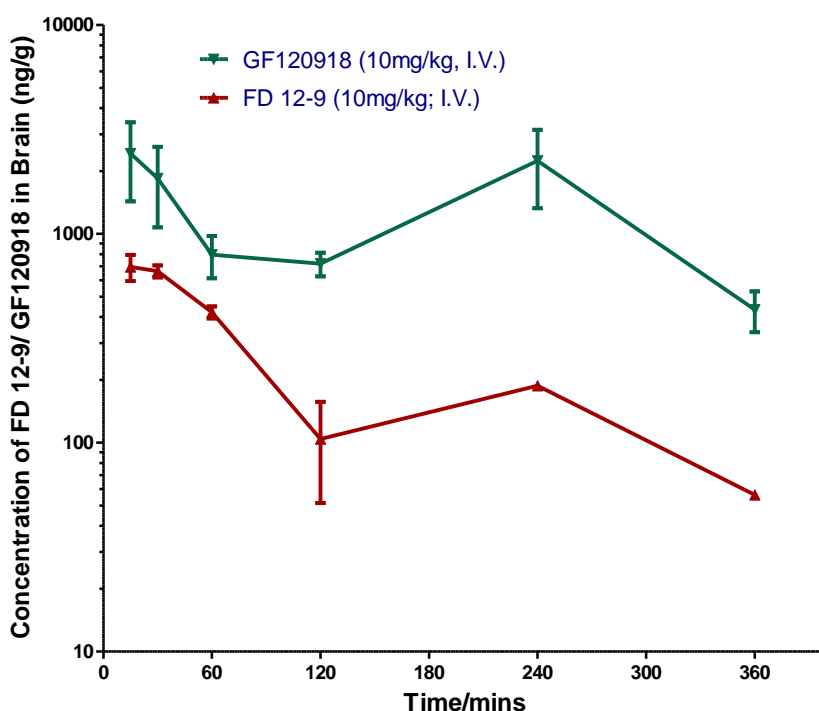


Figure 5.2.2D Pharmacokinetic studies of FD 12-9 and GF120918 in brain. Sorafenib (10 mg/kg) was co-administered with FD 12-9 (10 mg/kg) or GF 120918 (10mg/kg) as in Figure 5.2.2A and Figure 5.2.2B. Brain level of FD 12-9 or GF120918 was determined by LC-MS/MS at up to 360 minutes post administration (n = 3 – 6).

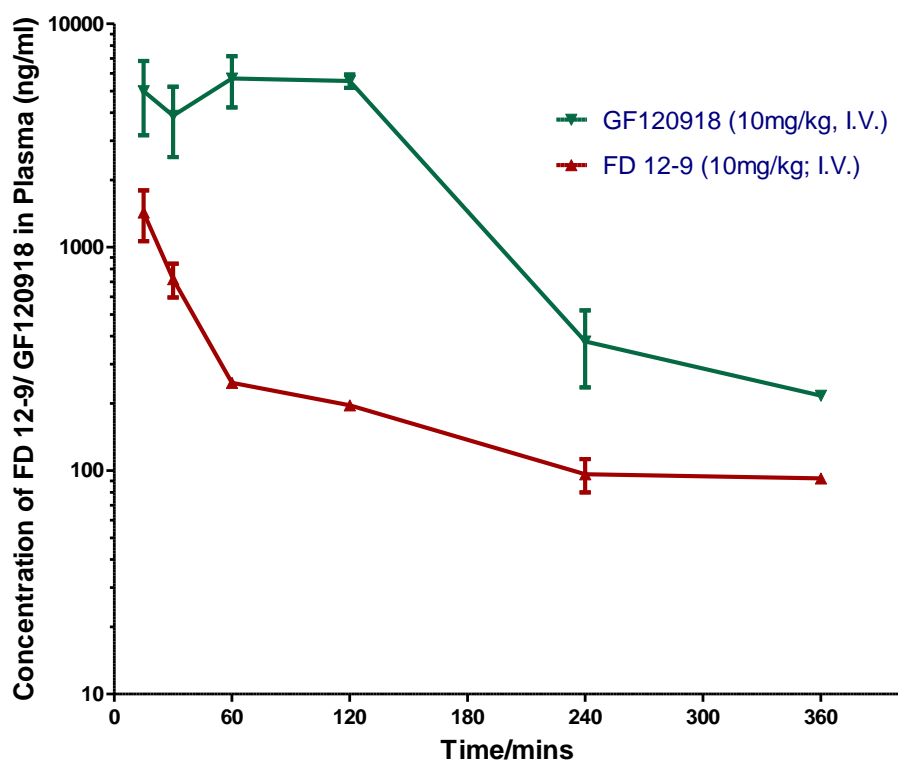


Figure 5.2.2E Pharmacokinetic studies of FD 12-9 and GF120918 in Plasma.

Sorafenib (10 mg/kg) was co-administered with FD 12-9 (10 mg/kg) or GF 120918 (10mg/kg) as in Figure 5.2.2A and Figure 5.2.2B. Plasma level of FD 12-9 or GF120918 was determined by LC-MS/MS at up to 360 minutes post administration (n = 3 – 6).

5.3 Summary

By comparing different formulations as carriers for FD 12-9, it was found that formulation B (NMP : Cremophor : 5%-Tween80 = 5 : 5 : 90) can be used safely to increase the brain concentration of FD 12-9 to the highest extent (Figure

5.2.1A). This formulation was used in all subsequent pharmacokinetic studies. Co-treatment of FD 12-9 (10 mg/kg) with sorafenib (10 mg/kg) can increase $AUC_{brain}/dose$ to a level of 96,515 $ng \cdot min \cdot ml^{-1}/mg \cdot kg^{-1}$ with a 3-fold increase in AUC_{brain}/AUC_{plasma} from 0.06 to 0.18 (Table 5.2.2). Combination of GF120918 (10 mg/kg) and sorafenib (10 mg/kg) exhibited an even stronger activity in increasing $AUC_{brain}/dose$ of sorafenib (214,200 $ng \cdot min \cdot ml^{-1}/mg \cdot kg^{-1}$), which might be due to the higher brain accumulation of GF120918 (Figure 5.2.2D). GF120918 penetrated into the brain before the FD 12-9 and perhaps had a longer impact on elevating brain level of sorafenib than FD 12-9.

CHAPTER 6: THE *IN VIVO* EFFICACY STUDIES OF SORAFENIB ON U87MG-REDFLUC ORTHOTOPIC XENOGRAFT GLIOBLASTOMA IN BALB/C NUDE MICE

6.1 Introduction

Most human cancer models are established in immunocompromised mice like Balb/c nude (nu nu) mice and NOD-SCID (non-obese diabetic-severe combined immunodeficiency) mice. Depending on the implantation location in the mouse host, xenograft model can be classified as subcutaneous or orthotopic. Subcutaneous xenograft tumor model is obtained by transplanting human cancer cells subcutaneously in nude mice. Changes in the tumor volume can be easily monitored in subcutaneous xenograft model. Such model, however, cannot reflect the real situation of tumors in human patients as the site of transplantation is different from the location where the tumor was originally derived. This is particularly problematic for GBM model which is protected by the BBB and in the subcutaneous xenograft model cannot reflect such situation. In contrast, orthotopic xenograft model is another xenograft model in which human cancer cells are injected into a mouse organ that in the same as the human origin. For example, human lung cancer cells are injected into the lung of a mouse. The major advantage of such orthotopic xenograft

cancer model is that it can provide a similar kind of tissue microenvironment similar to that of patient origin. As a result, the problems that may occur in patients will also be reflected in the orthotopic xenograft cancer model. The disadvantages of the orthotopic model are obvious: complicated implantation procedure, low success rate and difficulty in monitoring.

As a well-established GBM cell line, U87MG-RedFluc cells are often used to evaluate the effectiveness of anti-cancer drugs for brain cancers both *in vitro* and *in vivo*. U87MG-RedFluc cell line was established by stable transfection with red-shifted firefly luciferase gene. In this chapter, an orthotopic xenograft GBM model was established by inoculating U87MG-RedFluc cells into the brain of Balb/c nude mice according to the protocol mentioned in **Chapter 2**. When injected with luciferin in animal bearing an orthotopic U87MG-RedFluc xenograft, the tumor size can be determined by monitoring the luciferase activity at the wavelength of 620 nm. This orthotopic GBM animal model will be used to assess the effectiveness of FD 12-9 in enhancing sorafenib penetration cross the BBB.

6.2 Results

6.2.1 *In vivo* toxicity studies in Balb/c mice

Before the *in vivo* efficacy experiments were carried out, the toxicity of various treatments was evaluated. Six different treatments, 1) solvent control (i.v.), 2)

sorafenib (10 mg/kg, i.v.) alone, 3) FD 12-9 (10 mg/kg, i.v.) alone, 4) sorafenib (10 mg/kg, i.v.) + FD 12-9 (10 mg/kg, i.v.), 5) GF120918 (10 mg/kg, i.v.) alone, and 6) sorafenib (10 mg/kg, i.v.) + GF120918 (10 mg/kg, i.v.), were administered to six groups of Balb/c mice every other day (q.o.d.) for 10 times respectively (Figure 6.2.1). All treatments were prepared in the same formulation freshly on treatment day. Toxicity symptoms like loss of weight and appetite, slowness in activity or treatment-related mortality, if there were any, were recorded during treatment from day 0 to 18 and for 10 days after treatment from day 18 to 28 (Figure 6.2.1).

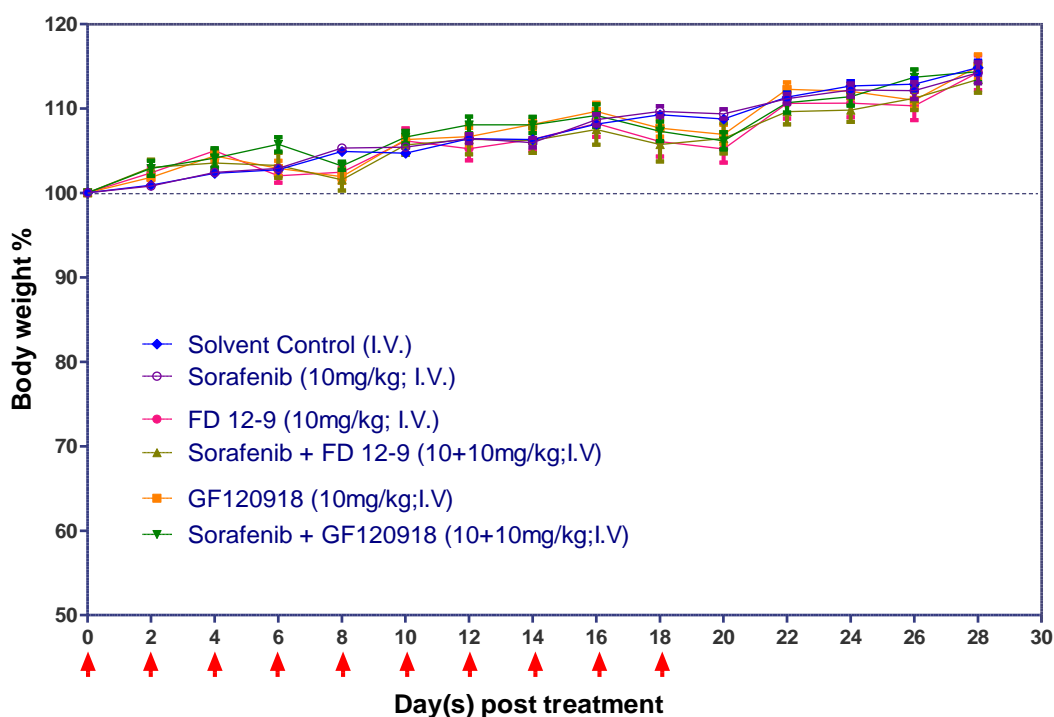


Figure 6.2.1 *In vivo* toxicity evaluation studies in Balb/c mice with different treatments.

Twenty-Four Balb/c mice were divided into six groups. Different treatments were made to different groups every other day for ten times respectively. Weight changes were recorded from day 0 to day 28 and showed in mean \pm SEM (n=4).

It was found that animals in all treatment groups gained body weight by 13.4 % to 15.0 % with similar rate. No mice died during or after the treatments in the whole experiment from day 0 to 28 (Table 6.2.1). These results suggested that the repeated administration of sorafenib (10 mg/kg) were safe to Balb/c mice with or without modulators (10 mg/kg; q.o.d x 10).

Table. 6.2.1 *In vivo* toxicity evaluation studies in BALB/c mice with different treatments.

Groups	Treatment	Deaths	Weight Changes (%)
1	solvent control (NMP: Cremophor EL: 5% Tween-80 = 5: 5: 90)	0/4	14.8±0.8
2	sorafenib (10 mg/kg)	0/4	14.2±1.2
3	FD 12-9 (10 mg/kg)	0/4	14.2±2.0
4	sorafenib (10 mg/kg) + FD 12-9 (10 mg/kg)	0/4	13.4±1.6
5	GF120918 (10 mg/kg)	0/4	15.0±1.4
6	sorafenib (10 mg/kg) + GF120918 (10 mg/kg)	0/4	14.3±1.2

Twenty-Four Balb/c mice were divided into six groups. Treatments were given every other day for ten times. All treatment mixtures were prepared using the same solvent as solvent control. Loss of weight, loss of appetite, slowdown of activity or treatment-related mortality was monitored and recorded as toxicity symptoms from day 0 to day 28. Weight changes were showed in mean ± SEM (n=4).

6.2.2 *In vivo* efficacy studies of sorafenib on U87MG-RedFluc orthotopic xenograft GBM in Balb/c nude (nu nu) mice with or without modulators

To establish an orthotopic GBM model, human GBM U87MG-RedFluc cells were implanted intracranially in the striatum of Balb/c nude (nu nu) mouse as described in the protocol in **Chapter 2**. (Figure 6.2.2A). Tumor-bearing nude mice were monitored by IVIS after the implantation.

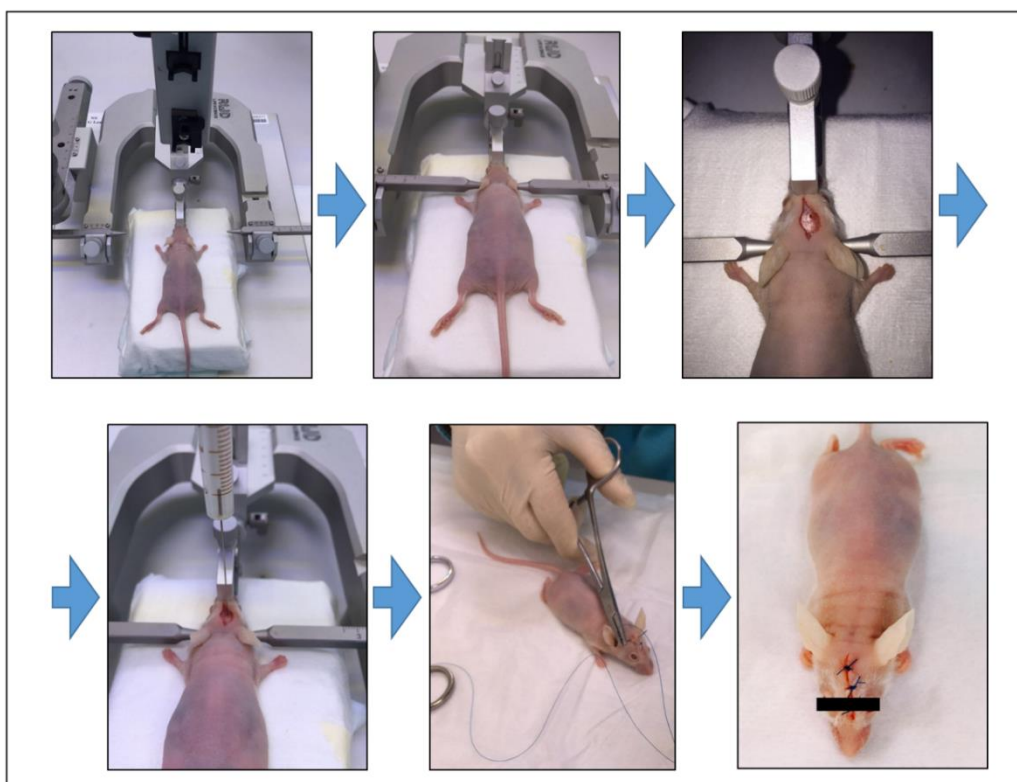


Figure 6.2.2A Implantation of U87MG-RedFluc cells in the brain of nude mice to establish orthotopic model of GBM.

U87MG-RedFluc cells were implanted into the brain of Balb/c nude mice. The major procedures included anesthesia, fixation, cranium drilling, cells implantation, and suture. Tumor growth was monitored by IVIS. Only mice with suitable size of tumor would be used for efficacy studies.

In the first efficacy study, Balb/c nu nu mice with intracranial U87MG-RedFluc orthotopic xenograft ($2-3 \times 10^8$ photons/s) were randomly divided into 4 treatment groups (n = 3 - 4 mice per group), namely (1) untreated control, (2) solvent control (NMP: Cremophor EL: 5% Tween-80 = 5: 5: 90), (3) sorafenib (10 mg/kg) and (4) sorafenib (10 mg/kg) + FD 12-9 (10 mg/kg). A total of seven injections (I.V.) were administered to each group every other day from day 0 to day 12 (q.o.d. X 7). Bioluminescent imaging (BLI) signal, which correlated to the tumor growth, was monitored during and after the treatment period till day 20 (Figure 6.2.2B, C). It was found that sorafenib treatment (10mg/kg/injection; q.o.d. X 7) resulted in no growth inhibition of U87MG-RedFluc orthotopic xenograft compared to untreated or solvent control. In contrast, combination of sorafenib (10 mg/kg/injection; q.o.d. X 7) and FD 12-9 (10 mg/kg/injection; q.o.d. X 7) resulted in a strong inhibitory effect on the tumor growth (Figure 6.2.2B, C). It also prolonged overall survival of mice (Figure 6.2.2D). All treatment groups have a gradual decrease in body weight during the treatment period with the combination group (sorafenib + FD 12-9) slower than others. The average body weight of the mice in the untreated control group increased again on day 14 because of the death of some mice (Figure 6.2.2E). These results suggested that sorafenib alone cannot control GBM orthotopic xenograft model whereas co-administration of FD 12-9 with sorafenib can, likely because FD 12-9 allow sorafenib to pass through BBB.

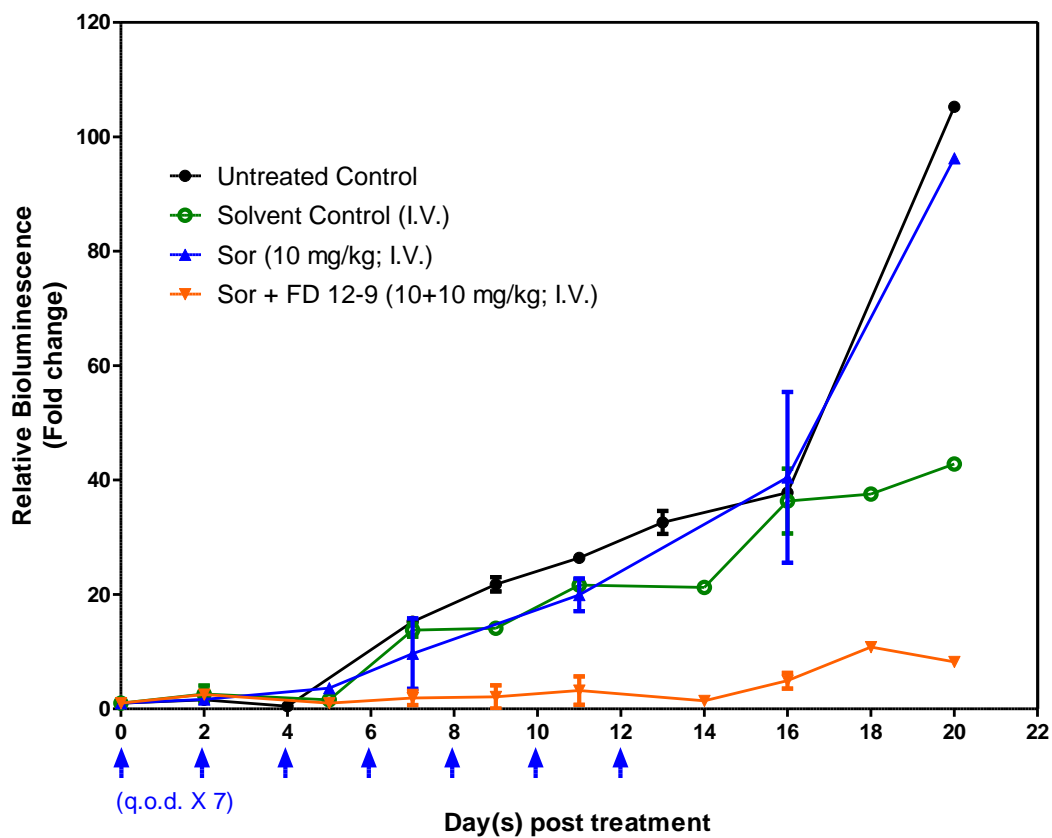


Figure 6.2.2B *In vivo* efficacy of sorafenib against orthotopic model of GBM with or without FD 12-9.

Nude mice with orthotopically-implanted U87MG-RedFluc cells were monitored for their luminescence level using IVIS. Four treatment groups included untreated control, solvent control, sorafenib (I.V. 10 mg/kg) and combination of sorafenib (I.V. 10 mg/kg) and FD 12-9 (I.V. 10 mg/kg) with a frequency of q.o.d.x7 (indicated as arrow head). Each group has 3-4 animals. Relative bioluminescent imaging (BLI) signals of each mouse was normalized to its BLI signal on the first day of treatment.

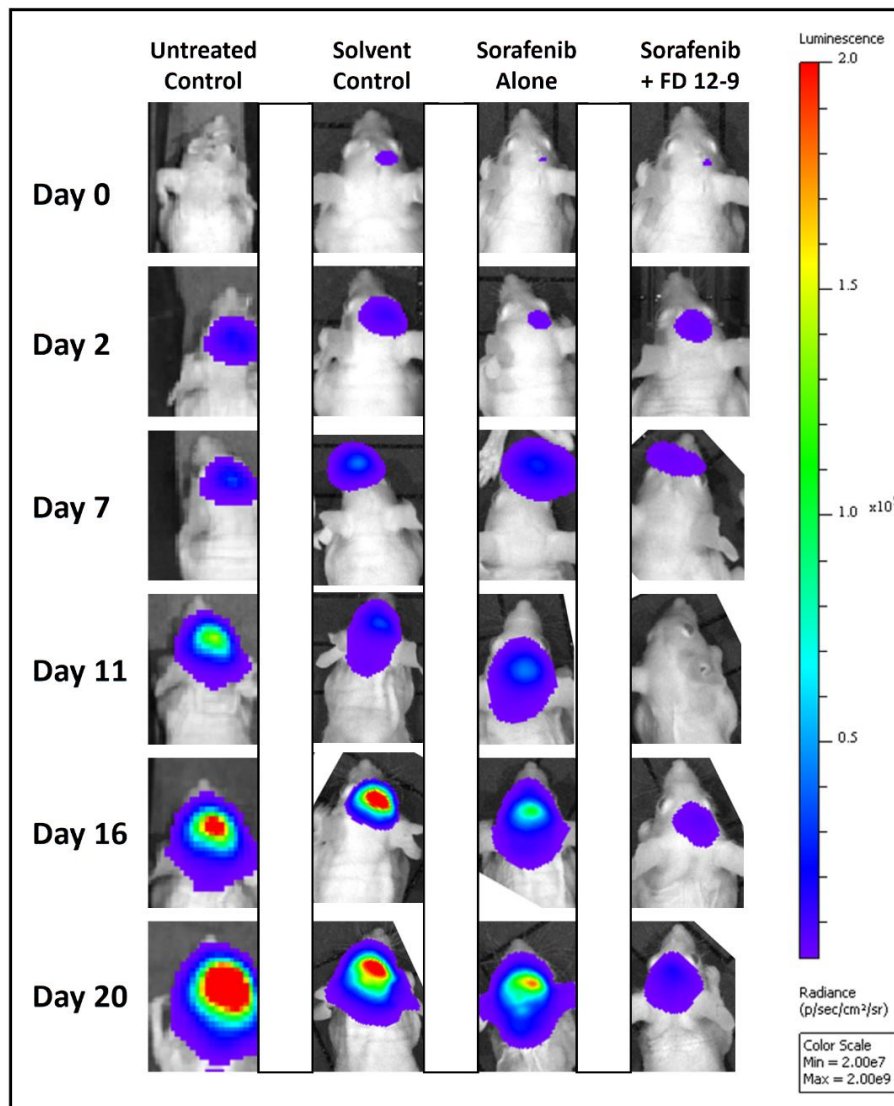


Figure 6.2.2C *In vivo* efficacy of sorafenib against orthotopic model of GBM as monitored by IVIS technique.

Nude mice from Figure 6.2.2B were monitored on the days indicated using IVIS. On the day of imaging, all mice were treated with ketamine/xylazine solution for anesthesia (100 mg/kg: 10 mg/kg; I.P.), followed by an injection of D-luciferin (150 mg/kg; I.P.). After thirty images were taken in 30 minutes by IVIS, the highest signal among the 30 images was taken as the BLI signal. All images were presented in the same range of color scale for comparison (n = 3 - 4).

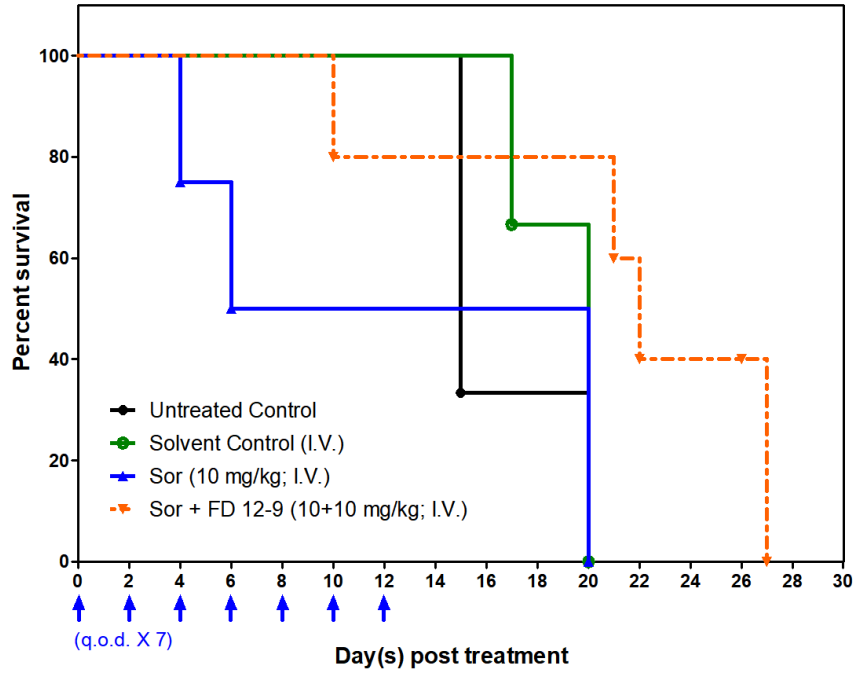


Figure 6.2.2D Survival curve of orthotopic GBM-bearing mice after receiving treatment of sorafenib with or without FD 12-9.

Animal survival from the previous experiment in Figure 6.2.2B were recorded and shown here (n = 3 - 4).

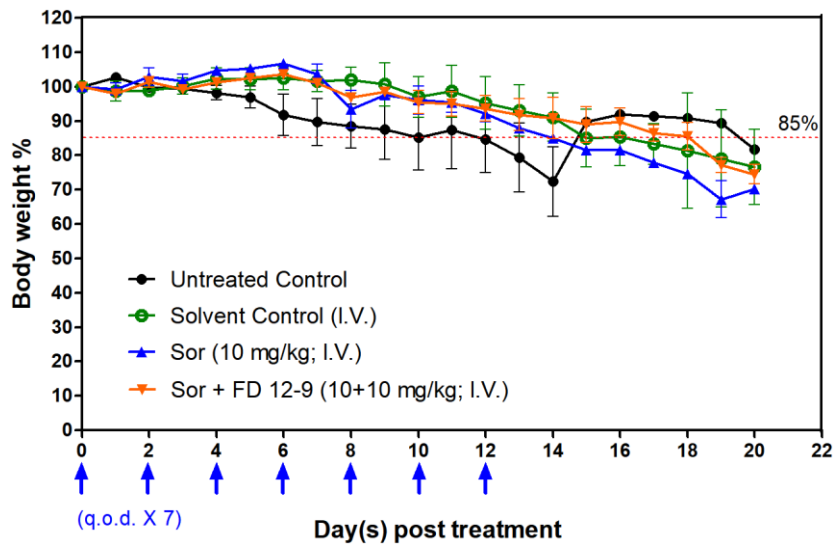


Figure 6.2.2E Body weight changes in U87MG-RedFluc-bearing mice receiving treatment of sorafenib with or without FD 12-9.

Body weight was normalized to day 0 and recorded every other day. Animal death might induce sudden increase in the average of body weight. Data were shown in mean \pm SEM (n = 3 - 4).

To further improve the efficacy, the treatment frequency was increased from 7 to 10. In addition, GF120918 was included for comparison. Six groups of Balb/c nu nu mice (6-9 mice/group) with similar intracranial U87MG-RedFluc xenograft ($1 - 2 \times 10^8$ photons/s) were treated for 10 times every other day (q.o.d. X 10). The six treatment groups were (1) untreated control, (2) sorafenib (10 mg/kg), (3) sorafenib (10 mg/kg) + FD 12-9 (10 mg/kg), (4) FD 12-9 (10 mg/kg), (5) sorafenib (10 mg/kg) + GF120918 (10 mg/kg) and (6) GF120918 (10 mg/kg). Increasing the treatment frequency to 10 times allowed sorafenib to have a slight effect on suppressing tumor growth (Tukey test, $P = 0.004$) (Figure 6.2.2F, G). Co-treatment of sorafenib with FD 12-9 has a strong inhibitory effect on tumor growth in comparison to both untreated control group (Tukey test, $P < 0.001$) and sorafenib alone group (Tukey test, $P = 0.005$) (Figure 6.2.2F, G). Meanwhile, FD 12-9 alone (10 mg/kg; I.V.; q.o.d. X 10) did not show any suppressive effect on tumor growth (Figure 6.2.2F, G). Sorafenib combined with GF120918 also manifested very potent inhibitory effect on tumor growth (Figure 6.2.2F, G).

Median overall survival of sorafenib alone group (26.1 days) and FD 12-9 alone group (24.8 days) showed no significant difference compared to untreated control group (25.2 days) (Log-Rank test, $P = 0.364$ and $P = 0.712$ respectively) (Figure 6.2.2G, H). In contrast, the median overall survival of treatment group of sorafenib with FD 12-9 was significantly different from the untreated control

(Log-Rank test, $P < 0.001$) (Figure 6.2.2H). No animals died at the end of the treatment period, suggesting that co-treatment of FD 12-9 and sorafenib was safe to use. Although GF120918 can also enhance the sorafenib in the efficacy experiments, mice in that group started to die earlier and suffered from bodyweight loss sooner than other groups (Figure 6.2.2G, H). GF120918 alone (10 mg/kg; I.V.; q.o.d.x10) demonstrated even more severe toxicity effect on mice than the co-treatment group of GF120918 and sorafenib (Figure 6.2.2G, H).

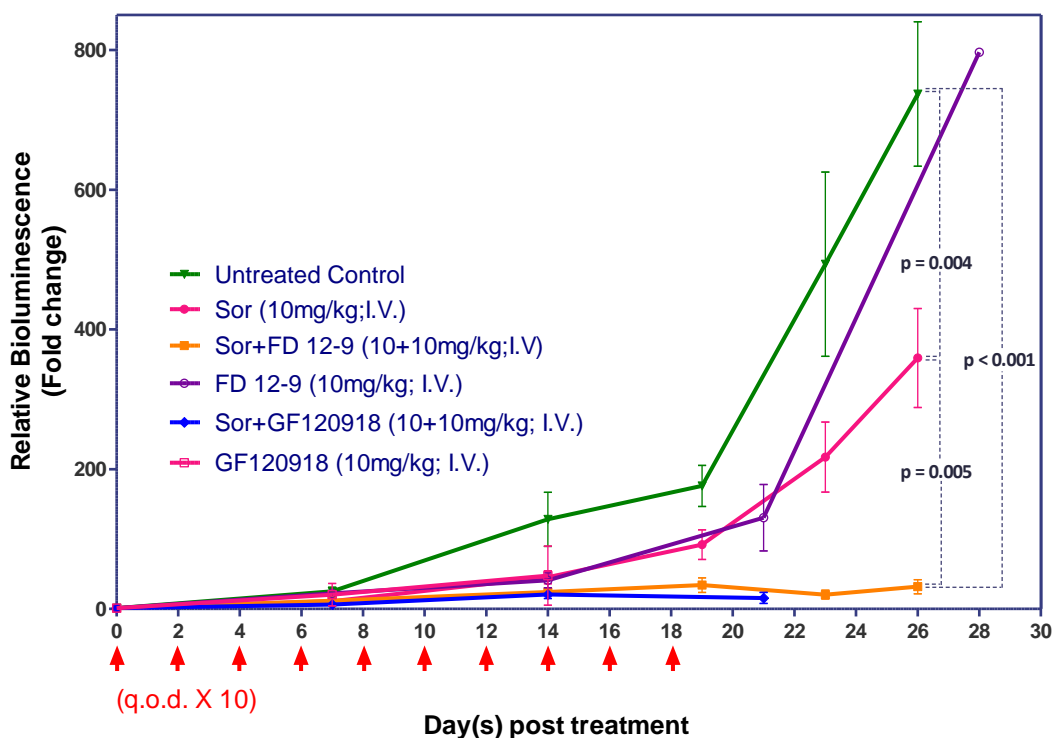


Figure 6.2.2F Relative BLI signal changes of U87MG-RedFluc tumors in 6 different groups of mice receiving sorafenib with or without FD 12-9 or GF120918.

Six groups of mice (6-9 mice/group) with implanted U87MG-RedFluc cells were treated with sorafenib (10 mg/kg), sorafenib (10 mg/kg) + FD 12-9 (10 mg/kg), FD 12-9 (10 mg/kg), sorafenib (10 mg/kg) + GF120918 (10 mg/kg) and

GF120918 (10 mg/kg) or no treatment. Treatment groups involving GF120918 ended abruptly because animals were all dead in those treatment groups. A total of ten treatments (q.o.d. x 10) were given. Fold changes were shown in mean \pm SEM (n = 6 - 9).

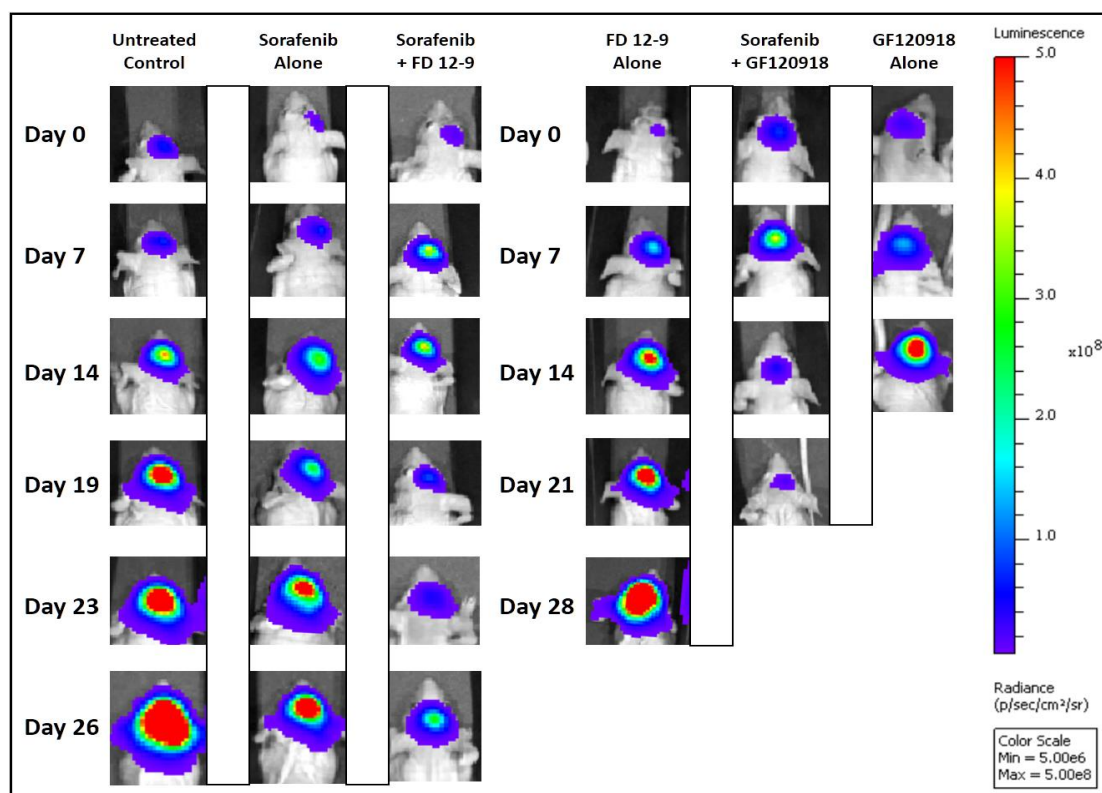


Figure 6.2.2G *In vivo* efficacy of sorafenib with or without different modulators against orthotopic model of GBM as monitored by IVIS technique.

Nude mice from Figure 6.2.2F were monitored on the days indicated using IVIS. On the day of imaging, all mice were treated with ketamine/xylazine solution for anesthesia (100 mg/kg: 10 mg/kg; I.P.), followed by an injection of D-luciferin (150 mg/kg; I.P.). After thirty images were taken in 30 minutes by IVIS, the highest signal among the 30 images was taken as the BLI signal. All images were presented in the same range of color scale (n = 6 - 9).

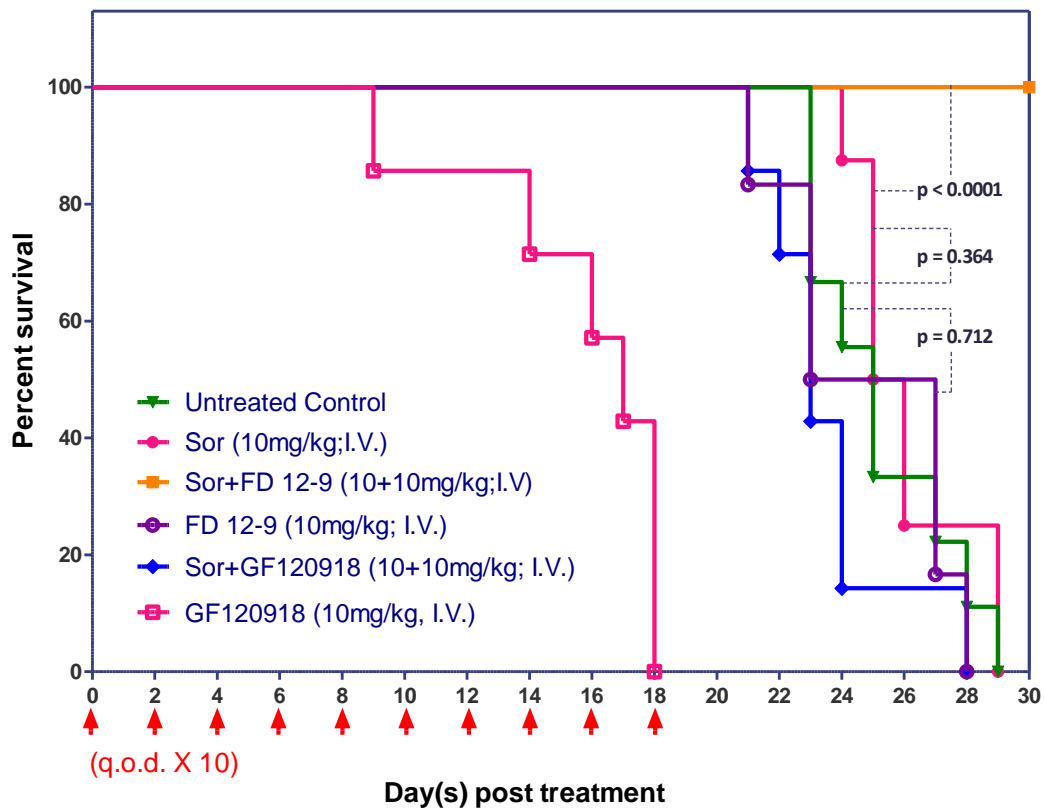


Figure 6.2.2H Survival curve of orthotopic GBM-bearing mice after receiving treatment of sorafenib with or without different modulators.

Animal survival from the previous experiment in Figure 6.2.2F were recorded and shown here. Mice in treatment group of sorafenib combined FD 12-9 survive for the longest period. Treatment of GF120918 alone has the shortest survival span. The Log-Rank test was used to evaluate the significances of different survival curves (n = 6 - 9).

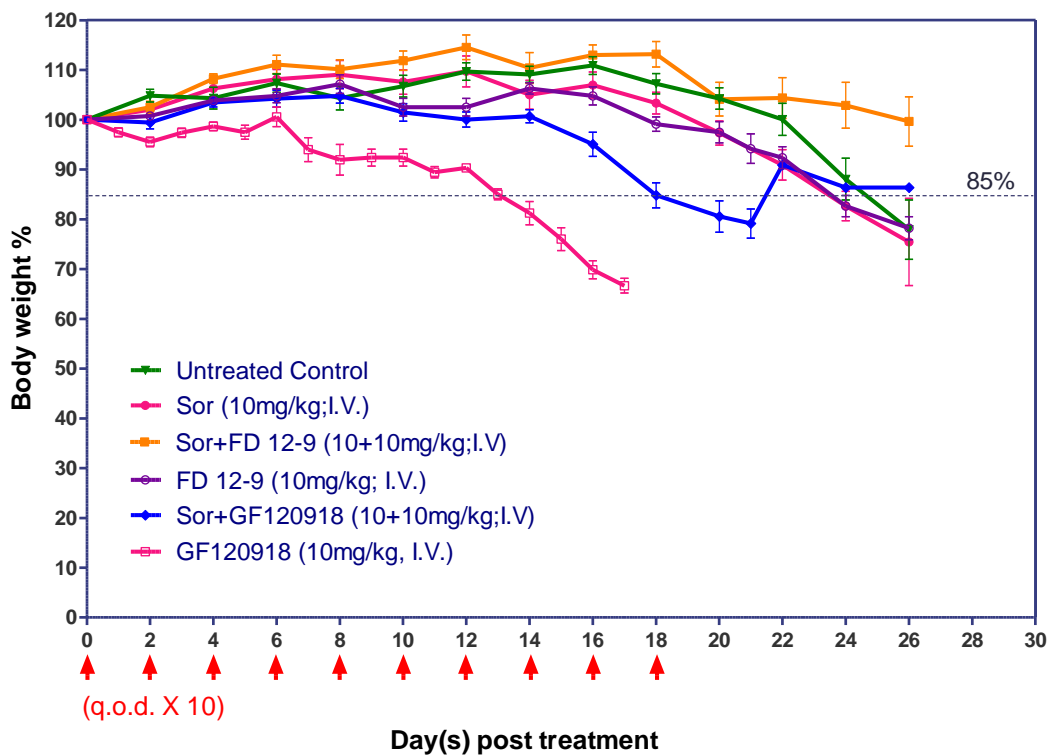


Figure 6.2.2I Body weight changes of U87MG-RedFluc-bearing mice after receiving sorafenib with or without FD 12-9 or GF120918.

The body weight of mice receiving treatments of sorafenib combined with FD 12-9 decrease slower than that of other treatment groups. Treatment of sorafenib plus GF120918 and GF120918 alone demonstrated severe toxicity effect. Weight changes were shown in mean \pm SEM (n = 6 - 9).

The body weight measurements also indicated that the group with co-administration of FD 12-9 and sorafenib can maintain a steady body weight gain and has the highest body weight among all treatment groups. On the contrary, sickness behaviors, including decrease of motor activity, decrease of body temperature and loss of appetite, were found in the treatment group with GF120918, resulting in the highest drop in body weight. This result suggests a potential toxicity of GF120918.

6.2.3 The *in vivo* efficacy study of sorafenib combined with FD 12-9 in mice with TMZ-resistant recurrent GBM tumor

As a first-line anti-cancer drug for GBM, TMZ has become the standard treatment for GBM patients. Unfortunately, relapse has been observed in most GBM patients treated with TMZ. TMZ does not work anymore in recurrent GBM patients. To understand the efficacy of the combination sorafenib and FD 12-9 in recurrent GBM which is TMZ-resistant, a TMZ-resistant animal model was developed by *in vivo* selection with TMZ.

To mimic the standard treatment of TMZ, a group of Balb/c nude mice with orthotopic implantation of U87MG-RedFluc cells was treated with TMZ (10 mg/kg; I.V.) every other day for ten times (q.o.d. x 10) (Figure 6.2.3A). The efficacy of TMZ in the first round treatment was monitored by IVIS every few days. After the completion of the first round treatment, mice were monitored further (Figure 6.2.3A, B). Once relapse was observed in any mouse, it would be selected and assigned to one of three groups of second round treatment (1) untreated control, 2) sorafenib + FD 12-9 (10 + 10 mg/kg; I.V.) or 3) TMZ (10 mg/kg; I.V.)). The second round treatment was similar to the first round: every other day for ten times (q.o.d. x 10). Mice were monitored for another 26 days from the relapse (Figure 6.2.3A, B). At the same time, the body weight change and animal death were also recorded (Figure 6.2.3B, C).

It was found that, in the first round treatment, TMZ (10 mg/kg; I.V., q.o.d.x10) could effectively inhibit the tumor growth (Figure 6.2.3A, B). Relapse, however,

occurred in almost all mice. Second round of TMZ treatment (10 mg/kg; I.V., q.o.d.x10) failed to suppress tumor growth suggesting that the relapse U87MG xenograft was TMZ-resistant. The growth rate of TMZ-treated group was similar to that of the untreated group. On the contrary, when mice were treated with sorafenib combined with FD 12-9 (10 +10 mg/kg; I.V., q.o.d.x10), tumor growth of recurrent GBM were inhibited significantly (Figure 6.2.3A, B). These results indicated that the strong inhibitory effect of TMZ on GBM was only limited to newly diagnosed GBMs which have not been treated with TMZ. But once GBM recurred, TMZ showed very limited inhibition on GBM. This animal model closely resembled the clinical picture. In contrast, the combination of sorafenib and FD 12-9 remained effective in treating TMZ-resistant GBM.

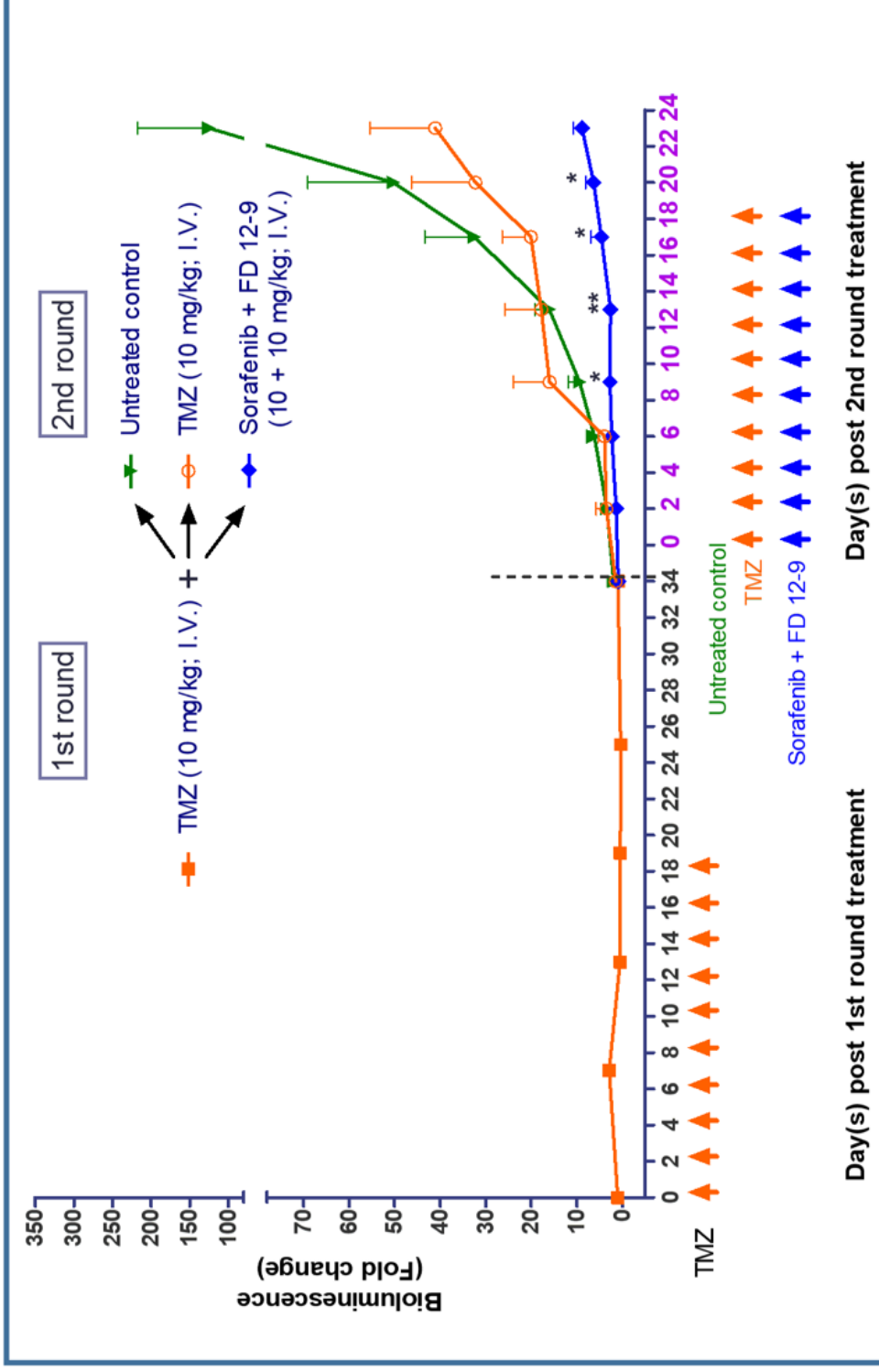


Figure 6.2.3A Establishment of TMZ-resistant relapse model of GBM and its response to combination treatment of TMZ and FD 12-9.

Mice with orthotopically-implanted U87MG-RedFluc were treated with TMZ in the first round of treatment every other day for 10 days (10 mg/kg; I.V.; n=20) as indicated by the arrows. When relapse occurred, mice were treated with one of the 3 second round treatments including 1) untreated control, 2) sorafenib + FD 12-9 (10 + 10 mg/kg; I.V.) or 3) TMZ (10 mg/kg; I.V.). Finally, 18 mice out of 20 were used in second round treatment. Treatment frequency of second round was the same as the first-round treatments as indicated by arrows. The BLI signals of each animal were obtained by IVIS and normalized to the initial day when treatment started. Fold changes of second treatment were shown in mean \pm SEM (n=6). *, $p < 0.05$; **, $p < 0.01$ (group 1) versus group 2).

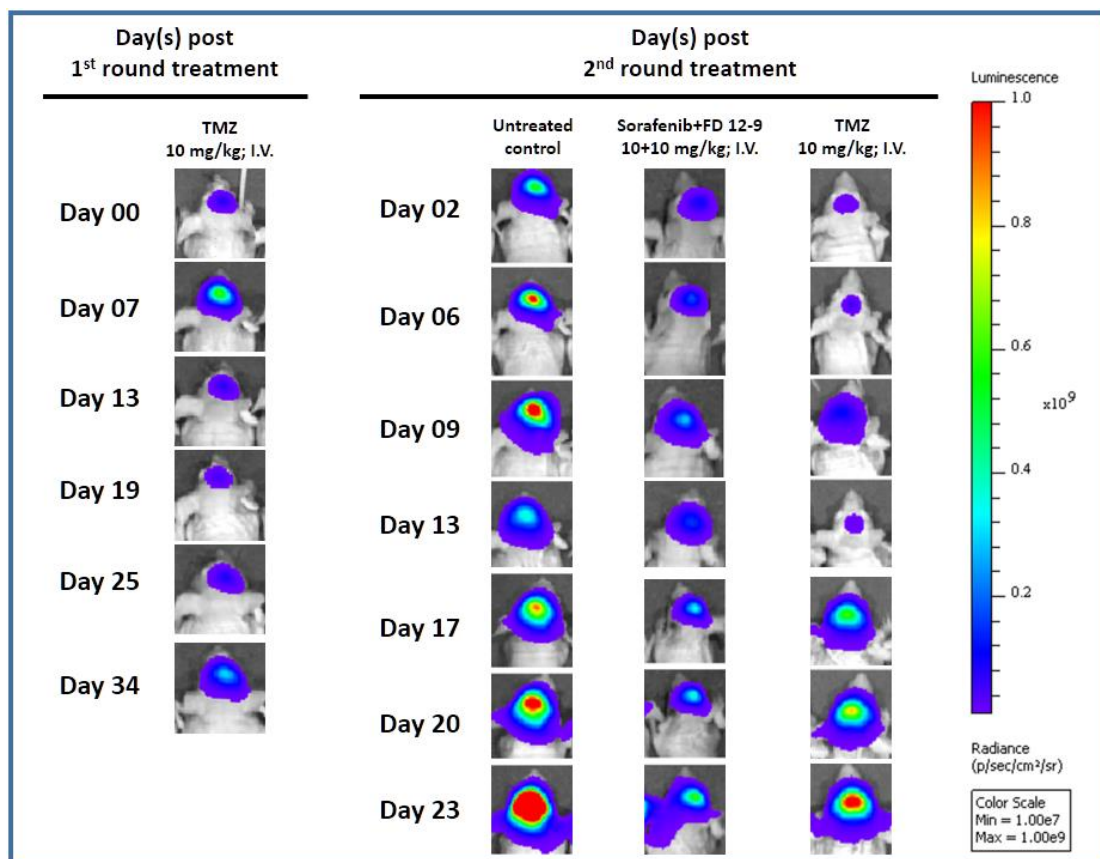


Figure 6.2.3B Establishment of TMZ-resistant relapse model of GBM and its response to combination treatment of TMZ and FD 12-9 (IVIS signals). Nude mice from Figure 6.2.2B were monitored on the days indicated using IVIS. All images were presented in the same range of color scale.

In the second round treatment, no death was observed in the combination group of sorafenib and FD 12-9. Mice in untreated control group started to die early on day 17, and half of them died by the end of the experiment. One mouse in TMZ group also die early on day 11 (Figure 6.2.3C). Body weight of untreated control group dropped rapidly for more than 15% weight on day 14. TMZ-treated group also have a significant weight loss. Conversely, only slight body weight decrease (smaller than 5%) was observed in combination group (Figure 6.2.3D). These data suggested that TMZ did not inhibit the tumor growth in 2nd round

treatment, while sorafenib in combination with FD 12-9 did, which was reflected on the body weight loss and survival rate.

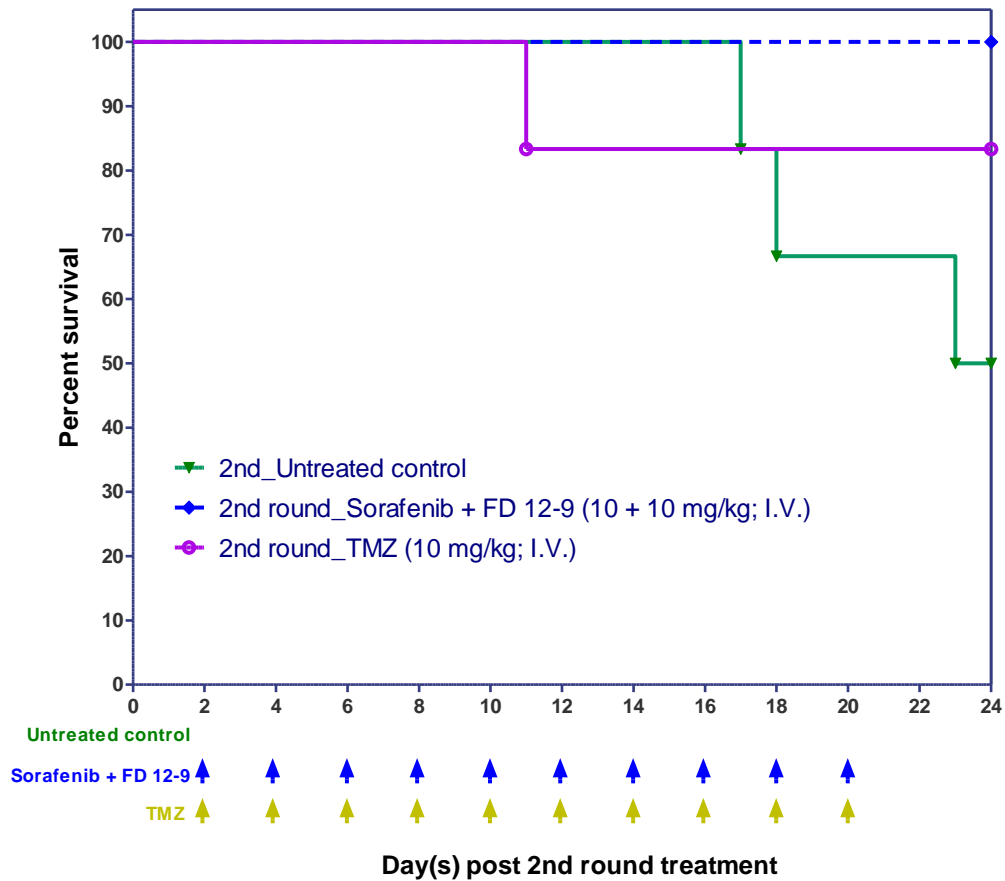


Figure 6.2.2C Survival curve of TMZ-resistant GBM animal model in response to TMZ or combination.

Survival data for the second-round treatment of TMZ-resistant GBM animal model in Figure 6.2.3A was recorded here (n = 6).

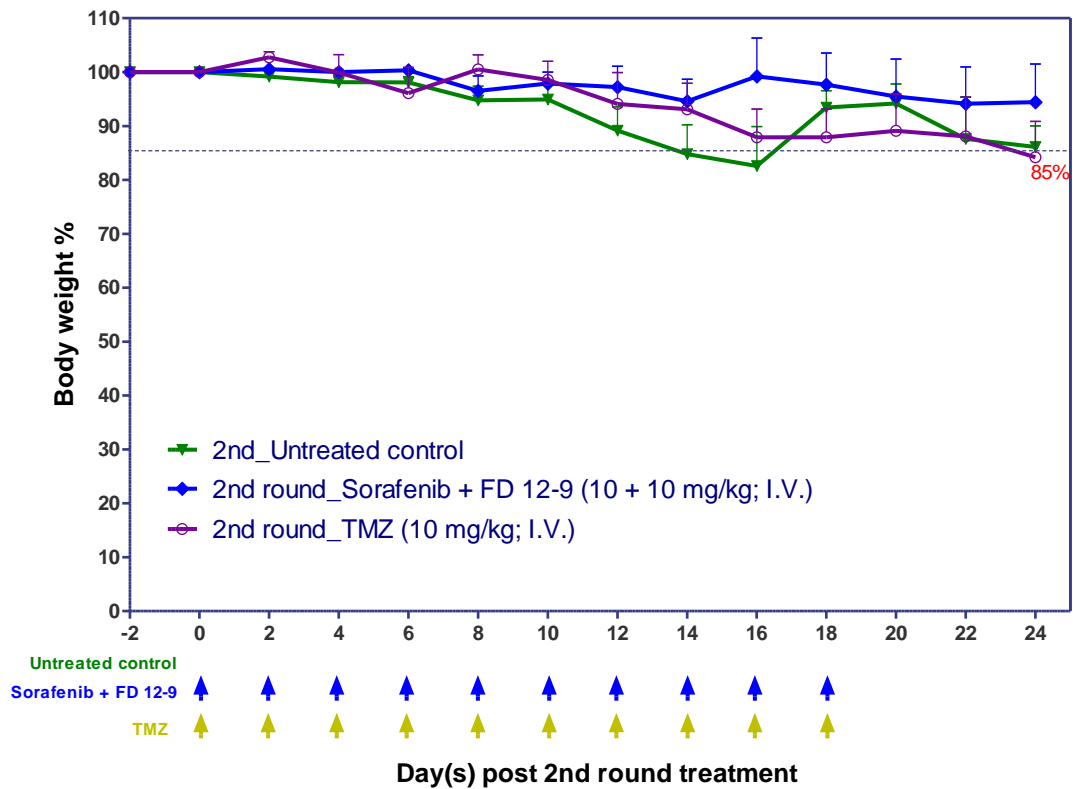


Figure 6.2.3D Body weight changes of TMZ-resistant GBM-bearing mice in response to TMZ or combination (FD 12-9 + sorafenib) treatment.

Body weight changes for the second-round treatment of TMZ-resistant GBM animal model in Figure 6.2.3A was recorded here. Weight changes were shown in mean \pm SEM (n = 6).

6.3 Discussion and summary

The annual incidence of malignant gliomas in Hong Kong (1 case per 100,000) is much lower than that of United States (5.97 cases per 100,000) (Chan et al., 2017; Pu, 2016). Among these malignant gliomas, GBM is the most aggressive brain cancer constituting 42% of all malignant gliomas in Hong Kong. The incidence of GBM (primary and secondary) in the U.S.A. is 3.2 per 100,000 (Ostrom et al., 2014), which is 7-fold higher than that of Hong Kong. In the past four decades, no significant improvement of prognosis has been found and few treatments have been developed. The most widely-used anti-cancer drug for GBM is still temozolomide (TMZ) approved in 2000.

In this project, sorafenib is selected as the candidate to treat GBM, though clinical trials of using sorafenib to treat GBM did not yield significant difference compared with controls (Table 1.2.3) in the past ten years. It is hypothesized that the failure of clinical trials for GBM involving sorafenib is possibly due to the limited penetration of sorafenib to pass through BBB. Based on the knocked-out mice experiments (Lagas et al., 2010b), BCRP and P-gp expressing in BBB are working together to restrict the penetration of sorafenib synergistically. Although co-administration of GF120918 can inhibit the efflux of sorafenib by inhibiting both P-gp and BCRP, its use is limited by severe toxicity. Nevertheless, this demonstrated the possibility of using a dual selective inhibitor to modulate BCRP and P-gp for treating GBM.

Taking the advantage of the large library of synthetic flavonoid dimers

discovered in our group, a series of flavonoid dimers with dual selective modulating effect against P-gp and BCRP was synthesized and used in this project for discovering new dual inhibitors of P-gp and BCRP. Among those flavonoid dimers, FD 12-9 was selected as the candidate for subsequent pharmacokinetic studies and *in vivo* efficacy studies because of its potent BCRP modulating effect (at sub-nanomolar range) and strong P-gp modulating effect (at around 200 nM range) and low toxicity to human fibroblast cells (Table 3.2.2). Pharmacokinetics studies of sorafenib in the presence and absence of FD 12-9 suggested that the brain accumulation of sorafenib can be improved by FD 12-9 as well as the brain-to-plasma ratio (Figure 5.2.2A&C).

Together with the potency of sorafenib against U87MG cells *in vitro* (Table 3.2.1) and the modulating effect of FD 12-9 against P-gp and BCRP *in vitro* (Table 3.2.2) and *in vivo* (Figure 5.2.2A-C), a combination of FD 12-9 and sorafenib was used to inhibit P-gp and BCRP in BBB to potentiate the accumulation of sorafenib in brain to treat GBM in subsequent animal model.

Before the efficacy studies were conducted, an experiment focusing on the toxicity of different treatments had been done and result showed that all treatments were safe to Balb/c mice under the treatment protocol (10 mg/kg; I.V.; q.o.d. X 10) (Figure 6.2.1).

Three efficacy experiments were performed using U87MG-RedFluc tumor-bearing Balb/c nude mice in this chapter. The objective of the first experiment is to prove that FD 12-9 can enhance the penetration of sorafenib in the brain,

thereby increasing its potency against GBM. The combination treatment of sorafenib and FD 12-9 displayed a potent inhibitory effect on GBM tumor growth in nude mice, while sorafenib alone did not. The GBM xenograft tumor in the combination group, however, grew back from day 14 onwards after a total of 7 injections (Figure 6.2.2B, E). As the combination treatment was safe, resulting in a relatively small decrease in body weight (Figure 6.2.2C) and the survival rate was high (Figure 6.2.2D), it was possible to increase the dosing frequency from 7 to 10 in the second trial (q.o.d. x 10). In addition, a positive control, GF120918 was included for comparison. Combination treatment of sorafenib and FD 12-9 displayed an even more potent inhibitory effect on tumor growth (Figure 6.2.2F, G). Interestingly, sorafenib alone, when dosed at q.o.d X10 also showed a small, but significant effect compared to untreated control. However, the effect was not as potent as that in the combination group (Figure 6.2.2F, G). The mice in the sorafenib alone group started to lose body weight from day 16 and lost more than 15% of their initial body weight from day 24 onwards when animal deaths also appeared (Figure 6.2.2G, H). These results suggested that sorafenib had a modest inhibitory effect on GBM tumor when administered alone. Only when it was combined with FD 12-9 (q.o.d. X 10) will a significant inhibition of tumor growth be observed. No body weight loss or death can be achieved. These results indicated that sorafenib alone was not effective in treating GBM due to the limited accumulation in brain. With the modulating effect of FD 12-9 on P-gp and BCRP in BBB, the efficacy of sorafenib could be

significantly improved.

GF120918 was more effective than FD 12-9 in elevating sorafenib level in the brain in pharmacokinetic experiment. It was, however, found to be too toxic compared to FD 12-9 in GBM orthotopic model. Indeed, GF120918 alone was significantly more toxic than FD 12-9. This result suggested that FD 12-9 was the most potent dual inhibitor in the literature and the safest one in rodents.

Combination of sorafenib and FD 12-9 also showed potent inhibitory effect on suppressing tumor growth in recurrent TMZ-resistant GBM model. Mice with GBM were treated with TMZ at the beginning (first round treatment) and then monitored until relapse occurred. Mice with recurrent GBM were assigned into three groups for different treatments. Without any treatment, recurrent GBM grew fast in mice (Figure 6.2.3A, B) and induced severe body weight loss and low survival rate (Figure 6.2.3C, D). TMZ did not show any significant inhibitory effect in the second-round treatment on tumor growth. Whereas the combination of sorafenib and FD 12-9 demonstrated striking effect on suppressing the growth of TMZ-resistant GBM. This encouraging result probably stems from the fact that TMZ and sorafenib have a different mechanism of action.

This recurrence and TMZ resistance in the recurrent model clearly reflect the clinical situation. This relapsed and TMZ-resistant GBM animal model might be useful in the future for drug screening studies. Overall, our data provides a possible treatment for recurrent and TMZ-resistant GBM.

CHAPTER 7: CONCLUSIONS AND PERSPECTIVES

As a first-line treatment for GBM patients, TMZ resistance has occurred in many cases. *In vitro* data suggest that sorafenib is much more potent than TMZ in treating U87MG-RedFluc cells (31-fold lower in term of IC₅₀, Table 3.2.1). The fact that sorafenib has already been approved for treating kidney cancer and hepatocellular carcinoma makes it more convenient to be developed as a drug for GBM. However, sorafenib has been tried in treating GBM but with unsatisfactory results (Amaravadi et al., 2007; Den et al., 2013; Hottinger et al., 2014a; Siegelin et al., 2010). Due to the unsatisfactory results in clinical trials, sorafenib is currently not considered as a viable therapeutic strategy for treating GBM (Hottinger et al., 2014b; Jakubowicz-Gil et al., 2014a).

One hypothesis is that the distribution sorafenib is restricted in the brain by the BBB. The *in vitro* MDCKII directional transport assay has proved that two ABC-transporters, BCRP and P-gp, play a major role in the efflux of sorafenib in this model. Addition of FD 12-9 or GF120918 to MDCKII cells expressing P-gp or BCRP can significantly inhibit the efflux of sorafenib back to the level of wild-type monolayer. These results indicate that sorafenib is a substrate for both P-gp and BCRP, and FD 12-9 and GF120918 are capable of inhibiting both P-gp and BCRP at the same time. Considering that the MDCKII monolayer is a well-established *in vitro* model for BBB, dual inhibitors like FD 12-9 and GF120918

for P-gp and BCRP are potential candidates to overcome the obstacle of the BBB to improve the accumulation of sorafenib in the brain.

To further confirm that FD 12-9 or GF120918 can help sorafenib to penetrate through BBB, pharmacokinetic studies of sorafenib with or without modulators have been carried out. The pharmacokinetic profiles of sorafenib in the brain was similar when mice were administered with a dose of 10 mg/kg or 20 mg/kg of sorafenib. Even when administered with 30 mg/kg of sorafenib, the AUC_{brain} of sorafenib could only be increased slightly, and the pharmacokinetic profile was similar to that of 10 mg/kg or 20 mg/kg alone. When sorafenib (10 mg/kg) was co-administered with FD 12-9 (10 mg/kg) or GF129118 (10 mg/kg), however, the AUC_{brain} of sorafenib was dramatically increased as well as the pharmacokinetic profile curve. The half-life of sorafenib was also prolonged. Meanwhile, the plasma concentration of sorafenib in the combination group was only moderately higher than those in sorafenib alone groups (10, 20 and 30 mg/kg). The brain-to-plasma ratios (AUC_{brain}/AUC_{plasma}) of sorafenib in two combination groups (sorafenib + FD 12-9 and sorafenib + GF120918), which were 0.18 and 0.42, respectively, were much higher than those of 20 mg/kg or 30 mg/kg of sorafenib alone, which were 0.03 and 0.04, respectively. GF120918 was more effective than FD 12-9. GF120918 also stayed longer in the brain with a higher concentration than FD 12-9. The pharmacokinetic studies of sorafenib with or without modulators clearly indicate that FD 12-9 can inhibit both P-gp and BCRP transporters in the BBB to elevate the accumulation of

sorafenib in the brain. Considering the potent cytotoxicity effect of sorafenib towards U87MG-RedFluc cancer cells, FD 12-9 is a promising modulator to be used together with sorafenib to treat GBM.

In vivo efficacy studies using U87MG-RedFluc orthotopic xenograft GBM model in Balb/c nude mice indicated that sorafenib alone displayed no inhibitory effect on tumor growth whereas co-administration of FD 12-9 and sorafenib resulted in strong inhibitory effect on tumor growth with only a few injections (q.o.d. X 7). In addition, once the number of injections was increased to 10 (q.o.d. X 10), the combination treatment of FD 12-9 and sorafenib worked even better. Treatment of FD 12-9 alone did not show any inhibitory effect on tumor growth. Although combination group of GF120918 and sorafenib did exhibit quite good inhibitory effect, such combination was toxic in the mice as indicated in reduced survival and body weight loss. This was possibly due the toxicity of GF120918 alone as such GF120918 alone group also suffered from significant body weight loss, and mice in this group died early.

Overall survival of combination treatment group of FD 12-9 and sorafenib achieved the longest survival span under both treatment frequency (q.o.d X 7 and q.o.d. X 10). Both GF120918 alone or in combination with sorafenib presented serious toxicity to mice. The longer survival span of the group of GF120918 plus sorafenib might have benefited from the shrinkage of tumor, because GF120918 did help sorafenib to get into the brain.

The third *in vivo* efficacy experiment used TMZ-treated GBM-bearing mice to

mimic the relapse of GBM in patients who took TMZ as the standard treatment. Without any treatment, tumor size in the mice grew very fast with severe weight loss and low survival rate. With TMZ alone, no significant effect was observed suggesting TMZ-resistance once relapse occurred. The combination treatment group of FD 12-9 and sorafenib, however, not only showed potent suppressing effect on tumor growth but also induced no death and no significant decrease in body weight. These results suggested that sorafenib combined with FD 12-9 can inhibit GBM growth even in TMZ-resistant mice. Sorafenib combined with FD 12-9 might be a promising second-line therapy for GBM patients, for both newly-diagnosed and recurrent GBM patients.

In summary, FD 12-9 can reverse P-gp and BCRP mediated active efflux in the BBB. As expected, FD 12-9 can not only elevate the accumulation of sorafenib in the brain but also help sorafenib to suppress GBM tumor growth in mice model significantly. Unlike GF120918, FD 12-9 showed no toxicity effect, which confers FD 12-9 a significant safety advantage.

This project can be further developed in two directions. First one is the search of more potent modulators for the BBB and more potential clinically-used anti-cancer drugs for treating GBM. The second one is to set up a patient-derived tumor xenograft which will have more clinical significance.

Modulators for the BBB is the most important part in this study. Once we find a safe and reliable way to overcome the BBB, the choices of anti-cancer drugs will increase enormously as many of them are excluded from BBB due to the

efflux by P-gp and BCRP. Furthermore, recurrence of GBM occurs in most GBM patients. Even though a novel treatment is proved effective to GBM in nude mice, it remains uncertain whether it would work in recurrent GBM because the tumor model used in this study was established by implanting naïve U87MG-RedFluc cells in nude mice. This is why we also established an *in vivo* model of recurrent GBM to compare the effect of TMZ and sorafenib combined with FD 12-9.

References

Abbott, N.J., Patabendige, A.A., Dolman, D.E., Yusof, S.R., and Begley, D.J. (2010). Structure and function of the blood–brain barrier. *Neurobiology of disease* 37, 13-25.

Adnane, L., Trail, P.A., Taylor, I., and Wilhelm, S.M. (2006). Sorafenib (BAY 43-9006, Nexavar®), a dual-action inhibitor that targets RAF/MEK/ERK pathway in tumor cells and tyrosine kinases VEGFR/PDGFR in tumor vasculature. *Methods in enzymology* 407, 597-612.

Agarwal, S., Jain, R., Pal, D., and Mitra, A.K. (2007). Functional characterization of peptide transporters in MDCKII–MDR1 cell line as a model for oral absorption studies. *International journal of pharmaceutics* 332, 147-152.

Agarwal, S., Sane, R., Ohlfest, J.R., and Elmquist, W.F. (2011). The role of the breast cancer resistance protein (ABCG2) in the distribution of sorafenib to the brain. *Journal of Pharmacology and Experimental Therapeutics* 336, 223-233.

Aller, S.G., Yu, J., Ward, A., Weng, Y., Chittaboina, S., Zhuo, R., Harrell, P.M., Trinh, Y.T., Zhang, Q., and Urbatsch, I.L. (2009). Structure of P-glycoprotein reveals a molecular basis for poly-specific drug binding. *science* 323, 1718-1722.

Allikmets, R., Gerrard, B., Hutchinson, A., and Dean, M. (1996). Characterization of the human ABC superfamily: isolation and mapping of 21 new genes using the expressed sequence tags database. *Human molecular genetics* 5, 1649-1655.

Amaravadi, R., Schuchter, L., McDermott, D., Kramer, A., Giles, L., Troxel, A., Medina, C., Nathanson, K., O'Dwyer, P., and Flaherty, K. (2007). Updated results of a randomized phase II study comparing two schedules of temozolomide in combination with sorafenib in patients with advanced melanoma. *Journal of clinical oncology* 25, 8527-8527.

Baglietto, L., Giles, G.G., English, D.R., Karahalios, A., Hopper, J.L., and Severi, G. (2011). Alcohol consumption and risk of glioblastoma; evidence from the Melbourne Collaborative Cohort Study. *International journal of cancer* 128, 1929-1934.

Ballabh, P., Braun, A., and Nedergaard, M. (2004). The blood–brain barrier: an overview: structure, regulation, and clinical implications. *Neurobiology of disease* 16, 1-13.

Barnholtz-Sloan, J.S., Sloan, A.E., and Schwartz, A.G. (2003). Relative survival rates and patterns of diagnosis analyzed by time period for individuals with primary malignant brain tumor, 1973–1997. *Journal of neurosurgery* 99, 458-466.

Basselin, M., Lawrence, F., and Robert-Gero, M. (1996). Pentamidine uptake in *Leishmania donovani* and *Leishmania amazonensis* promastigotes and axenic amastigotes. *Biochem J* 315, 631-634.

Baumann, B.C., Dorsey, J.F., Benci, J.L., Joh, D.Y., and Kao, G.D. (2012). Stereotactic intracranial implantation and in vivo bioluminescent imaging of tumor xenografts in a mouse model system of glioblastoma multiforme. *JoVE (Journal of Visualized Experiments)*, e4089-e4089.

Begley, D.J. (2004). ABC transporters and the blood-brain barrier. *Current pharmaceutical design* 10, 1295-1312.

Blackwell, K.L., Burstein, H.J., Storniolo, A.M., Rugo, H., Sledge, G., Koehler, M., Ellis, C., Casey, M., Vukelja, S., and Bischoff, J. (2010). Randomized study of Lapatinib alone or in combination with trastuzumab in women with ErbB2-positive, trastuzumab-refractory metastatic breast cancer. *Journal of clinical oncology* 28, 1124-1130.

Brandes, A., Tosoni, A., Cavallo, G., Bertorelle, R., Gioia, V., Franceschi, E., Biscuola, M., Blatt, V., Crino, L., and Ermani, M. (2006). Temozolomide 3 weeks on and 1 week off as first-line therapy for recurrent glioblastoma: phase II study from gruppo italiano cooperativo di neuro-oncologia (GICNO). *The British Journal of Cancer* 95, 1155.

Brandes, A.A., Tosoni, A., Basso, U., Reni, M., Valduga, F., Monfardini, S., Amistà, P., Nicolardi, L., Sotti, G., and Ermani, M. (2004). Second-line chemotherapy with irinotecan plus carmustine in glioblastoma recurrent or progressive after first-line temozolomide chemotherapy: a phase II study of the Gruppo Italiano Cooperativo di Neuro-Oncologia (GICNO). *Journal of clinical oncology* 22, 4779-4786.

Brose, M.S., Nutting, C., Jarzab, B., Elisei, R., Siena, S., Bastholt, L., de la Fouchardiere, C., Pacini, F., Paschke, R., and Shong, Y.K. (2013). Sorafenib in locally advanced or metastatic patients with radioactive iodine-refractory differentiated thyroid cancer: The phase III DECISION trial (American Society of Clinical Oncology).

Cavenee, W. (2000). High-grade gliomas with chromosome 1p loss. *Journal of neurosurgery* 92, 1080.

Chan, D., Hsieh, S.Y., Lau, C.K., Kam, M.K., Loong, H.H., Tsang, W., Poon, D., and Poon, W. (2017). Ten-year review of survival and management of malignant glioma in Hong Kong. *Hong Kong medical journal= Xianggang yi xue za zhi* 23, 134-139.

Chan, K.-F., Wong, I.L., Kan, J.W., Yan, C.S., Chow, L.M., and Chan, T.H. (2012). Amine linked flavonoid dimers as modulators for P-glycoprotein-based multidrug resistance: structure–activity relationship and mechanism of modulation. *Journal of medicinal chemistry* 55, 1999-2014.

Chan, K.-F., Zhao, Y., Burkett, B.A., Wong, I.L., Chow, L.M., and Chan, T.H. (2006). Flavonoid dimers as bivalent modulators for P-glycoprotein-based multidrug resistance: synthetic apigenin homodimers linked with defined-length poly (ethylene glycol) spacers increase drug retention and enhance chemosensitivity in resistant cancer cells. *Journal of medicinal chemistry* 49, 6742-6759.

Chan, K.F., Zhao, Y., Chow, T.W., Yan, C.S., Ma, D.L., Burkett, B.A., Wong, I.L., Chow, L., and Chan,

T.H. (2009). Flavonoid Dimers as Bivalent Modulators for P-Glycoprotein-Based Multidrug Resistance: Structure–Activity Relationships. *ChemMedChem* 4, 594-614.

Chang, Y.S., Adnane, J., Trail, P.A., Levy, J., Henderson, A., Xue, D., Bortolon, E., Ichetovkin, M., Chen, C., and McNabola, A. (2007). Sorafenib (BAY 43-9006) inhibits tumor growth and vascularization and induces tumor apoptosis and hypoxia in RCC xenograft models. *Cancer chemotherapy and pharmacology* 59, 561-574.

Chen, Y., Pan, L., Jiang, M., Li, D., and Jin, L. (2016). Nanostructured lipid carriers enhance the bioavailability and brain cancer inhibitory efficacy of curcumin both in vitro and in vivo. *Drug delivery* 23, 1383-1392.

Chen, Z.S., and Tiwari, A.K. (2011). Multidrug resistance proteins (MRPs/ABCCs) in cancer chemotherapy and genetic diseases. *FEBS journal* 278, 3226-3245.

Childs, S., and Ling, V. (1994). The MDR superfamily of genes and its biological implications. *Important advances in oncology*, 21.

Clark, A.J., Fakurnejad, S., Ma, Q., and Hashizume, R. (2016). Bioluminescence Imaging of an Immunocompetent Animal Model for Glioblastoma. *Journal of visualized experiments: JoVE*.

COBBS, C. (2009). A viral link to glioblastoma?

Cohen, M.H., Johnson, J.R., and Pazdur, R. (2005). Food and Drug Administration Drug approval summary: temozolomide plus radiation therapy for the treatment of newly diagnosed glioblastoma multiforme. *Clinical cancer research* 11, 6767-6771.

Cole, S., Bhardwaj, G., Gerlach, J., Mackie, J., Grant, C., Almquist, K., Stewart, A., Kurz, E., Duncan, A., and Deeley, R. (1992). Overexpression of a transporter gene in a multidrug-resistant human lung cancer cell line. *science* 258, 1650-1654.

Cole, S., and Deeley, R.G. (1993). Multidrug resistance-associated protein: sequence correction. *science* 260, 879-879.

Cooray, H.C., Blackmore, C.G., Maskell, L., and Barrand, M.A. (2002). Localisation of breast cancer resistance protein in microvessel endothelium of human brain. *Neuroreport* 13, 2059-2063.

Cordon-Cardo, C., O'Brien, J.P., Casals, D., Rittman-Grauer, L., Biedler, J.L., Melamed, M.R., and Bertino, J.R. (1989). Multidrug-resistance gene (P-glycoprotein) is expressed by endothelial cells at blood-brain barrier sites. *Proceedings of the National Academy of Sciences* 86, 695-698.

Culot, M., Lundquist, S., Vanuxeem, D., Nion, S., Landry, C., Delplace, Y., Dehouck, M.-P., Berezowski, V., Fenart, L., and Cecchelli, R. (2008). An in vitro blood-brain barrier model for high throughput (HTS) toxicological screening. *Toxicology in vitro* 22, 799-811.

de Vries, H.E., Kuiper, J., de Boer, A.G., Van Berkel, T.J., and Breimer, D.D. (1997). The blood-brain barrier in neuroinflammatory diseases. *Pharmacological reviews* 49, 143-156.

de Vries, N.A., Zhao, J., Kroon, E., Buckle, T., Beijnen, J.H., and van Tellingen, O. (2007). P-glycoprotein and breast cancer resistance protein: two dominant transporters working together in limiting the brain penetration of topotecan. *Clinical cancer research* 13, 6440-6449.

Dean, M., Hamon, Y., and Chimini, G. (2001). The human ATP-binding cassette (ABC) transporter superfamily. *Journal of lipid research* 42, 1007-1017.

Den, R.B., Kamrava, M., Sheng, Z., Werner-Wasik, M., Dougherty, E., Marinucchi, M., Lawrence, Y.R., Hegarty, S., Hyslop, T., and Andrews, D.W. (2013). A phase I study of the combination of sorafenib with temozolomide and radiation therapy for the treatment of primary and recurrent high-grade gliomas. *International Journal of Radiation Oncology* Biology* Physics* 85, 321-328.

Dolecek, T.A., Propp, J.M., Stroup, N.E., and Kruchko, C. (2012). CBTRUS statistical report: primary brain and central nervous system tumors diagnosed in the United States in 2005–2009. *Neuro-oncology* 14, v1-v49.

Doyle, L.A., Yang, W., Abruzzo, L.V., Krogmann, T., Gao, Y., Rishi, A.K., and Ross, D.D. (1998). A multidrug resistance transporter from human MCF-7 breast cancer cells. *Proceedings of the National Academy of Sciences* 95, 15665-15670.

Eisen, T., Ahmad, T., Flaherty, K., Gore, M., Kaye, S., Marais, R., Gibbens, I., Hackett, S., James, M., and Schuchter, L. (2006). Sorafenib in advanced melanoma: a Phase II randomised discontinuation trial analysis. *British journal of cancer* 95, 581-586.

Estudante, M., Morais, J.G., Soveral, G., and Benet, L.Z. (2013). Intestinal drug transporters: an overview. *Advanced drug delivery reviews* 65, 1340-1356.

Ewend, M.G., Brem, S., Gilbert, M., Goodkin, R., Penar, P.L., Varia, M., Cush, S., and Carey, L.A. (2007). Treatment of single brain metastasis with resection, intracavity carmustine polymer wafers, and radiation therapy is safe and provides excellent local control. *Clinical cancer research* 13, 3637-3641.

Ferreira, R.J., Ferreira, M.-J.U., and dos Santos, D.J. (2012). Insights on P-glycoprotein's efflux mechanism obtained by molecular dynamics simulations. *Journal of Chemical Theory and Computation* 8, 1853-1864.

Fonkem, E., and Wong, E.T. (2012). NovoTTF-100A: a new treatment modality for recurrent glioblastoma. *Expert review of neurotherapeutics* 12, 895-899.

Fulton, D., Urtasun, R., Scott-Brown, I., Johnson, E., Mielke, B., Curry, B., Huyser-Wierenga, D., Hanson, J., and Feldstein, M. (1992). Increasing radiation dose intensity using hyperfractionation in patients with malignant glioma. *Journal of neuro-oncology* 14, 63-72.

Gabathuler, R. (2010). Approaches to transport therapeutic drugs across the blood–brain barrier to treat brain diseases. *Neurobiology of disease* 37, 48-57.

Galanis, E., Anderson, S.K., Lafky, J.M., Uhm, J.H., Giannini, C., Kumar, S.K., Kimlinger, T.K., Northfelt, D.W., Flynn, P.J., Jaeckle, K.A., *et al.* (2013). Phase II study of bevacizumab in combination with sorafenib in recurrent glioblastoma (N0776): a north central cancer treatment group trial. *Clinical cancer research : an official journal of the American Association for Cancer Research* 19, 4816-4823.

Gallego, O. (2015). Nonsurgical treatment of recurrent glioblastoma. *Current oncology* 22, e273.

Gettinger, S., Rizvi, N., Chow, L., Borghaei, H., Brahmer, J., Juergens, R., Shepherd, F., Laurie, S., Gerber, D., and Goldman, J. (2014). Nivolumab (Anti-PD-1; BMS-936558, ONO-4538) in Combination With Platinum-Based Doublet Chemotherapy (PT-DC) in Advanced Non-Small Cell Lung Cancer (NSCLC). *Annals of Oncology* 25, iv363-iv363.

Goldstein, L.J., Pastan, I., and Gottesman, M.M. (1992). Multidrug resistance in human cancer. *Critical reviews in oncology/hematology* 12, 243-253.

Hansson, G.C., Simons, K., and van Meer, G. (1986). Two strains of the Madin-Darby canine kidney (MDCK) cell line have distinct glycosphingolipid compositions. *The EMBO journal* 5, 483.

Higgins, C.F. (1992). ABC transporters: from microorganisms to man. *Annual review of cell biology* 8, 67-113.

Hottinger, A., Aissa, A., Espeli, V., Squiban, D., Dunkel, N., Vargas, M., Hundsberger, T., Mach, N., Schaller, K., and Weber, D. (2014a). Phase I study of sorafenib combined with radiation therapy and temozolomide as first-line treatment of high-grade glioma. *British journal of cancer* 110, 2655-2661.

Hottinger, A.F., Aissa, A.B., Espeli, V., Squiban, D., Dunkel, N., Vargas, M.I., Hundsberger, T., Mach, N., Schaller, K., Weber, D.C., *et al.* (2014b). Phase I study of sorafenib combined with radiation therapy and temozolomide as first-line treatment of high-grade glioma. *Br J Cancer* 110, 2655-2661.

Huncharek, M., Kupelnick, B., and Wheeler, L. (2003). Dietary cured meat and the risk of adult glioma: a meta-analysis of nine observational studies. *Journal of environmental pathology, toxicology and oncology* 22.

Hyde, S.C., Emsley, P., Hartshorn, M.J., Mimmack, M.M., Gileadi, U., Pearce, S.R., Gallagher, M.P., Gill, D.R., Hubbard, R.E., and Higgins, C.F. (1990). Structural model of ATP-binding proteing associated with cystic fibrosis, multidrug resistance and bacterial transport.

Inskip, P.D., Tarone, R.E., Hatch, E.E., Wilcosky, T.C., Shapiro, W.R., Selker, R.G., Fine, H.A., Black, P.M., Loeffler, J.S., and Linet, M.S. (2001). Cellular-telephone use and brain tumors. *New England Journal of Medicine* 344, 79-86.

Jacinto, F.V., and Esteller, M. (2007). MGMT hypermethylation: a prognostic foe, a predictive friend. *DNA repair* 6, 1155-1160.

Jakubowicz-Gil, J., Langner, E., Bądziul, D., Wertel, I., and Rzeski, W. (2014a). Quercetin and sorafenib as a novel and effective couple in programmed cell death induction in human gliomas. *Neurotox Res* 26, 64-77.

Jakubowicz-Gil, J., Langner, E., Bądziul, D., Wertel, I., and Rzeski, W. (2014b). Quercetin and sorafenib as a novel and effective couple in programmed cell death induction in human gliomas. *Neurotoxicity research* 26, 64-77.

Kane, R.C., Farrell, A.T., Madabushi, R., Booth, B., Chattopadhyay, S., Sridhara, R., Justice, R., and Pazdur, R. (2009). Sorafenib for the treatment of unresectable hepatocellular carcinoma. *The oncologist* 14, 95-100.

Kane, R.C., Farrell, A.T., Saber, H., Tang, S., Williams, G., Jee, J.M., Liang, C., Booth, B., Chidambaram, N., and Morse, D. (2006). Sorafenib for the treatment of advanced renal cell carcinoma. *Clinical cancer research* 12, 7271-7278.

Karavasilis, V., Kotoula, V., Pentheroudakis, G., Televantou, D., Lambaki, S., Chrisafi, S., Bobos, M., and Fountzilias, G. (2013). A phase I study of temozolomide and lapatinib combination in patients with recurrent high-grade gliomas. *Journal of neurology* 260, 1469-1480.

Kirson, E.D., Gurchik, Z., Schneiderman, R., Dekel, E., Itzhaki, A., Wasserman, Y., Schatzberger, R., and Palti, Y. (2004). Disruption of cancer cell replication by alternating electric fields. *Cancer research* 64, 3288-3295.

Krex, D., Klink, B., Hartmann, C., von Deimling, A., Pietsch, T., Simon, M., Sabel, M., Steinbach, J.P., Heese, O., and Reifenberger, G. (2007). Long-term survival with glioblastoma multiforme. *Brain* 130, 2596-2606.

Krishna, R., and Mayer, L.D. (2000). Multidrug resistance (MDR) in cancer: mechanisms, reversal using modulators of MDR and the role of MDR modulators in influencing the pharmacokinetics of anticancer drugs. *European Journal of Pharmaceutical Sciences* 11, 265-283.

Kusuhara, H., and Sugiyama, Y. (2005). Active efflux across the blood-brain barrier: role of the solute carrier family. *NeuroRx* 2, 73-85.

Kyte, J.A., Gaudernack, G., Dueland, S., Trachsel, S., Julsrud, L., and Aamdal, S. (2011). Telomerase peptide vaccination combined with temozolomide: a clinical trial in stage IV melanoma patients. *Clinical cancer research* 17, 4568-4580.

Löscher, W., and Potschka, H. (2005). Role of drug efflux transporters in the brain for drug disposition and treatment of brain diseases. *Progress in neurobiology* 76, 22-76.

Lacroix, M., Abi-Said, D., Fourney, D.R., Gokaslan, Z.L., Shi, W., DeMonte, F., Lang, F.F.,

McCutcheon, I.E., Hassenbusch, S.J., and Holland, E. (2001). A multivariate analysis of 416 patients with glioblastoma multiforme: prognosis, extent of resection, and survival. *Journal of neurosurgery* 95, 190-198.

Lagas, J.S., van Waterschoot, R.A., Sparidans, R.W., Wagenaar, E., Beijnen, J.H., and Schinkel, A.H. (2010a). Breast cancer resistance protein and P-glycoprotein limit sorafenib brain accumulation. *Molecular cancer therapeutics* 9, 319-326.

Lagas, J.S., van Waterschoot, R.A., Sparidans, R.W., Wagenaar, E., Beijnen, J.H., and Schinkel, A.H. (2010b). Breast cancer resistance protein and P-glycoprotein limit sorafenib brain accumulation. *Molecular cancer therapeutics* 9, 319-326.

Lander, E.S., Linton, L.M., Birren, B., Nusbaum, C., Zody, M.C., Baldwin, J., Devon, K., Dewar, K., Doyle, M., and FitzHugh, W. (2001). Initial sequencing and analysis of the human genome. *Nature* 409, 860-921.

Lee, E.Q., Kuhn, J., Lamborn, K.R., Abrey, L., DeAngelis, L.M., Lieberman, F., Robins, H.I., Chang, S.M., Yung, W.K., Drappatz, J., *et al.* (2012). Phase I/II study of sorafenib in combination with temsirolimus for recurrent glioblastoma or gliosarcoma: North American Brain Tumor Consortium study 05-02. *Neuro Oncol* 14, 1511-1518.

Lee, S.Y. (2016). Temozolomide resistance in glioblastoma multiforme. *Genes & Diseases* 3, 198-210.

Lehrer, S. (2010). Anopheles mosquito transmission of brain tumor. *Medical hypotheses* 74, 167-168.

Litman, T., Jensen, U., Hansen, A., Covitz, K.-M., Zhan, Z., Fetsch, P., Abati, A., Hansen, P.R., Horn, T., and Skovsgaard, T. (2002). Use of peptide antibodies to probe for the mitoxantrone resistance-associated protein MXR/BCRP/ABCP/ABCG2. *Biochimica et Biophysica Acta (BBA)-Biomembranes* 1565, 6-16.

Llovet, J.M., Ricci, S., Mazzaferro, V., Hilgard, P., Gane, E., Blanc, J.-F., de Oliveira, A.C., Santoro, A., Raoul, J.-L., and Forner, A. (2008). Sorafenib in advanced hepatocellular carcinoma. *New England Journal of Medicine* 359, 378-390.

Lundquist, S., Renftel, M., Brillault, J., Fenart, L., Cecchelli, R., and Dehouck, M.-P. (2002). Prediction of drug transport through the blood-brain barrier in vivo: a comparison between two in vitro cell models. *Pharmaceutical research* 19, 976-981.

Miller, V.A., Hirsh, V., Cadranet, J., Chen, Y.-M., Park, K., Kim, S.-W., Zhou, C., Su, W.-C., Wang, M., and Sun, Y. (2012). Afatinib versus placebo for patients with advanced, metastatic non-small-cell lung cancer after failure of erlotinib, gefitinib, or both, and one or two lines of chemotherapy (LUX-Lung 1): a phase 2b/3 randomised trial. *The lancet oncology* 13, 528-538.

Molenaar, R.J., Radivoyevitch, T., Maciejewski, J.P., van Noorden, C.J., and Bleeker, F.E. (2014a). The driver and passenger effects of isocitrate dehydrogenase 1 and 2 mutations in oncogenesis

and survival prolongation. *Biochimica et Biophysica Acta (BBA)-Reviews on Cancer* 1846, 326-341.

Molenaar, R.J., Verbaan, D., Lamba, S., Zanon, C., Jeuken, J.W., Boots-Sprenger, S.H., Wesseling, P., Hulsebos, T.J., Troost, D., and Van Tilborg, A.A. (2014b). The combination of IDH1 mutations and MGMT methylation status predicts survival in glioblastoma better than either IDH1 or MGMT alone. *Neuro-oncology*, nou005.

Molnár, P. (2011). *Classification of Primary Brain Tumors: Molecular Aspects* (INTECH Open Access Publisher).

Monk, P., Lam, E., Mortazavi, A., Kendra, K., Lesinski, G.B., Mace, T.A., Geyer, S., Carson III, W.E., Tahiri, S., and Bhinder, A. (2014). A phase I study of high-dose interleukin-2 with sorafenib in patients with metastatic renal cell carcinoma and melanoma. *Journal of Immunotherapy* 37, 180-186.

Nabors, L.B., Supko, J.G., Rosenfeld, M., Chamberlain, M., Phuphanich, S., Batchelor, T., Desideri, S., Ye, X., Wright, J., Gujar, S., *et al.* (2011). Phase I trial of sorafenib in patients with recurrent or progressive malignant glioma. *Neuro Oncol* 13, 1324-1330.

Nagasawa, D.T., Chow, F., Yew, A., Kim, W., Cremer, N., and Yang, I. (2012). Temozolomide and other potential agents for the treatment of glioblastoma multiforme. *Neurosurgery clinics of North America* 23, 307-322.

Nakagawa, S., Deli, M.A., Kawaguchi, H., Shimizudani, T., Shimono, T., Kittel, A., Tanaka, K., and Niwa, M. (2009). A new blood–brain barrier model using primary rat brain endothelial cells, pericytes and astrocytes. *Neurochemistry international* 54, 253-263.

Narayana, A., Gruber, D., Kunnakkat, S., Golfinos, J.G., Parker, E., Raza, S., Zagzag, D., Eagan, P., and Gruber, M.L. (2012). A clinical trial of bevacizumab, temozolomide, and radiation for newly diagnosed glioblastoma: clinical article. *Journal of neurosurgery* 116, 341-345.

Nielsen, D., and Skovsgaard, T. (1992). P-glycoprotein as multidrug transporter: a critical review of current multidrug resistant cell lines. *Biochimica et Biophysica Acta (BBA)-Molecular Basis of Disease* 1139, 169-183.

Norden, A.D., Drappatz, J., and Wen, P.Y. (2009). Antiangiogenic therapies for high-grade glioma. *Nature Reviews Neurology* 5, 610-620.

Nupponen, N.N., and Joensuu, H. (2006). Molecular pathology of gliomas. *Current Diagnostic Pathology* 12, 394-402.

Ogura, J., Kuwayama, K., Sasaki, S., Kaneko, C., Koizumi, T., Yabe, K., Tsujimoto, T., Takeno, R., Takaya, A., and Kobayashi, M. (2015). Reactive oxygen species derived from xanthine oxidase interrupt dimerization of breast cancer resistance protein, resulting in suppression of uric acid excretion to the intestinal lumen. *Biochemical pharmacology* 97, 89-98.

Ohgaki, H., and Kleihues, P. (2007). Genetic pathways to primary and secondary glioblastoma. *The American journal of pathology* *170*, 1445-1453.

Ohgaki, H., and Kleihues, P. (2013). The definition of primary and secondary glioblastoma. *Clinical cancer research* *19*, 764-772.

Ostrom, Q.T., Bauchet, L., Davis, F.G., Deltour, I., Fisher, J.L., Langer, C.E., Pekmezci, M., Schwartzbaum, J.A., Turner, M.C., and Walsh, K.M. (2014). The epidemiology of glioma in adults: a “state of the science” review. *Neuro-oncology* *16*, 896-913.

Ostrom, Q.T., Gittleman, H., Farah, P., Ondracek, A., Chen, Y., Wolinsky, Y., Stroup, N.E., Kruchko, C., and Barnholtz-Sloan, J.S. (2013). CBTRUS statistical report: Primary brain and central nervous system tumors diagnosed in the United States in 2006-2010. *Neuro-oncology* *15*, ii1-ii56.

Ozawa, T., and James, C.D. (2010). Establishing intracranial brain tumor xenografts with subsequent analysis of tumor growth and response to therapy using bioluminescence imaging. *JoVE (Journal of Visualized Experiments)*, e1986-e1986.

Pan, G., Winter, T.N., Roberts, J.C., Fairbanks, C.A., and Elmquist, W.F. (2010). Organic cation uptake is enhanced in bcrp1-transfected MDCKII cells. *Molecular pharmaceutics* *7*, 138.

Pardridge, W.M. (2005). The blood-brain barrier: bottleneck in brain drug development. *NeuroRx* *2*, 3-14.

Paz-Ares, L., Hirsh, V., Zhang, L., de Marinis, F., Yang, J., Wakelee, H., Seto, T., Wu, Y., Novello, S., and Juhász, E. (2015a). MISSION Trial-A phase III, multi-center, placebo-controlled trial of sorafenib in patients with relapsed or refractory predominantly non-squamous NSCLC after 2 or 3 previous treatment regimens. *Journal of thoracic oncology: official publication of the International Association for the Study of Lung Cancer*.

Paz-Ares, L., Hirsh, V., Zhang, L., De Marinis, F., Yang, J.C.-H., Wakelee, H.A., Seto, T., Wu, Y.-L., Novello, S., and Juhász, E. (2015b). Monotherapy Administration of Sorafenib in Patients With Non–Small Cell Lung Cancer (MISSION) Trial: A Phase III, Multicenter, Placebo–Controlled Trial of Sorafenib in Patients with Relapsed or Refractory Predominantly Nonsquamous Non–Small-Cell Lung Cancer after 2 or 3 Previous Treatment Regimens. *Journal of Thoracic Oncology* *10*, 1745-1753.

Pegg, A.E. (1990). Mammalian O6-alkylguanine-DNA alkyltransferase: regulation and importance in response to alkylating carcinogenic and therapeutic agents. *Cancer research* *50*, 6119-6129.

Pegg, A.E., Dolan, M.E., and Moschel, R.C. (1995). Structure, function, and inhibition of O 6-alkylguanine-DNA alkyltransferase. *Progress in nucleic acid research and molecular biology* *51*, 167-223.

Pizzo, P.A., and Poplack, D.G. (2015). *Principles and practice of pediatric oncology* (Lippincott

Williams & Wilkins).

Poller, B., Iusuf, D., Sparidans, R.W., Wagenaar, E., Beijnen, J.H., and Schinkel, A.H. (2011a). Differential impact of P-glycoprotein (ABCB1) and breast cancer resistance protein (ABCG2) on axitinib brain accumulation and oral plasma pharmacokinetics. *Drug Metabolism and Disposition*, dmd. 110.037317.

Poller, B., Wagenaar, E., Tang, S.C., and Schinkel, A.H. (2011b). Double-Transduced MDCKII Cells To Study Human P-Glycoprotein (ABCB1) and Breast Cancer Resistance Protein (ABCG2) Interplay in Drug Transport across the Blood– Brain Barrier. *Molecular pharmaceutics* 8, 571-582.

Polli, J.W., Olson, K.L., Chism, J.P., John-Williams, L.S., Yeager, R.L., Woodard, S.M., Otto, V., Castellino, S., and Demby, V.E. (2009). An unexpected synergist role of P-glycoprotein and breast cancer resistance protein on the central nervous system penetration of the tyrosine kinase inhibitor lapatinib (N-{3-chloro-4-[(3-fluorobenzyl) oxy] phenyl}-6-[5-{{2-(methylsulfonyl) ethyl} amino} methyl]-2-furyl}-4-quinazolinamine; GW572016). *Drug Metabolism and Disposition* 37, 439-442.

Prados, M.D., Chang, S.M., Butowski, N., DeBoer, R., Parvataneni, R., Carliner, H., Kabuubi, P., Ayers-Ringler, J., Rabbitt, J., and Page, M. (2008). Phase II study of erlotinib plus temozolomide during and after radiation therapy in patients with newly diagnosed glioblastoma multiforme or gliosarcoma. *Journal of clinical oncology* 27, 579-584.

Preston-Martin, S., Mack, W., and Henderson, B.E. (1989). Risk factors for gliomas and meningiomas in males in Los Angeles County. *Cancer research* 49, 6137-6143.

Pu, K.-s. (2016). Malignant glioma in Hong Kong Chinese. HKU Theses Online (HKUTO).

Raza, M.W., Shad, A., Pedler, S.J., and Karamat, K.A. (2005). Penetration and activity of antibiotics in brain abscess. *J Coll Physicians Surg Pak* 15, 165-167.

Reeve, J., Koch, G., and Twentyman, P. (1987). Evidence that multidrug resistance in Chinese hamster ovary cells is associated with alterations in the endoplasmic reticulum. *British journal of cancer* 56, 143.

Rini, B., Wilding, G., Hudes, G., Stadler, W., Kim, S., Tarazi, J., Bycott, P., Liau, K., and Dutcher, J. (2007). Axitinib (AG-013736; AG) in patients (pts) with metastatic renal cell cancer (RCC) refractory to sorafenib. *Journal of clinical oncology* 25, 5032-5032.

Sambuy, Y., De Angelis, I., Ranaldi, G., Scarino, M., Stamatii, A., and Zucco, F. (2005). The Caco-2 cell line as a model of the intestinal barrier: influence of cell and culture-related factors on Caco-2 cell functional characteristics. *Cell biology and toxicology* 21, 1-26.

Savitz, D.A., Checkoway, H., and Loomis, D.P. (1998). Magnetic field exposure and neurodegenerative disease mortality among electric utility workers. *Epidemiology* 9, 398-404.

- Schapira, A.H. (2007). *Neurology and clinical neuroscience*.
- Sheehan, J., Ionescu, A., Pouratian, N., Hamilton, D.K., Schlesinger, D., Oskouian Jr, R.J., and Sansur, C. (2008). Use of trans sodium crocetin for sensitizing glioblastoma multiforme to radiation.
- Sheehan, J.P., Shaffrey, M.E., Gupta, B., Larner, J., Rich, J.N., and Park, D.M. (2010). Improving the radiosensitivity of radioresistant and hypoxic glioblastoma. *Future oncology* 6, 1591-1601.
- Shigeta, J., Katayama, K., Mitsuhashi, J., Noguchi, K., and Sugimoto, Y. (2010). BCRP/ABCG2 confers anticancer drug resistance without covalent dimerization. *Cancer science* 101, 1813-1821.
- Shitara, Y., Maeda, K., Ikejiri, K., Yoshida, K., Horie, T., and Sugiyama, Y. (2013). Clinical significance of organic anion transporting polypeptides (OATPs) in drug disposition: their roles in hepatic clearance and intestinal absorption. *Biopharmaceutics & drug disposition* 34, 45-78.
- Showalter, T.N., Andrel, J., Andrews, D.W., Curran, W.J., Daskalakis, C., and Werner-Wasik, M. (2007). Multifocal glioblastoma multiforme: prognostic factors and patterns of progression. *International Journal of Radiation Oncology* Biology* Physics* 69, 820-824.
- Siegelin, M.D., Raskett, C.M., Gilbert, C.A., Ross, A.H., and Altieri, D.C. (2010). Sorafenib exerts anti-glioma activity in vitro and in vivo. *Neuroscience letters* 478, 165-170.
- Smalley, K.S., Xiao, M., Villanueva, J., Nguyen, T.K., Flaherty, K.T., Letrero, R., Van Belle, P., Elder, D.E., Wang, Y., and Nathanson, K.L. (2009). CRAF inhibition induces apoptosis in melanoma cells with non-V600E BRAF mutations. *Oncogene* 28, 85-94.
- Stamatovic, S.M., Keep, R.F., and Andjelkovic, A.V. (2008). Brain endothelial cell-cell junctions: how to “open” the blood brain barrier. *Current neuropharmacology* 6, 179-192.
- Stevens, G.H. (2006). Antiepileptic therapy in patients with central nervous system malignancies. *Current neurology and neuroscience reports* 6, 311-318.
- Stupp, R., Taillibert, S., Kanner, A.A., Kesari, S., Steinberg, D.M., Toms, S.A., Taylor, L.P., Lieberman, F., Silvani, A., and Fink, K.L. (2015). Maintenance therapy with tumor-treating fields plus temozolomide vs temozolomide alone for glioblastoma: a randomized clinical trial. *Jama* 314, 2535-2543.
- Stupp, R., Wong, E., and Scott, C. Interim analysis of the EF-14 trial: a prospective, multicenter trial of NovoTTF-100A together with temozolomide compared to temozolomide alone in patients with newly diagnosed GBM; November 13–16; Miami, FL. 2014. Society for Neuro-Oncology.
- Swanson, K.D., Lok, E., and Wong, E.T. (2016). An overview of alternating electric fields therapy (NovoTTF Therapy) for the treatment of malignant glioma. *Current neurology and neuroscience reports* 16, 8.

Tait, M., Petrik, V., Loosemore, A., Bell, B., and Papadopoulos, M. (2007). Survival of patients with glioblastoma multiforme has not improved between 1993 and 2004: analysis of 625 cases. *British journal of neurosurgery* *21*, 496-500.

Thiebaut, F., Tsuruo, T., Hamada, H., Gottesman, M.M., Pastan, I., and Willingham, M.C. (1987). Cellular localization of the multidrug-resistance gene product P-glycoprotein in normal human tissues. *Proceedings of the National Academy of Sciences* *84*, 7735-7738.

Thomas, L., Lai, S.Y., Dong, W., Feng, L., Dadu, R., Regone, R.M., and Cabanillas, M.E. (2014). Sorafenib in metastatic thyroid cancer: a systematic review. *The oncologist* *19*, 251-258.

Tryfonidis, K., Basaran, G., Bogaerts, J., Debled, M., Dirix, L., Thery, J.-C., Tjan-Heijnen, V.C., Van den Weyngaert, D., Cufer, T., and Piccart, M. (2016). A European Organisation for Research and Treatment of Cancer randomized, double-blind, placebo-controlled, multicentre phase II trial of anastrozole in combination with gefitinib or placebo in hormone receptor-positive advanced breast cancer (NCT00066378). *European Journal of Cancer* *53*, 144-154.

Ueda, K., Clark, D., Chen, C., Roninson, I., Gottesman, M., and Pastan, I. (1987). The human multidrug resistance (mdr1) gene. cDNA cloning and transcription initiation. *Journal of Biological Chemistry* *262*, 505-508.

Van Dorpe, S., Bronselaer, A., Nielandt, J., Stalmans, S., Wynendaele, E., Audenaert, K., Van De Wiele, C., Burvenich, C., Peremans, K., and Hsuchou, H. (2012). Brainpeps: the blood–brain barrier peptide database. *Brain Structure and Function* *217*, 687-718.

Van Tellingen, O., Yetkin-Arik, B., De Gooijer, M., Wesseling, P., Wurdinger, T., and De Vries, H. (2015). Overcoming the blood–brain tumor barrier for effective glioblastoma treatment. *Drug Resistance Updates* *19*, 1-12.

Van Wijngaarden, E., and Dosemeci, M. (2006). Brain cancer mortality and potential occupational exposure to lead: findings from the National Longitudinal Mortality Study, 1979–1989. *International journal of cancer* *119*, 1136-1144.

Venter, J.C., Adams, M.D., Myers, E.W., Li, P.W., Mural, R.J., Sutton, G.G., Smith, H.O., Yandell, M., Evans, C.A., and Holt, R.A. (2001). The sequence of the human genome. *science* *291*, 1304-1351.

Vilchez, R.A., Kozinetz, C.A., Arrington, A.S., Madden, C.R., and Butel, J.S. (2003). Simian virus 40 in human cancers. *The American journal of medicine* *114*, 675-684.

Vlaming, M.L., Lagas, J.S., and Schinkel, A.H. (2009). Physiological and pharmacological roles of ABCG2 (BCRP): recent findings in *Abcg2* knockout mice. *Advanced drug delivery reviews* *61*, 14-25.

Walker, M.D., Alexander Jr, E., Hunt, W.E., MacCarty, C.S., Mahaley Jr, M.S., Mealey Jr, J., Norrell, H.A., Owens, G., Ransohoff, J., and Wilson, C.B. (1978). Evaluation of BCNU and/or radiotherapy in the treatment of anaplastic gliomas: a cooperative clinical trial. *Journal of*

neurosurgery *49*, 333-343.

Wang, Z., Pal, D., Patel, A., Kwatra, D., and Mitra, A.K. (2013). Influence of overexpression of efflux proteins on the function and gene expression of endogenous peptide transporters in MDR-transfected MDCKII cell lines. *International journal of pharmaceutics* *441*, 40-49.

Wick, W. (2016). *TTFIELDS: where does all the skepticism come from?* (Oxford University Press).

Wilhelm, S.M., Adnane, L., Newell, P., Villanueva, A., Llovet, J.M., and Lynch, M. (2008). Preclinical overview of sorafenib, a multikinase inhibitor that targets both Raf and VEGF and PDGF receptor tyrosine kinase signaling. *Molecular cancer therapeutics* *7*, 3129-3140.

Yan, C.S., Wong, I.L., Chan, K.-F., Kan, J.W., Chong, T.C., Law, M.C., Zhao, Y., Chan, S.W., Chan, T.H., and Chow, L.M. (2015). A new class of safe, potent, and specific P-gp modulator: Flavonoid dimer FD18 reverses P-gp-mediated multidrug resistance in human breast xenograft in vivo. *Molecular pharmaceutics* *12*, 3507-3517.

Young, R.M., Jamshidi, A., Davis, G., and Sherman, J.H. (2015). Current trends in the surgical management and treatment of adult glioblastoma. *Annals of translational medicine* *3*.

Zhang, Y., Li, C.S., Ye, Y., Johnson, K., Poe, J., Johnson, S., Bobrowski, W., Garrido, R., and Madhu, C. (2006). Porcine brain microvessel endothelial cells as an in vitro model to predict in vivo blood-brain barrier permeability. *Drug Metabolism and Disposition* *34*, 1935-1943.

Zheng, T., Cantor, K.P., Zhang, Y., Chiu, B.C., and Lynch, C.F. (2001). Risk of brain glioma not associated with cigarette smoking or use of other tobacco products in Iowa. *Cancer Epidemiology and Prevention Biomarkers* *10*, 413-414.

Zhou, C., Wu, Y.-L., Chen, G., Feng, J., Liu, X.-Q., Wang, C., Zhang, S., Wang, J., Zhou, S., and Ren, S. (2011). Erlotinib versus chemotherapy as first-line treatment for patients with advanced EGFR mutation-positive non-small-cell lung cancer (OPTIMAL, CTONG-0802): a multicentre, open-label, randomised, phase 3 study. *The lancet oncology* *12*, 735-742.

Zustovich, F., Landi, L., Lombardi, G., Porta, C., Galli, L., Fontana, A., Amoroso, D., Galli, C., Andreuccetti, M., and Falcone, A. (2013). Sorafenib plus daily low-dose temozolomide for relapsed glioblastoma: a phase II study. *Anticancer research* *33*, 3487-3494.

PUBLICATIONS

1. Wong IL, Wang BC, Yuan J, Duan LX, Liu Z, Liu T, Li XM, **Hu X**, Zhang XY, Jiang T, Wan SB, Chow LM. Potent and Nontoxic Chemosensitizer of P-Glycoprotein-Mediated Multidrug Resistance in Cancer: Synthesis and Evaluation of Methylated Epigallocatechin, Gallocatechin, and Dihydromyricetin Derivatives. *J Med Chem*. 2015 Jun 11;58(11):4529-49.
2. Bin JW, Wong IL, **Hu X**, Yu ZX, Xing LF, Jiang T, Chow LM, Biao WS. Structure-activity relationship study of permethyl ningalin B analogues as P-glycoprotein chemosensitizers. *J Med Chem*. 2013 Nov 27;56(22):9057-70.

CONFERENCE PRESENTATIONS

1. **X. Hu**, Iris L. K. Wong, K. F. Chan, T. Z. Chong, T. H. Chan* and Larry M. C. Chow* Flavonoid heterodimers as nanomolar dual inhibitor of P-glycoprotein (P-gp) and breast cancer resistance protein (BCRP). Gordon Research Conference, Multi-Drug Efflux System, Italy, 2015.
2. **X. Hu**, Iris L. K. Wong, K. F. Chan, T. Z. Chong, T. H. Chan* and Larry M. C. Chow* Flavonoid heterodimers as nanomolar dual inhibitor of P-glycoprotein (P-gp) and breast cancer resistance protein (BCRP). International Symposium on Frontiers in Cancer Biology & Drug Development, Hong Kong, 2015.

AWARD AND SCHOLARSHIP

Hong Kong PhD Fellowship Scheme, Research Grants Council (RGC) of Hong Kong,
2012 – 2015.

GRANT SUPPORT

This Ph.D study was supported in part by Hong Kong Research Grants Council
General Research Fund.